6.4.1 Concrete mix design

The four concrete mixes were designed using the absolute volume method as shown below:

6.4.1.1 Mix No. (1): f_{cu} = 30MPa, w/c = 0.32

$$Absolute\ volume = \frac{C}{G_c} + \frac{S}{G_S} + \frac{G}{G_G} + \frac{W}{1.0} + \frac{Adm.}{G_{adm}} = 1000\ Liters$$

$$Percentage\ of\ sand\ in\ concrete\ aggregate = 40\%$$

$$Percentage\ of\ crushed\ stone\ in\ concrete\ aggregate = 60\%$$

$$Weight\ of\ cement\ per\ cubic\ meter$$

$$= concrete\ target\ strength\ after\ 28\ days\left(\frac{kg}{cm^2}\right) + 50 \rightarrow 100$$

$$Weight\ of\ cement = 300 + 50 = 350\ {}^{kg}/_{m^3}$$

$$Required\ {}^{W}/_{C} = 0.32 \quad \rightarrow \quad water\ volume = 0.32 * 350 = 112\ {}^{Liters}/_{m^3}$$

$$Nominal\ maximum\ size = 20mm$$

$$Percentage\ of\ superplasticizers = 1.5\%\ of\ cement\ weight = 5.25\ kg$$

$$Weight\ of\ crushed\ stone = 1.5\ weight\ of\ sand$$

$$Absolute\ volume = \frac{350}{3.15} + \frac{S}{2.63} + \frac{1.5S}{2.56} + \frac{112}{1.0} + \frac{5.25}{1.18} = 1000\ Liters$$

$$Weight\ of\ sand\ per\ cubic\ meter\ of\ concrete = 800\ kg$$

$$Weight\ of\ crushed\ stone\ per\ cubic\ meter\ of\ concrete = 1200\ kg$$

6.4.1.2 Mix No. (2): f_{cu} = 44MPa, w/c = 0.52

$$Absolute\ volume = \frac{C}{G_c} + \frac{S}{G_S} + \frac{G}{G_G} + \frac{W}{1.0} = 1000\ Liters$$

$$Percentage\ of\ sand\ in\ concrete\ aggregate = 40\%$$

$$Percentage\ of\ crushed\ stone\ in\ concrete\ aggregate = 60\%$$

$$Weight\ of\ cement\ per\ cubic\ meter$$
$$= concrete\ target\ strength\ after\ 28\ days\left(\frac{kg}{cm^2}\right) + 50 \rightarrow 100$$

$$Weight\ of\ cement = 440 + 100 = 540\ {}^{kg}/{}_{m^3}$$

$$Nominal\ maximum\ size = 20mm$$

$$Required\ {}^{W}/{}_{C} = 0.52 \quad \rightarrow \quad water\ volume = 0.52 * 540 = 280.8\ {}^{Liters}/{}_{m^3}$$

$$Weight\ of\ crushed\ stone = 1.5\ weight\ of\ sand$$

$$Absolute\ volume = \frac{540}{3.15} + \frac{S}{2.63} + \frac{1.5S}{2.56} + \frac{280.8}{1.0} = 1000\ Liters$$

$$Weight\ of\ sand\ per\ cubic\ meter\ of\ concrete = 567\ kg$$

$$Weight\ of\ crushed\ stone\ per\ cubic\ meter\ of\ concrete = 850\ kg$$

6.4.1.3 Mix No. (3): f_{cu} = 44MPa, w/c = 0.32

$$Absolute\ volume = \frac{C}{G_c} + \frac{S}{G_S} + \frac{G}{G_G} + \frac{W}{1.0} + \frac{Adm.}{G_{adm}} = 1000\ Liters$$

$$Percentage\ of\ sand\ in\ concrete\ aggregate = 40\%$$

$$Percentage\ of\ crushed\ stone\ in\ concrete\ aggregate = 60\%$$

$$Weight\ of\ cement\ per\ cubic\ meter$$
$$= concrete\ target\ strength\ after\ 28\ days\left(\frac{kg}{cm^2}\right) + 50 \rightarrow 100$$

$$Weight\ of\ cement = 440 + 50 = 490\ {}^{kg}/_{m^3}$$

$$Required\ {}^{W}/_{C} = 0.32 \quad \rightarrow \quad water\ volume = 0.32 * 490 = 156.8\ {}^{Liters}/_{m^3}$$

$$Nominal\ maximum\ size = 20mm$$

$$Percentage\ of\ superplasticizers = 1.5\%\ of\ cement\ weight = 7.35\ kg$$

$$Weight\ of\ crushed\ stone = 1.5\ weight\ of\ sand$$

$$Absolute\ volume = \frac{490}{3.15} + \frac{S}{2.63} + \frac{1.5S}{2.56} + \frac{156.8}{1.0} + \frac{7.35}{1.18} = 1000\ Liters$$

$$Weight\ of\ sand\ per\ cubic\ meter\ of\ concrete = 705\ kg$$

$$Weight\ of\ crushed\ stone\ per\ cubic\ meter\ of\ concrete = 1058\ kg$$

6.4.1.4 Mix No. (4): f_{cu} = 60MPa, w/c = 0.32

$$Absolute\ volume = \frac{C}{G_c} + \frac{S}{G_S} + \frac{G}{G_G} + \frac{W}{1.0} + \frac{Adm.}{G_{adm}} = 1000\ Liters$$

$$Percentage\ of\ sand\ in\ concrete\ aggregate = 40\%$$

$$Percentage\ of\ crushed\ stone\ in\ concrete\ aggregate = 60\%$$

$$Weight\ of\ cement\ per\ cubic\ meter$$
$$= concrete\ target\ strength\ after\ 28\ days\left(\frac{kg}{cm^2}\right) + 50 \rightarrow 100$$

$$Weight\ of\ cement = 600 + 50 = 650\ {}^{kg}/_{cm^2}$$

$$Required\ {}^{W}/_{C} = 0.32 \quad \rightarrow \quad water\ volume = 0.32 * 650 = 208\ {}^{Liters}/_{m^3}$$

$$Nominal\ maximum\ size = 20mm$$

$$Percentage\ of\ superplasticizers = 2.0\%\ of\ cement\ weight = 13\ kg$$

$$Weight\ of\ crushed\ stone = 1.5\ weight\ of\ sand$$

$$Absolute\ volume = \frac{650}{3.15} + \frac{S}{2.63} + \frac{1.5S}{2.56} + \frac{208}{1.0} + \frac{13}{1.18} = 1000\ Liters$$

$$Weight\ of\ sand\ per\ cubic\ meter\ of\ concrete = 594.5\ kg$$

$$Weight\ of\ crushed\ stone\ per\ cubic\ meter\ of\ concrete = 891.5\ kg$$

Table 6.14 summarizes the concrete mix proportioning for the four mixes.

Table 6.14: Concrete mix proportions per cubic meter

	Cement (kg)	**Sand (kg)**	**Coarse aggregate (kg)**	**Water (Liters)**	**Admixtures (kg)**
Mix No.1	350	800	1200	112	5.25
Mix No.2	540	567	850	281	0.0
Mix No.3	490	705	1058	157	7.35
Mix No.4	650	595	892	208	13

Six concrete cylinders (150 mm diameter and 300 mm height) for each concrete type were prepared, measured and tested for tensile strengths (after 28 and 56 days of casting) in accordance with ASTM C496-96 as shown in Figs. 6.11a through 6.11d, and the splitting tensile strength (f_t) was calculated as follows:

$$f_t = {}^{2p}/_{\pi.l.d} \qquad \text{6-1}$$

Where:

f_t = splitting tensile strength (MPa)
p = maximum applied load (N)
l = length of the specimen (mm)
d = diameter of the specimen (mm)

Fig. 6.11a

Fig. 6.11b

Fig. 6.11c

Fig. 6.11d

Fig. 6.11: Tensile Splitting Test

The compressive strength test was carried out for six concrete cubes 150 mm for each type of concrete after 28 and 56 days of casting according to BS using 2000 KN compression testing machine. The results of the compressive strength tests as well as the splitting tensile strength are presented in Tables 6.15 through 6.18.

Table 6.15: The results of compressive strength and splitting tensile strength tests for **mix No. (1)**

Test Type	Sample Code	Curing Duration	Sample Weight (kg)	Maximum Load (N)	Maximum Stress (MPa)	Average Stress (MPa)
Compressive Strength	1.1	28 days	7.83	699200	31.08	30.91
	1.2	28 days	7.81	698000	31.02	
	1.3	28 days	7.78	689500	30.64	
	1.4	56 days	7.06	762210	33.88	33.74
	1.5	56 days	7.35	763530	33.93	
	1.6	56 days	7.04	751540	33.4	
Splitting Tensile Strength	1.7	28 days	12.48	220000	3.11	3.14
	1.8	28 days	12.41	227300	3.22	
	1.9	28 days	12.44	219200	3.1	
	1.10	56 days	12.51	264500	3.74	3.69
	1.11	56 days	12.47	260900	3.69	
	1.12	56 days	12.56	256600	3.63	

Table 6.16: The results of compressive strength and splitting tensile strength tests for **mix No. (2)**

Test Type	Sample Code	Curing Duration	Sample Weight (kg)	Maximum Load (N)	Maximum Stress (MPa)	Average Stress (MPa)
Compressive Strength	2.1	28 days	8.03	968600	43.05	44.083
	2.2	28 days	8.17	1001000	44.49	
	2.3	28 days	7.83	1006000	44.71	
	2.4	56 days	8.3	1142000	50.76	49.88
	2.5	56 days	7.99	1165000	51.78	
	2.6	56 days	7.96	1060000	47.11	
Splitting Tensile Strength	2.7	28 days	12.31	205500	2.91	3.54
	2.8	28 days	12.54	268700	3.8	
	2.9	28 days	12.56	275600	3.9	
	2.10	56 days	12.43	282000	3.99	3.98
	2.11	56 days	12.28	268000	3.79	
	2.12	56 days	12.61	294000	4.16	

Table 6.17: The results of compressive strength and splitting tensile strength tests for **mix No. (3)**

Test Type	Sample Code	Curing Duration	Sample Weight (kg)	Maximum Load (N)	Maximum Stress (MPa)	Average Stress (MPa)
Compressive Strength	3.1	28 days	7.84	1008000	44.8	44.43
	3.2	28 days	7.843	1025000	45.56	
	3.3	28 days	7.85	966200	42.94	
	3.4	56 days	7.91	1267000	56.31	48.58
	3.5	56 days	7.63	1031000	45.82	
	3.6	56 days	7.53	981400	43.62	
Splitting Tensile Strength	3.7	28 days	12.63	338000	4.78	4.32
	3.8	28 days	12.72	288800	4.09	
	3.9	28 days	12.79	289200	4.09	
	3.10	56 days	12.53	341000	4.82	4.604
	3.11	56 days	12.69	294000	4.16	
	3.12	56 days	12.71	341570	4.83	

Table 6.18: The results of compressive strength and splitting tensile strength tests for **mix No. (4)**

Test Type	Sample Code	Curing Duration	Sample Weight (kg)	Maximum Load (N)	Maximum Stress (MPa)	Average Stress (MPa)
Compressive Strength	4.1	28 days	7.86	1299000	57.73	53.096
	4.2	28 days	7.88	1268000	56.36	
	4.3	28 days	7.75	1017000	45.2	
	4.4	56 days	7.9	1321000	58.71	62.904
	4.5	56 days	7.88	1491000	66.27	
	4.6	56 days	7.74	1434000	63.73	
Splitting Tensile Strength	4.7	28 days	12.39	300100	4.25	4.141
	4.8	28 days	12.67	309000	4.37	
	4.9	28 days	12.56	269100	3.81	
	4.10	56 days	12.62	309200	4.37	4.397
	4.11	56 days	12.6	315200	4.46	
	4.12	56 days	12.73	308000	4.36	

6.5 Specimens preparation

In addition to the 48 concrete samples used to study the compressive strength and the indirect tensile strength, 24 cylindrical concrete specimens (100 mm diameter and 200 mm height reinforced axially with a single steel bar, and protruding at one end only) were prepared for each concrete type to study the bond strength under several corrosion stages.

The 24 cylindrical specimens for each concrete type were divided into three groups (8 specimens per group for each reinforcing steel type). Each group consists of: 2 specimens tested for zero cracking level and 2 specimens tested for each of pre-cracking, cracking and severe corrosion levels.

The cylindrical concrete specimen has a 16mm diameter bar embedded and protruding at one end only. The bar is 310 mm protruded out of the surface and 150 mm embedded in the bottom of the concrete cylinder (Figs. 6.12a and 6.12b).

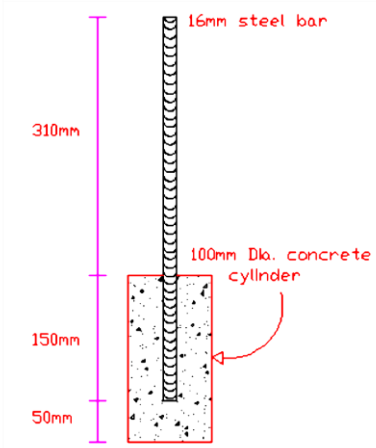

Fig. 6.12a

Fig. 6.12b

Fig. 6.12: Cylindrical concrete specimens

To protect the interface between the protruding steel bar and the surface of the concrete specimen from corrosion during the curing stage, 50 mm of the extension part of the bars along with another length of 25 mm within the specimen top, was epoxy coated (Figs. 6.13a, 6.13b and 6.13c)

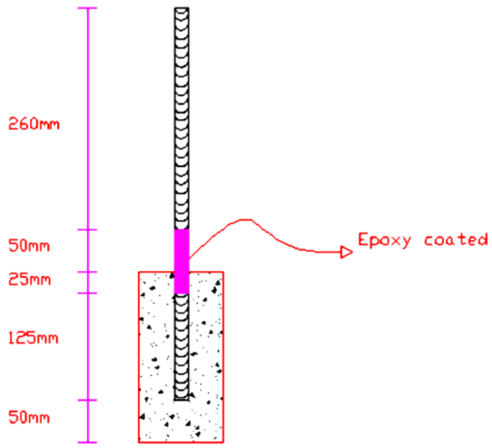

Fig. 6.13a

Fig. 6.13b

Fig. 6.13c

Fig. 6.13: Interface between the protruding steel bar and the surface of the concrete

To maintain the bar verticality during casting, a circular steel piece with a centered steel hollow tube with an inner diameter 18 mm, was mounted on the cylinder mold quickly after casting the concrete and the bar was then hammered until reaching the required depth (Figs. 6.14a and 6.14b).

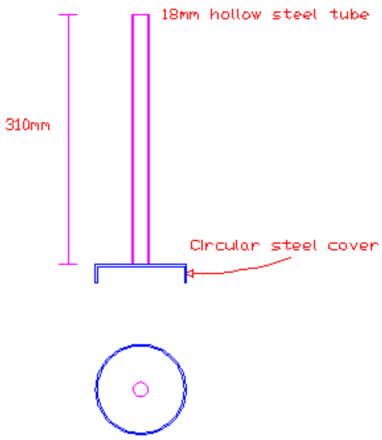

Fig. 6.14a

Fig. 6.14b

Fig. 6.14: A circular steel piece to maintain bar verticality

The concrete specimens were cast in steel moulds. All specimens were compacted using a standard steel rod and a vibrating table directly after casting. The specimens were left to set for 24 hours, and then they were demolded and cured in a standard moist curing tank (at 22 ± 2°C and 100% relative humidity) to different stages (Figs. 6.15a and 6.15b).

Fig. 6.15a

Fig. 6.15b

Fig. 6.15: Curing of concrete specimens

6.6 Accelerated Corrosion

Accelerated corrosion tests are used to obtain qualitative information on corrosion behavior in a relative short period compared to the field corrosion test. Accelerated corrosion tests have been used successfully to determine the susceptibility of the reinforcing and other forms of structural steel to localized attacks such as pitting corrosion, stress corrosion and other forms of corrosion, *Al Hassan (2003).*

The accelerated corrosion test in this program was terminated when the four stages of corrosion took place within the different steel types, based on the crack width; zero corrosion stage after two months of curing and before placing the specimens in the corrosion tank. Pre-cracking stage considered when the current started to increase but before any crack was visible. Cracking stage considered when the first crack appeared on the concrete specimen regardless the width of this crack, and severe corrosion stage considered when any crack extended up to 4 mm.

6.6.1 Test set up

After the 96 pullout specimens were cast and cured, 72 specimens were subjected to accelerated corrosion by placing them in the accelerated corrosion tank, while the rest of the 24 specimens (2 specimens per steel type per concrete type) served as the control specimens (zero corrosion stage).

The accelerated corrosion setup consists of 1650 x 850 mm fiber tank, electrolytic solution [5% sodium chloride NaCl by the weight of water] and a steel mesh placed in the bottom of the tank connected to a single steel bar (Fig. 6.16).

Fig. 6.16(a): 1650x850 mm fiber tank

Fig. 6.16(b): Bottom steel mesh.

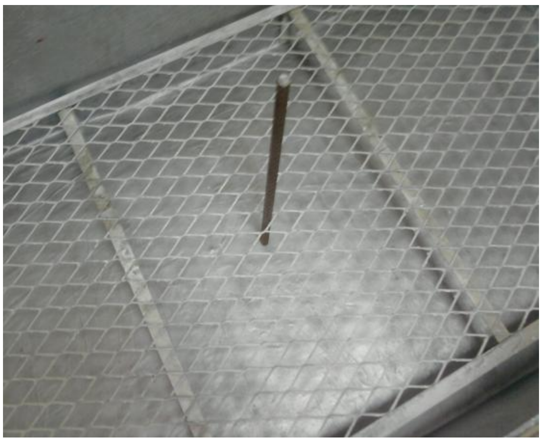

Fig. 6.16(c): A steel bar connected to the steel mesh

The specimens were placed in the accelerated corrosion tank and partially immersed with the electrolytic solution up to two thirds of its height. To eliminate any change in the concentration of the NaCl and ph of the solution, the electrolyte solution was changed weekly.

The single steel bar (connected to the steel mesh) and the specimens' bars were connected to electrical wires then connected to 12 V power supply (Fig. 6.17). The direction of the current was arranged so that the single steel bar served as cathode, while the specimens' bars served as anodes. The current was measured daily by means of a Digital Multimeter (Fig. 6.18) that read both current and the voltage. Figs. 5.19a and 5.19b illustrate the schematic drawing of the accelerated corrosion set up and a photograph taken during the test respectively.

Fig. 6.17: 12V power supply

Fig. 6.18: Digital Multimeter

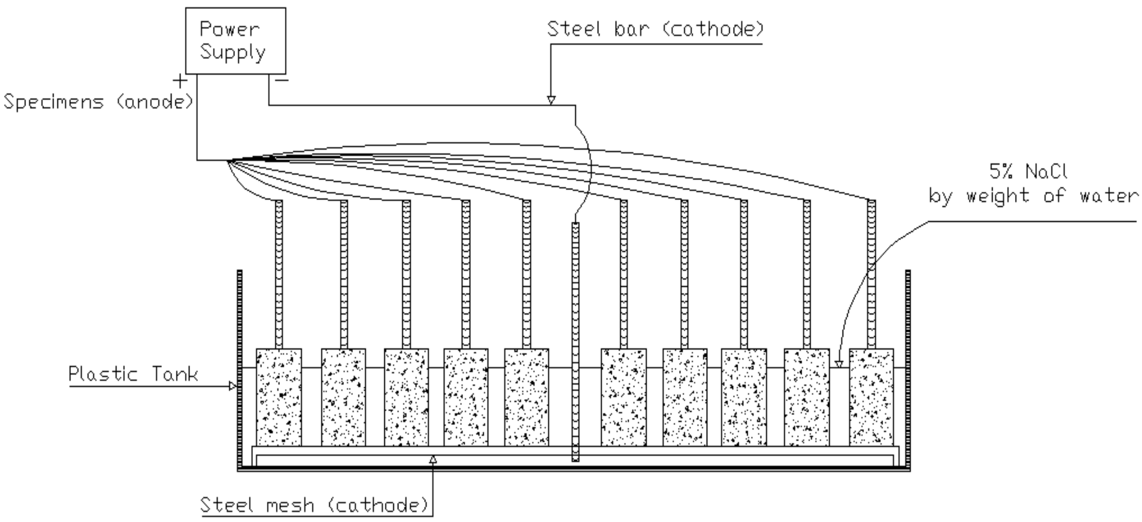

Fig. 6.19a: Schematic diagram of the accelerated corrosion tank.

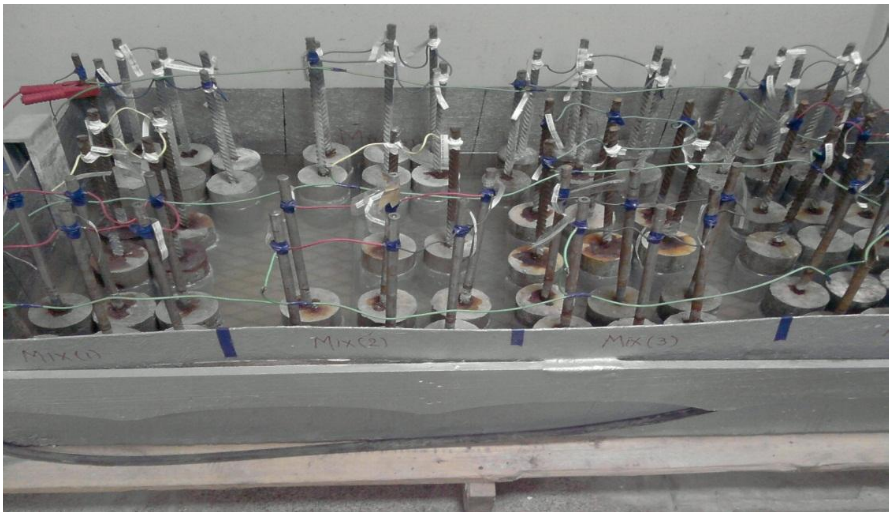

Fig. 6.19b: The accelerated corrosion tank during testing

6.7 Pull out test

The pull out test was conducted in the Arab Academy laboratory using an Instron Universal Testing Machine (Fig. 6.20). After establishing the specified levels of corrosion, the specimens were removed from the accelerated corrosion tank and a standard pull out test was performed. The relative displacement between the free end of the steel bar and the surface of concrete specimen was measured using a standard LVDT. Also the load readings were recorded from the machine loading cell.

Fig. 6.20: Instron Universal Testing Machine, *[AAST materials Lab]*

6.8 Percentage of mass loss

After the completion of the pull out test, the specimens were broken and then the reinforcing bar for each specimen was cleaned and scrubbed with a stiff brush to ensure that the bar was free from any adhering corrosion products. The mass loss of the steel reinforcing bar was then obtained as the difference between the mass of the corroded bar (after the removal of the loose corrosion products) and its mass before corrosion, *Amleh (2000).*

$$Percentage\ of\ mass\ loss = \frac{[uncorroded\ weight - corroded\ weight]}{[uncorroded\ weight]} * 100 \qquad 6-2$$

6.9 Bar profile loss

The degradation in the rib profile was determined by measuring the rib height before applying the impressed current and after the corrosion takes place in the steel bar. The percentage of rib loss was determined as follows:

$$Percentage\ of\ rib\ loss =$$

$$\frac{[Rib\ height\ of\ uncorroded\ bar - Rib\ height\ of\ corroded\ bar]}{[Rib\ height\ of\ uncorroded\ bar]} * 100 \qquad 6-3$$

TEST RESULTS AND DISCUSSION FOR ACCELERATED CORROSION SPECIMENS

7.1 Introduction

The test results presented in this chapter are divided into four groups. The first group uses the current measurements to study the effect of different concrete types and the different steel types on steel passivation and corrosion initiation. The second group uses the pullout test to study the bond strength for different steel-concrete types. The third group shows the effect of corrosion on the mechanical properties of steel including tensile strength and ductility. The fourth group shows the corrosion effect on the physical properties of steel including its mass and rib profile.

7.2 Current Measurement Results

The current readings were taken daily by means of a digital multi-meter. The samples were divided, in the corrosion tank, into 12 groups as shown in Fig. 7.1. Each group acts as one circuit and the current readings were taken for each circuit individually. Table 7.1 shows the division of theses circuits inside the accelerated corrosion tank.

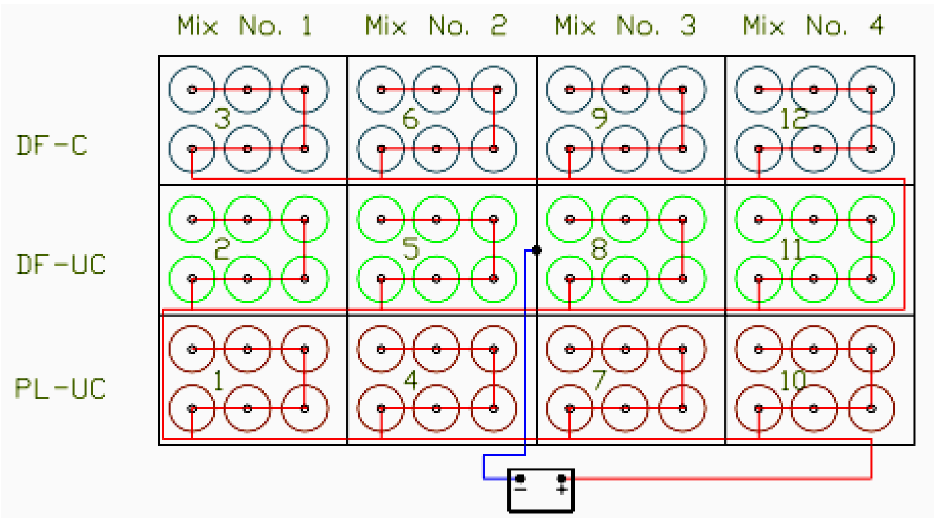

Fig. 7.1: Accelerated corrosion tank circuits division

Table 7.1: Distribution of circuits inside the corrosion tank

Circuit No.	Concrete Type		Steel Type
	Compressive Strength (MPa)	Water/cement	
1	30	0.32	Plain Un coated
2	30	0.32	Deformed Un coated
3	30	0.32	Deformed Coated
4	44	0.52	Plain Un coated
5	44	0.52	Deformed Un coated
6	44	0.52	Deformed Coated
7	44	0.32	Plain Un coated
8	44	0.32	Deformed Un coated
9	44	0.32	Deformed Coated
10	60	0.32	Plain Un coated
11	60	0.32	Deformed Un coated
12	60	0.32	Deformed Coated

7.2.1 Effect of steel types on the current measurements

Figs. 7.2 through 7.5 show the relationship between the current in mA and the immersion time in days for each steel type. As mentioned in previous chapters, the current is an indication of the passivation, depassivation and corrosion initiation on a steel bar surface.

From the curves it is obvious that the current readings decrease in the first stage for all types of bars. This stage resembles the passivation stage, where a passive film is formed on the bar surface protecting it from corrosion. After a while, the current readings start to increase again after depassivation and until reaching severe corrosion stage.

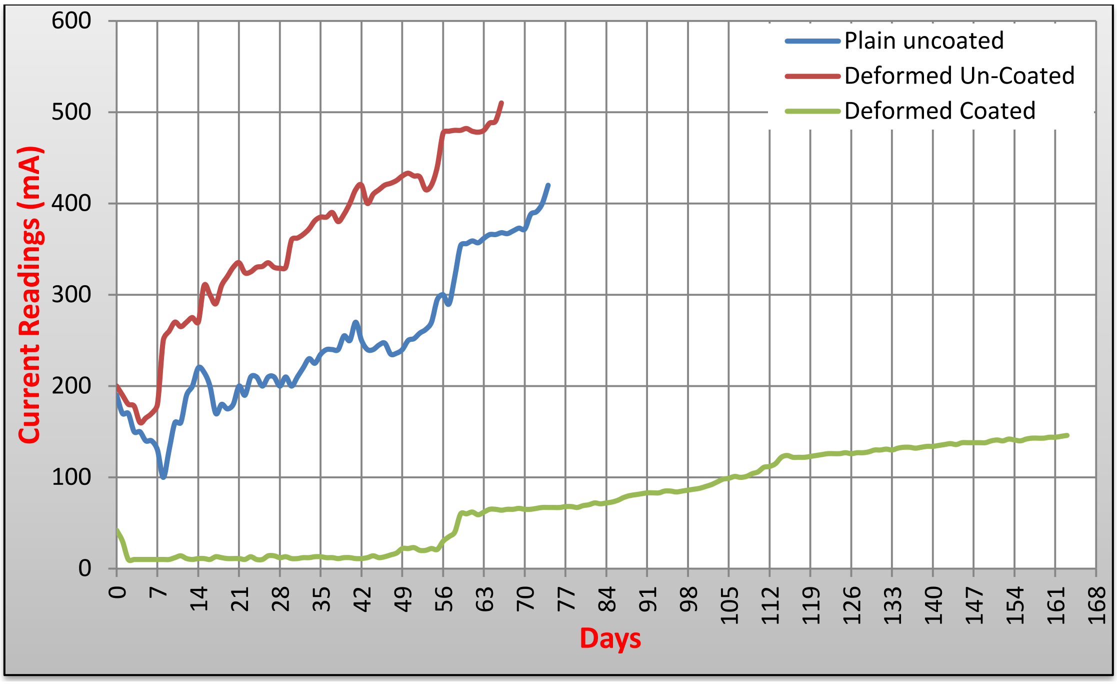

Fig. 7.2: Current readings vs. immersion time for 30 MPa concrete mixes (w/c=0.32) with different types of steel bars

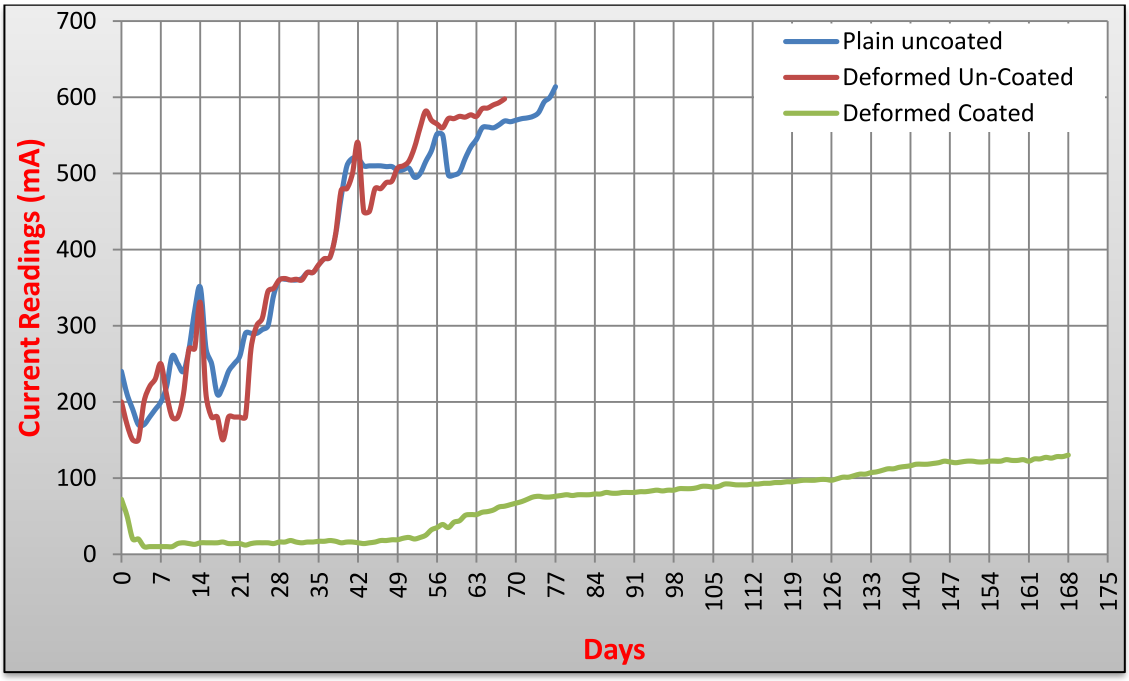

Fig. 7.3: Current readings vs. immersion time for 44 MPa concrete mixes (w/c=0.52) with different types of steel bars

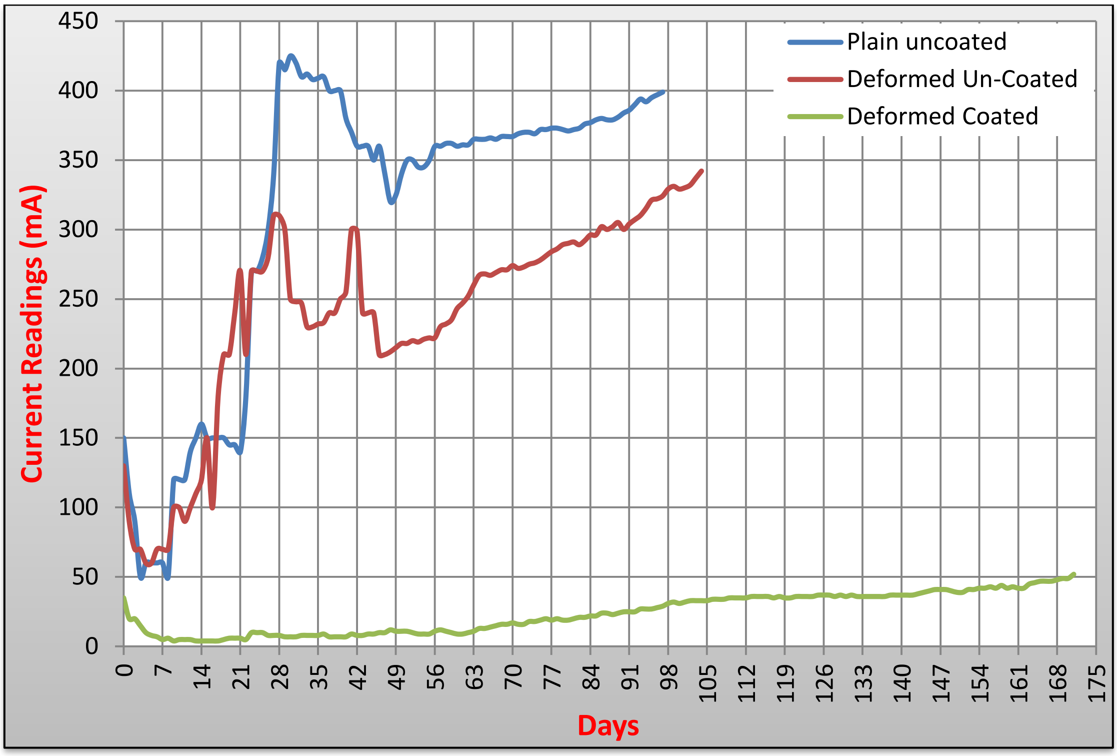

Fig. 7.4: Current readings vs. immersion time for 44 MPa concrete mixes (w/c=0.32) with different types of steel bars

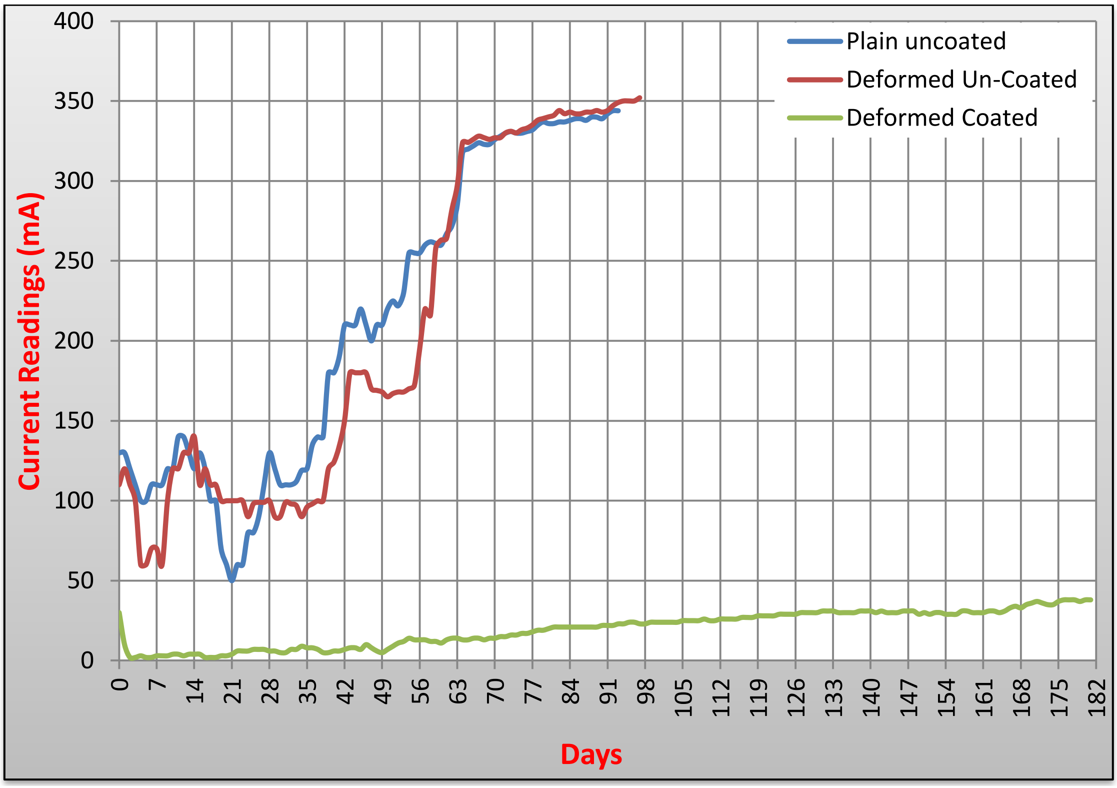

Fig. 7.5: Current readings vs. immersion time for 60 MPa concrete mixes (w/c=0.32) with different types of steel bars

The current passing through the deformed uncoated bars and the plain bars started with a low level at an early age then rapidly increased after a certain time according to the type of the steel and the concrete mix. This rapid increase is due to the cracking of the concrete cover which left the steel without protection and in direct contact with the electrolytic solution. In other words, the rate of corrosion of the steel bars was very slow at first, until depassivation of the steel occurred when corrosion started, and then the rate of corrosion increased significantly.

For epoxy coated steel bars, the current started at a low level and remained the same for a long time and then the current started to increase rapidly, since a sudden cracking was observed across the specimen passing through the embedded end of the bar (Fig. 7.6). This sudden cracking was due to corrosion concentration around the uncoated embedded end of the bar. Hence, the corrosion products accumulated and concentrated in a small area, which exerted tensile stresses inside the concrete.

Fig. 7.6: Cracks passing through the un-coated end of epoxy coated bars

The epoxy-coated bars showed the lowest current readings during the whole period of the immersion time, compared to the un-coated deformed and plain bars for all types of concrete mixes, even after cracking, where the coating acts as a barrier for current flow between the electrolyte and the reinforcing bar. The un-coated deformed and plain steel bars showed similarity in their current readings for each type of concrete, which corresponds to their similarity in reaching pre-cracking, cracking, and severe corrosion stage.

According to what was mentioned before that the current reading increases as the crack width increases, the relationship plotted must be directly proportional. However, some drops had appeared in the plotted curves during the test. This can be attributed to one of these reasons:

1- The concentration of the electrolyte in the accelerated corrosion tank decreased with time as the corrosion reactions continued between the cathode and anode. The current started to return to its normal values as the electrolyte was changed by the end of each weak.

2- The corrosion products formed a layer around the bar which acted as a barrier to the current flow. As the reactions continued, these products propagated away from the bar surface and the current started to increase again.

7.2.2 Effect of concrete types on the current measurements

Figs. 7.7 through 7.9 show the relationship between the current readings in mA and the immersion time in days for different concrete types for each type of steel bars.

As expected, the [44MPa, 0.52 w/c mix] demonstrated the highest current values in the beginning of the test, approximately 240 mA with plain bars, 200 mA with deformed uncoated bars, and 72 mA with the epoxy coated bars, followed by the [30MPa, 0.32 w/c mix], approximately 190 mA with plain bars, 200 mA with deformed uncoated bars, and 34 mA with the epoxy coated bars. The [44MPa, 0.32 w/c mix] demonstrated lower initial current reading, approximately 150 mA with plain bars, 130 mA with deformed uncoated bars, and 35 mA with the epoxy coated bars. The [60MPa, 0.32 w/c mix] showed the lowest initial current reading, approximately 130 mA with plain bars, 110 mA with deformed uncoated bars, and 30 mA with the epoxy coated bars.

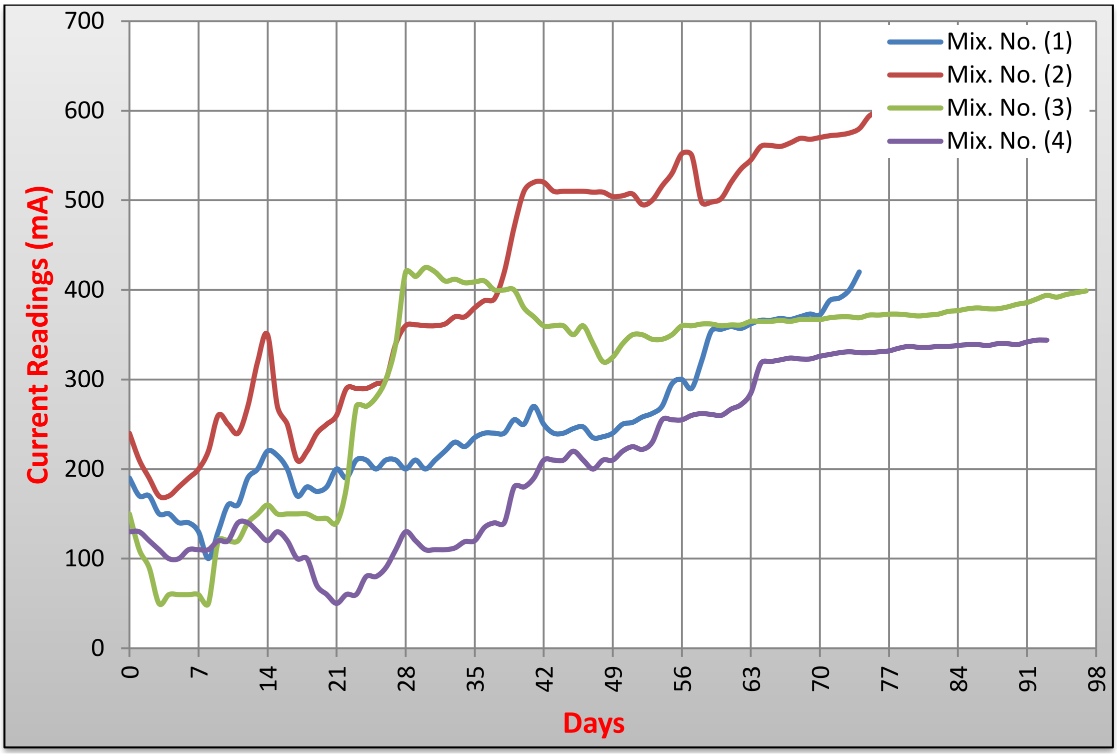

Fig. 7.7: Current readings vs. immersion time for un-coated plain bars with different types of concrete mixes

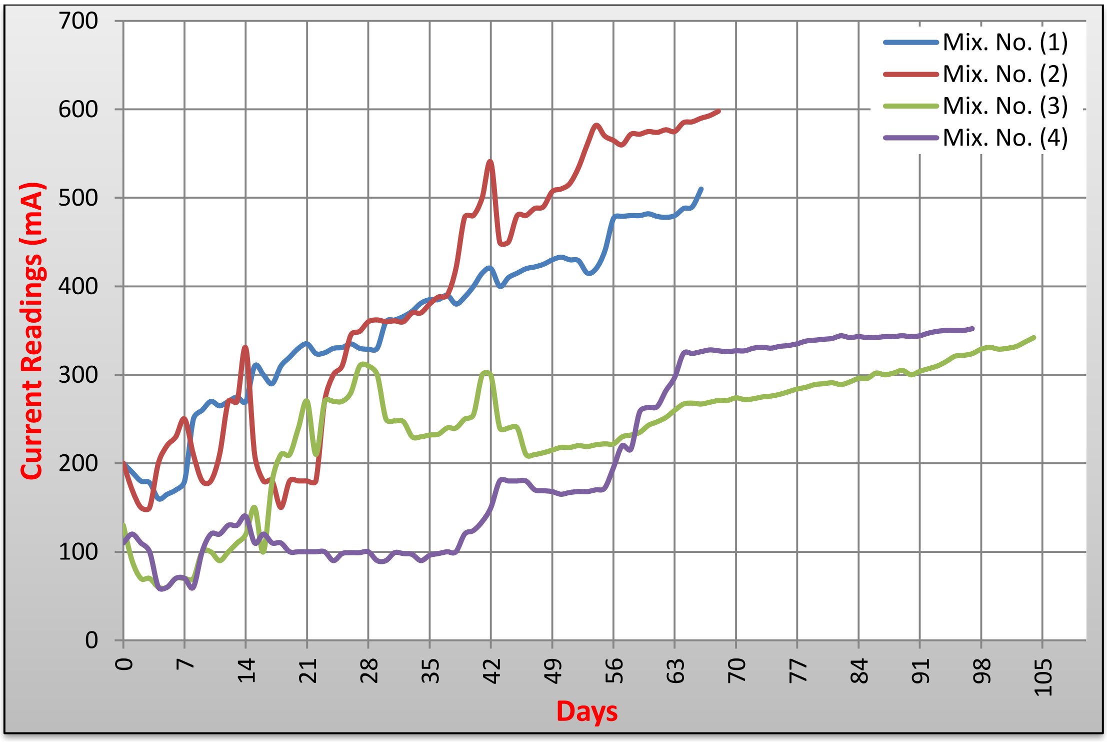

Fig. 7.8: Current readings vs. immersion time for un-coated deformed bars with different types of concrete mixes.

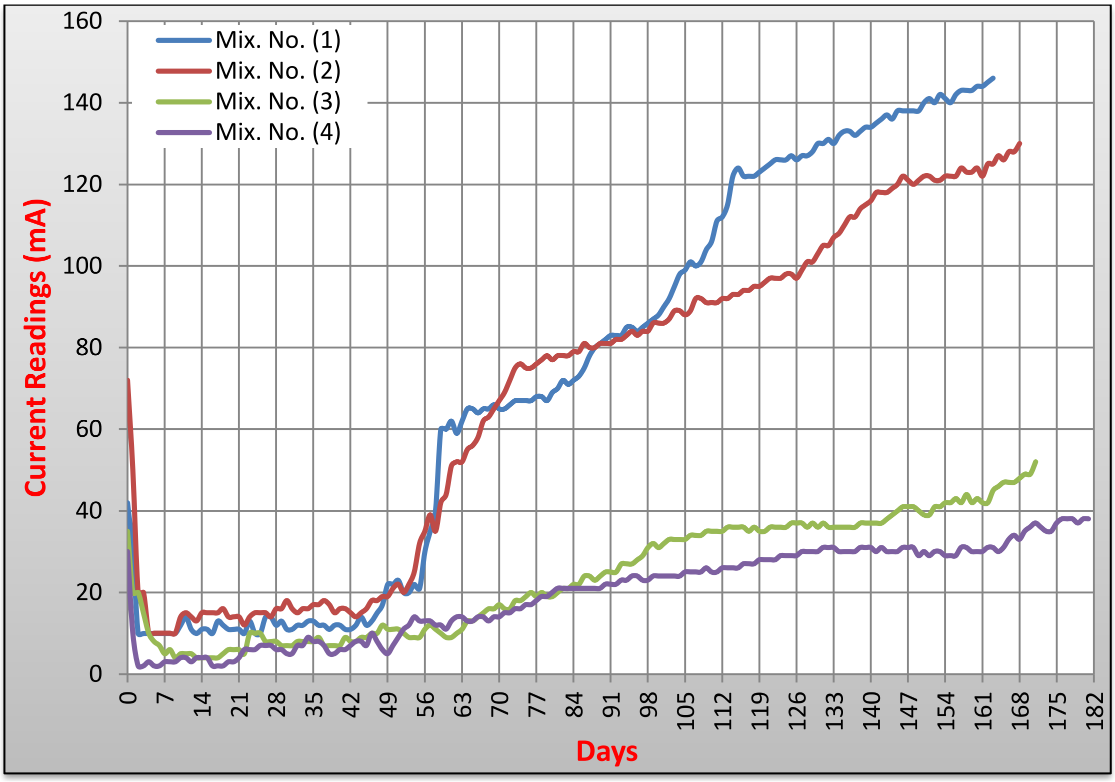

Fig. 7.9: Current readings vs. immersion time for epoxy coated deformed bars with different types of concrete mixes.

The current passing through the concrete specimens depends mainly on the resistivity of the concrete. Higher water/cement ratio results in a higher permeability concrete, since the excess water in the concrete matrix occupies more voids, *Neville, 1981*. On the other hand, the concrete with lower water/cement ratio and using workability admixtures exhibit lower permeability.

As void ratio decreases, permeability decreases and this increases the concrete resistivity. The three concrete types with low water/cement ratio showed differences in their current readings, this is due to the variations in their resistivity. The concrete void ratio is inversely proportional to the concrete cement content; this means that the lowest permeability and highest resistivity concrete specimens are those of the [60MPa, 0.32 w/c] mix.

The maximum current reading corresponding to severe corrosion stages in all steel types was always higher in the [30MPa] and [44MPa, 0.52 w/c] concrete mixes. This can be attributed to the high permeability and low resistivity for these two mixes, where mix No. 2 has the highest water/cement ratio (0.52) and mix No. 1 contains the lowest cement content (350 kg/m^3). The [44MPa, 0.52 w/c] mix showed higher current readings for both un-coated deformed and plain steel bars, however, the [30MPa] was the highest for epoxy coated deformed bars. This can be attributed to the lower strength of mix No. 1 (30MPa) which couldn't withstand the high tensile stresses caused by the corrosion products concentrations at the un-coated end of the epoxy coated bars. However, in case of un-coated plain and deformed bars, the corrosion was mainly uniform that caused uniform stresses along the steel bar.

From the curves it can be observed that the [44MPa, 0.32 w/c] and the [60MPa] mixes showed similarities in their current readings. The [44MPa, 0.32 w/c] mix showed higher current readings for both un-coated plain and epoxy coated deformed bars. The [60MPa] mix was the higher for un-coated deformed bars. This was obvious during the operation of the accelerated corrosion tank, where the 60MPa samples showed sudden cracks for the un-coated deformed bars and the current readings started to increase rapidly (Fig. 7.10). This can be attributed to the larger surface area for the deformed bars compared with plain bars, and also their lower resistivity relative to the epoxy coated deformed bars. This have caused a higher corrosion rate for un-coated deformed bars, and the corrosion products caused high tensile stresses, since this mix contains the lowest void ratio, so sudden cracks have occurred and the bar was in direct contact with the electrolytic solution.

By comparing the current readings for the different strength mixes (1, 3 and 4), and different water/cement ratio mixes (2 and 3), it will be obvious that the effect of increasing the concrete strength is higher in case of un-coated plain and deformed bars, however, the effect of decreasing water/cement ratio will appear higher in the case of epoxy coated bars.

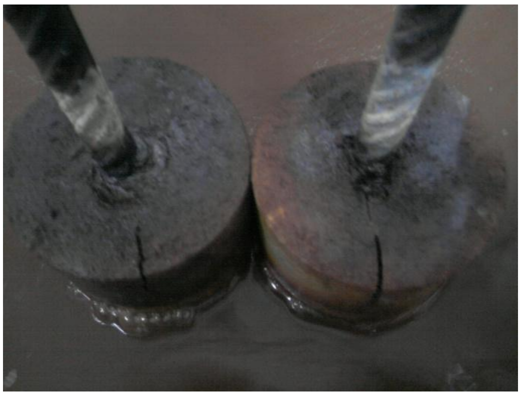

Fig. 7.10: Sudden cracks for mix No. 4 un-coated deformed samples in the accelerated corrosion tank.

7.3 Pullout Test Results

The pull out test was performed using an Instron Universal Testing machine in the AAST materials lab as shown in Fig. 7.11. After establishing the specified level of corrosion, the specimen was removed from the accelerated corrosion tank and the pullout test was performed at a rate of 2.0 mm/min. The bond stress was calculated by dividing the ultimate pullout force over the surface area of the embedded part of the bar.

Fig. 7.11(a): A pull-out specimen loaded in the Universal Testing machine
[AAST materials lab]

Fig. 7.11(b): Two rigid metal plates are used at the interaction between the specimen and the machine head to ensure good stress distribution.

Fig. 7.11(c): The protruding end of the bar is connected to the machine V-jaws.

7.3.1 Zero corrosion stage

Samples were removed from the corrosion tank as soon as they reached the required stage of corrosion. As mentioned before the four stages of corrosion are zero corrosion, pre-cracking, cracking and finally severe corrosion. The bond-slip relationships for the un-corroded bars (zero corrosion level) were evaluated for the different steel and concrete types. The effect of each steel and concrete type on the bond stress is demonstrated in Figs. 7.12 through 7.15.

From the figures, it is observed that plain steel bars have the least bond stress. This can be attributed to the smooth surface that bond by adhesion and low friction component compared to other deformed bars that have a good friction with concrete , in addition to their mechanical interlock between the ribs and the concrete.

Also it is obvious that un-coated deformed bars gives higher bonding values compared to those given by epoxy coated bars, although the two of them have nearly the same rib profile. This can be attributed to the smooth surface of the coated bars due to the presence of epoxy film at the bar concrete interface which decreases the friction of epoxy coated bars.

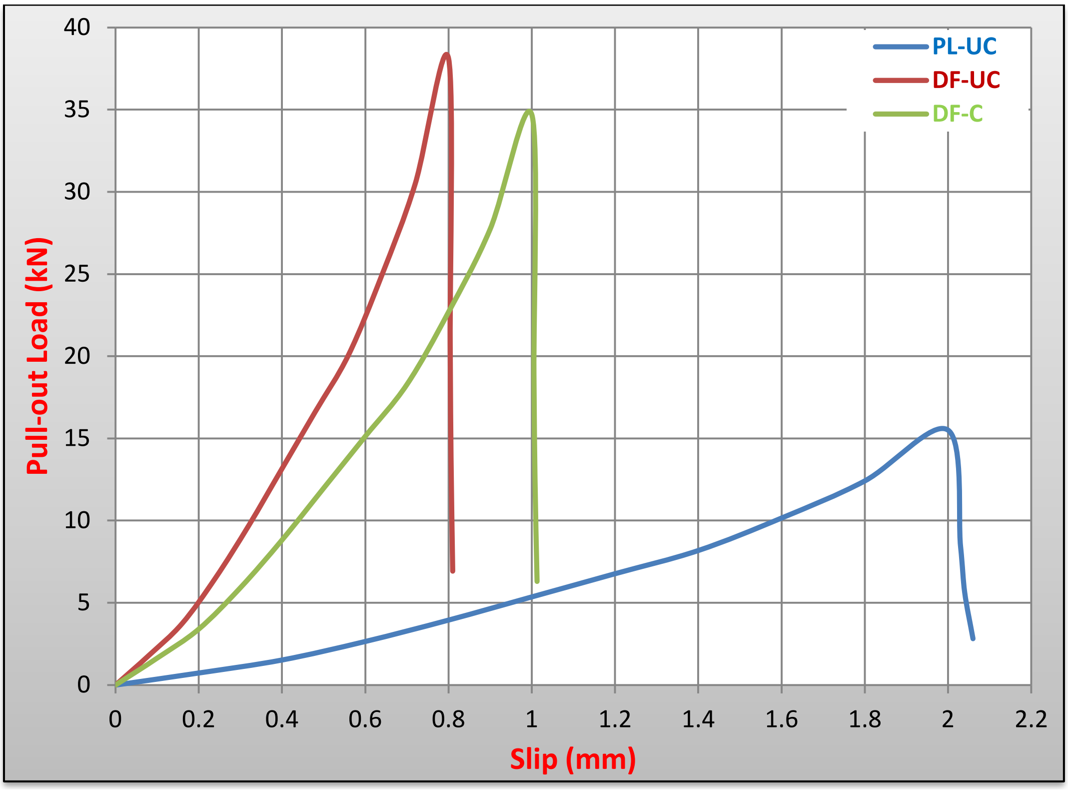

Fig. 7.12: Load-slip relationship for the 30MPa, 0.32 w/c mix with different types of steel bars, *Zero corrosion stage*

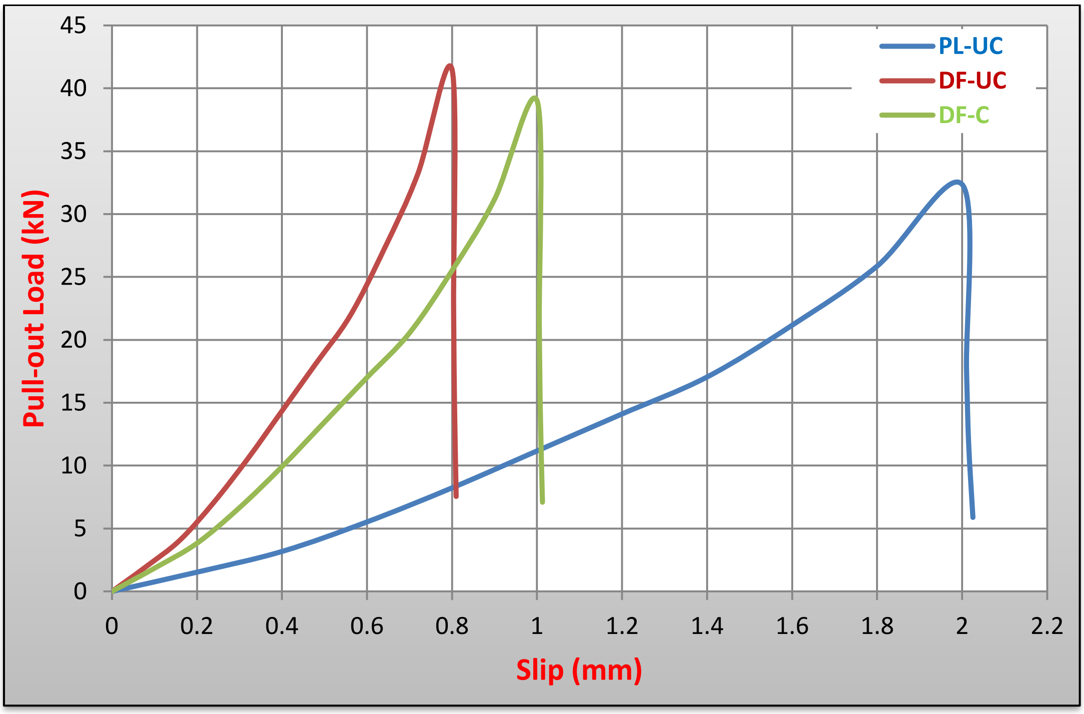

Fig. 7.13: Load-slip relationship for the 44MPa, 0.52 w/c mix with different types of steel bars, *Zero corrosion stage*

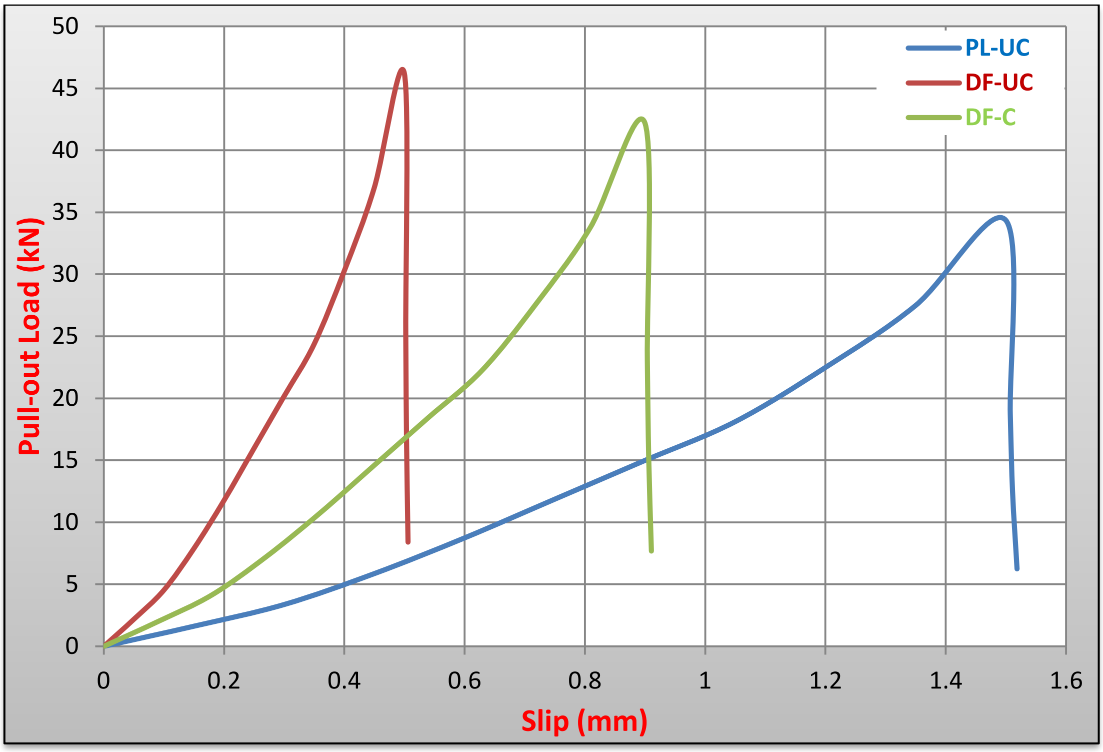

Fig. 7.14: Load-slip relationship for the 44MPa, 0.32 w/c mix with different types of steel bars, *Zero corrosion stage*

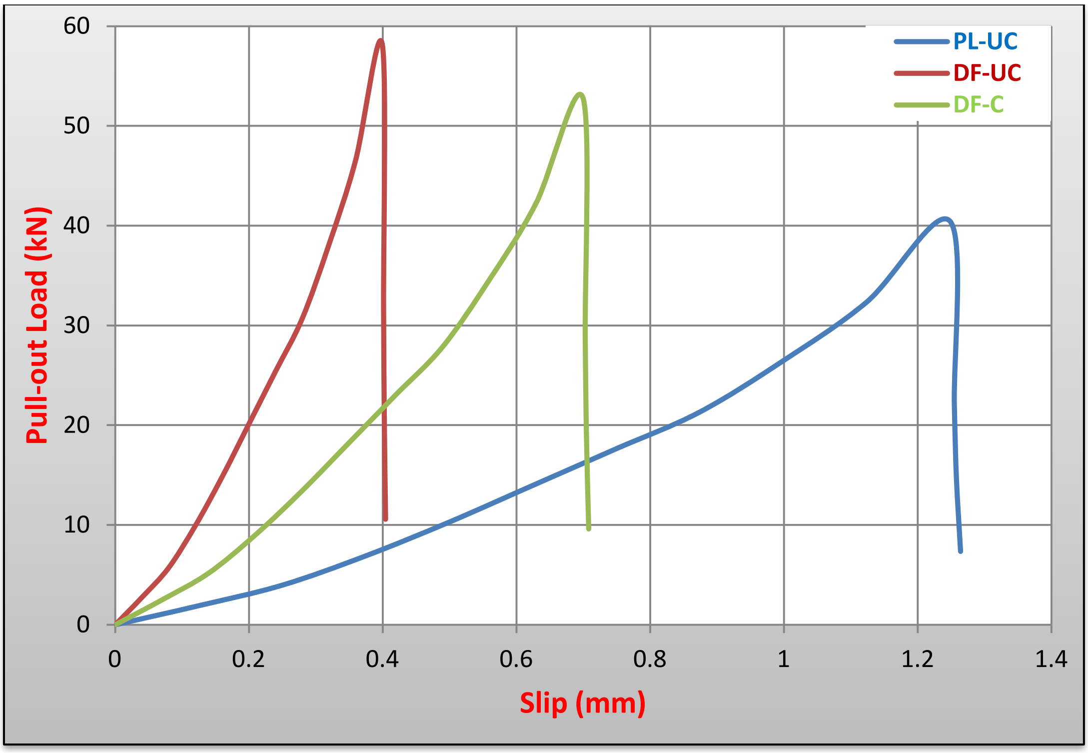

Fig. 7.15: Load-slip relationship for the 60MPa, 0.32 w/c mix with different types of steel bars, *Zero corrosion stage*

The bond stress was calculated by dividing the maximum pull-out force by the embedded surface area of the bar. The values of bond stresses and the shapes of failure are shown in Table 7.2. Four patterns of failure were considered during the pull-out tests: (a) small cracking, (b) longitudinal cracking, (c) splitting, and (d) sudden crushing (Figs. 7.16 through 7.19)

Table 7.2: Bond strength and shape of failure for each type of concrete and steel, *Zero corrosion*

Concrete Type	Steel Type	Zero Corrosion Level	
		Bond Strength (MPa)	**Shape of Failure**
30MPa, w/c=0.32	Plain	2.21	2mm slipping
	Deformed Uncoated	4.85	0.8mm slipping + small cracking
	Deformed Coated	4.66	1.0mm slipping + small cracking
44MPa, w/c=0.32	Plain	4.65	1mm slipping
	Deformed Uncoated	6.13	2mm slipping + crack
	Deformed Coated	5.35	4mm slipping + crack
60MPa, w/c=0.32	Plain	5.36	1.5mm slipping + small cracking
	Deformed Uncoated	7.51	Sudden crushing
	Deformed Coated	6.96	Sudden crushing
44MPa, w/c=0.52	Plain	4.46	2mm slipping
	Deformed Uncoated	5.38	0.8mm slipping + Longitudinal crack and splitting
	Deformed Coated	4.84	1.0mm slipping + small cracking


Fig. 7.16: Small cracking


Fig. 7.17: Longitudinal cracking


Fig. 7.18: Total splitting


Fig. 7.19: Sudden crushing

7.3.2 Pre-cracking, cracking and severe corrosion stages

After operating the accelerated corrosion set-up, the corrosion started to initiate and the corrosion products appeared on the outer surface of the concrete samples. Samples were removed as soon as they reached the required stage of corrosion. Pre-cracking stage was defined as the stage when the corrosion started to initiate, or after the depassivation of the steel bars, and this happened at the time when the current reading started to increase initially (Fig. 7.20). Samples are said to reach the cracking stage when any crack, regardless its width, appeared on the concrete surface; and this stage can be determined by naked eye, or when the current started to increase rapidly (Fig. 7.21). Severe corrosion was defined as the stage when any crack width reached 4 mm (Fig. 7.22).

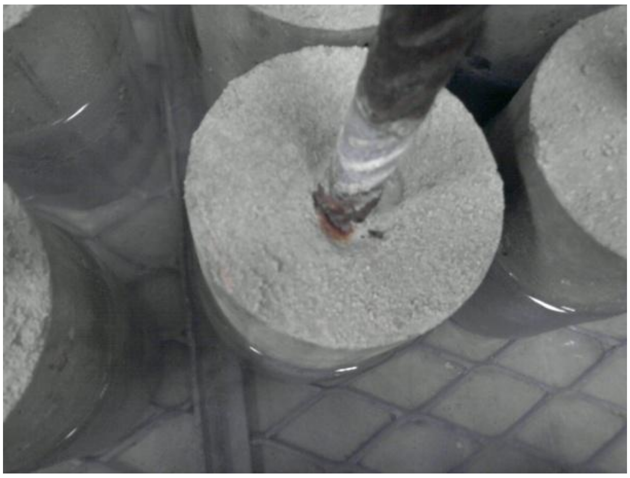

Fig. 7.20: Pre-cracking stage after steel depassivation and the corrosion products started to appear around the bar

Fig. 7.21: Cracking stage: the appearance of the first crack

Fig. 7.22: Severe corrosion stage

Table 7.3 and Figs 7.23 through 7.28 show the timing of corrosion stages for each type of concrete and each type of steel.

Table 7.3: Timing of corrosion stages for each type of concrete and steel bars

Concrete Type	Steel Type	Duration (days)		
		Pre-cracking	Cracking	Severe Corrosion
30MPa, w/c=0.32	Plain	14	37	74
	Deformed Uncoated	7	23	66
	Deformed Coated	------	60	163
44MPa, w/c=0.32	Plain	21	51	97
	Deformed Uncoated	14	52	106
	Deformed Coated	------	109	173
60MPa, w/c=0.32	Plain	39	44	93
	Deformed Uncoated	39	46	97
	Deformed Coated	------	166	------
44MPa, w/c=0.52	Plain	8	35	77
	Deformed Uncoated	4	23	68
	Deformed Coated	------	65	168

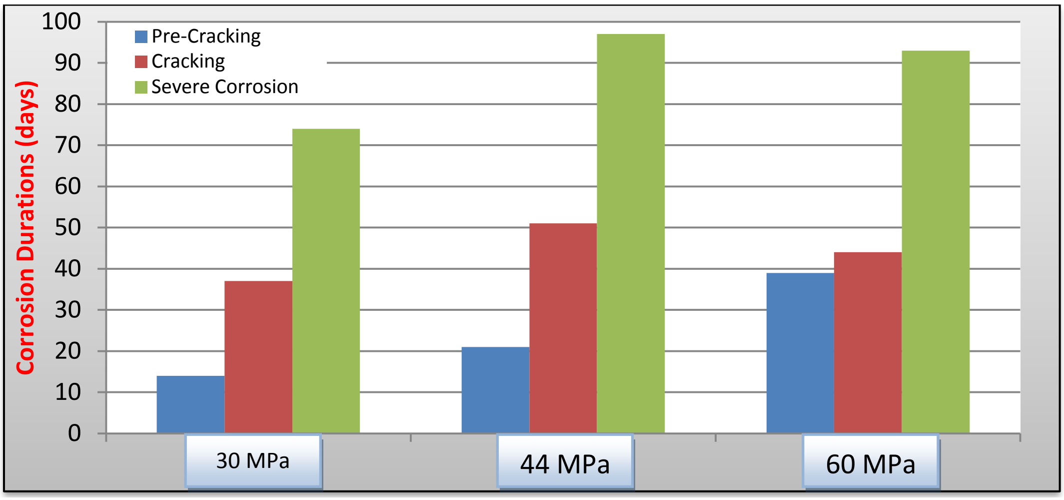

Fig. 7.23: Corrosion durations for un-coated plain bars embedded in different concrete strength mixes with the same water/cement ratio 0.32

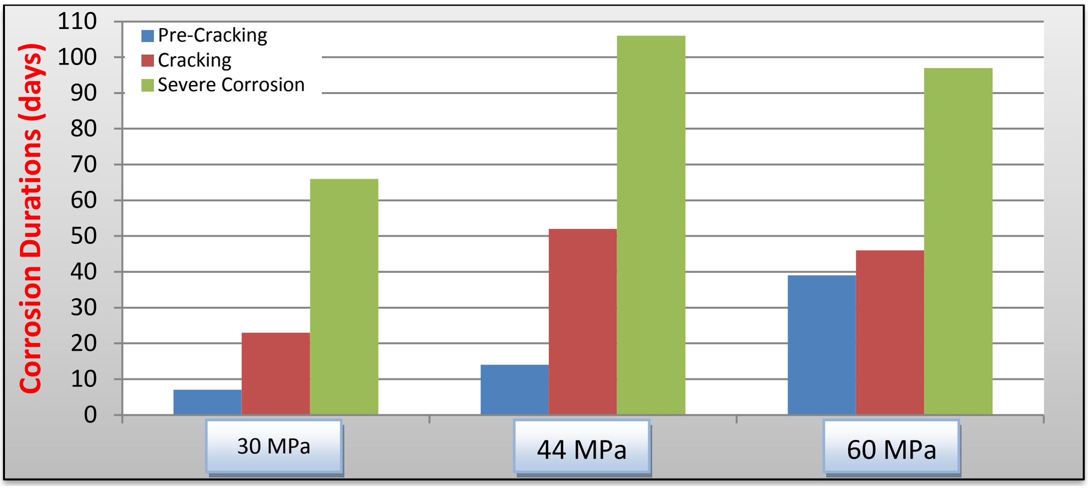

Fig. 7.24: Corrosion durations for un-coated deformed bars embedded in different concrete strength mixes with the same water/cement ratio 0.32

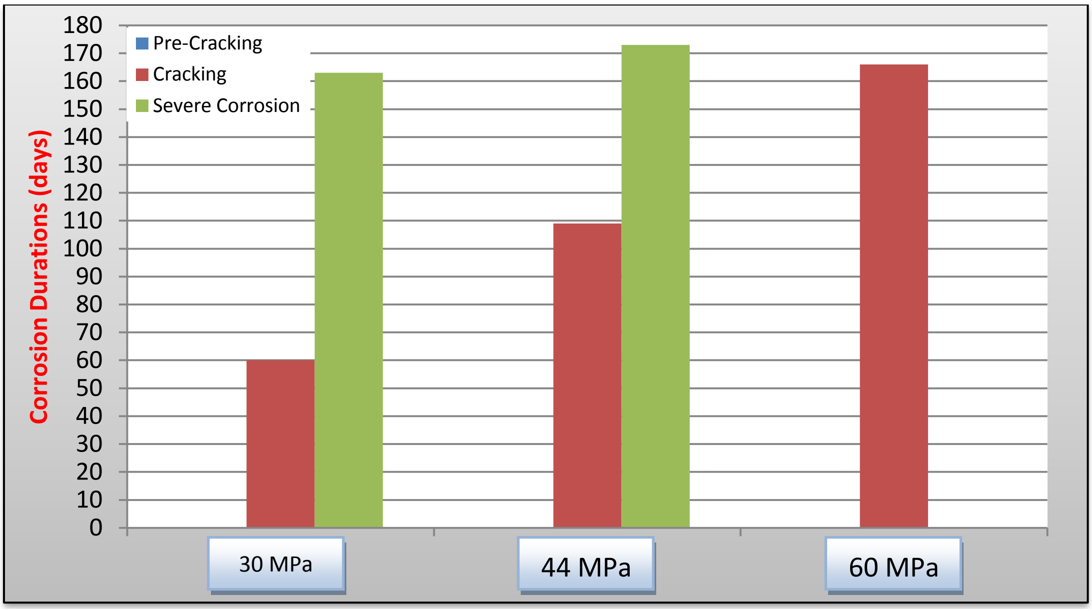

Fig. 7.25: Corrosion durations for epoxy coated deformed bars embedded in different concrete strength mixes with the same water/cement ratio 0.32

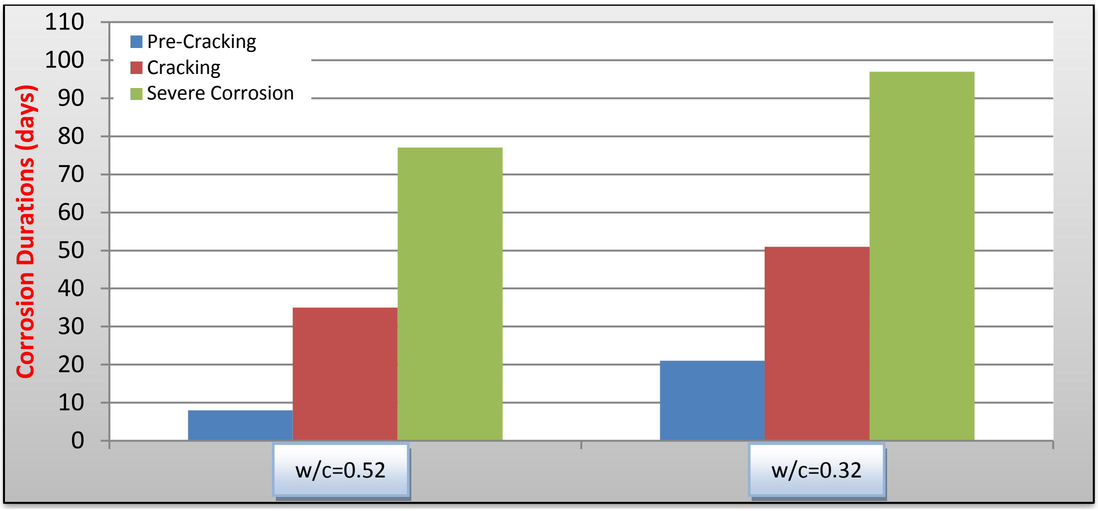

Fig. 7.26: Corrosion durations for un-coated plain bars embedded in different water/cement ratios concrete mixes with the same strength (44MPa)

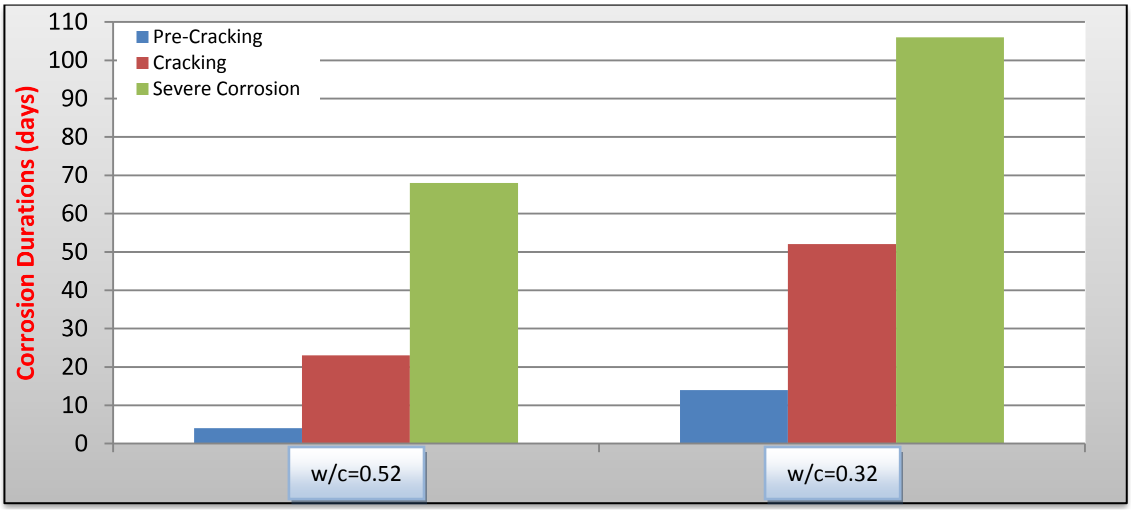

Fig. 7.27: Corrosion durations for un-coated deformed bars embedded in different water/cement ratios concrete mixes with the same strength (44MPa)

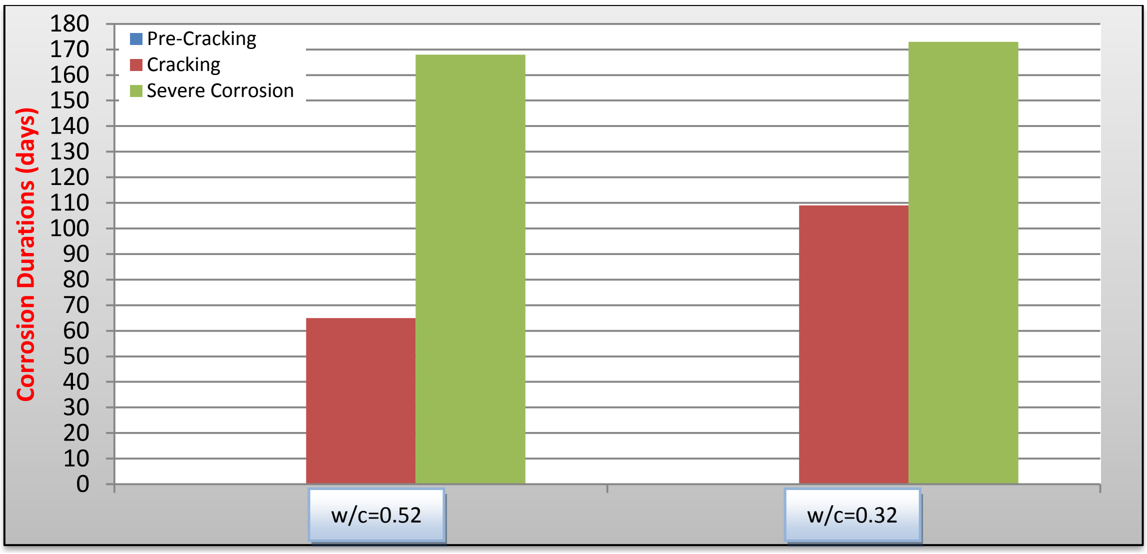

Fig. 7.28: Corrosion durations for epoxy coated deformed bars embedded in different water/cement ratios concrete mixes with the same strength (44MPa)

From the previous table, it is observed that the pre-cracking stage wasn't determined for epoxy coated bars for all types of concrete. The current readings were low for long time until cracks happened suddenly. Also the severe corrosion stage wasn't reached for epoxy coated bars for the [60MPa] concrete mix until the end of the experimental program (approximately 8 months subjected to accelerated corrosion).

Figs. 7.29 through 7.40 show the bond-slip relationships for each type of concrete and steel bars at pre-cracking and cracking stages.

30MPa, w/c=0.32:

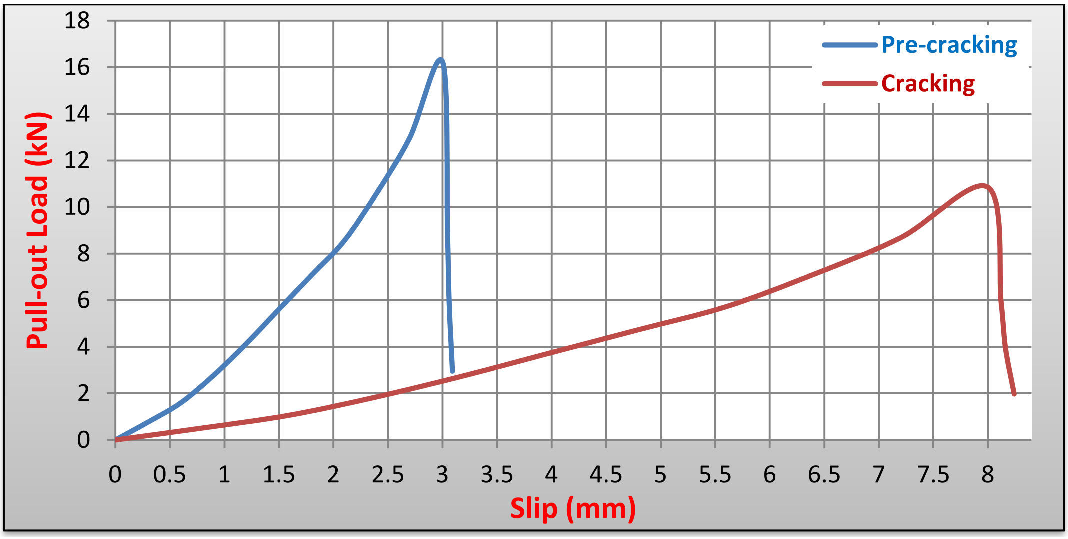

Fig. 7.29: Bond-slip relationship for Mix No. (1) Un-coated plain bars

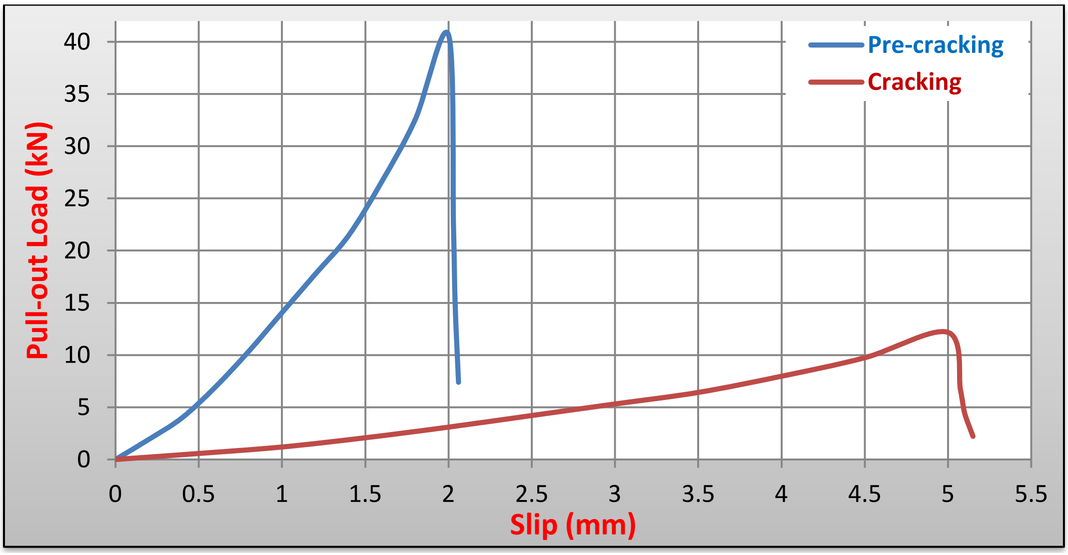

Fig. 7.30: Bond-slip relationship for Mix No. (1) Un-coated deformed bars

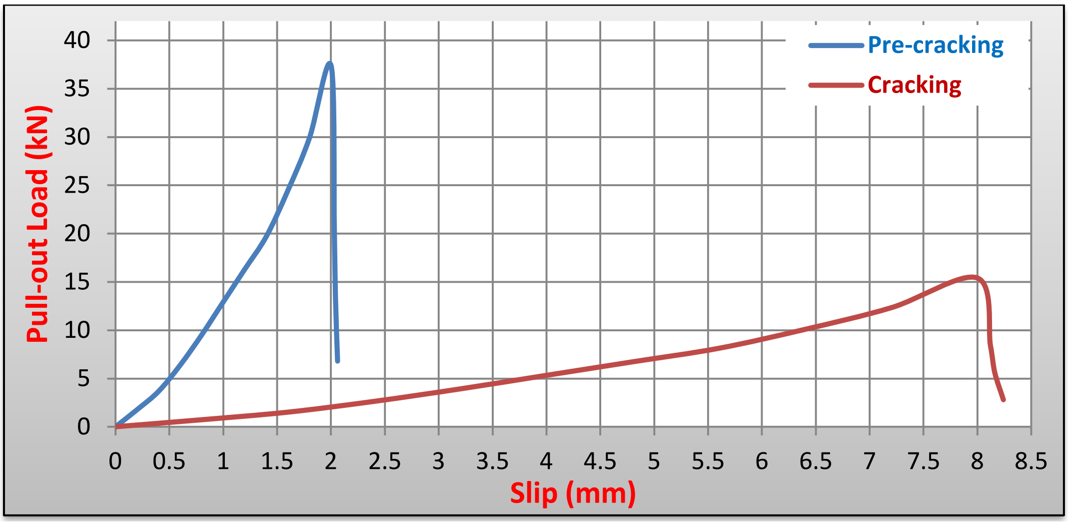

Fig. 7.31: Bond-slip relationship for Mix No. (1) Epoxy coated deformed bars

44MPa, w/c=0.52:

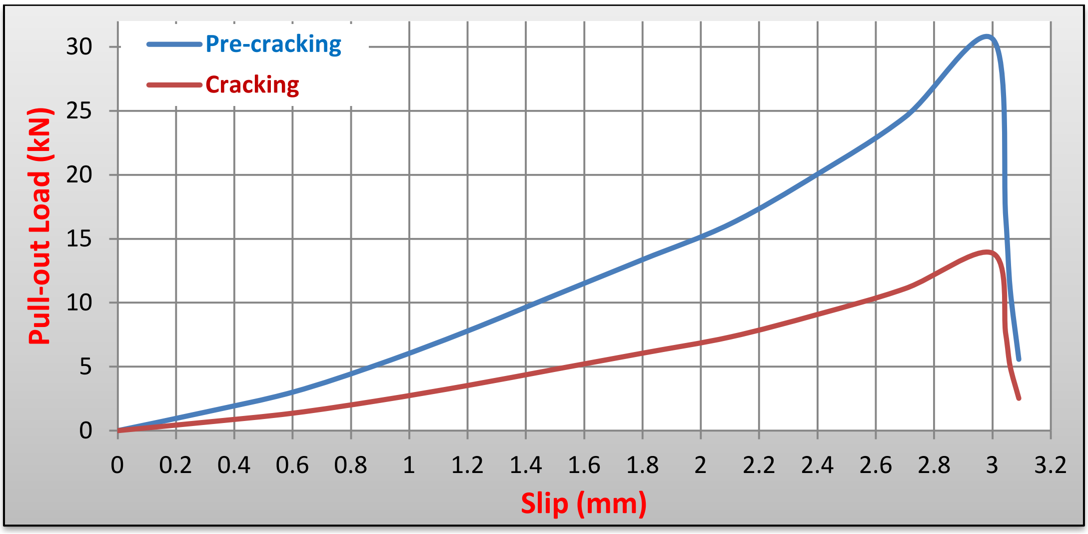

Fig. 7.32: Bond-slip relationship for Mix No. (2) Un-coated plain bars

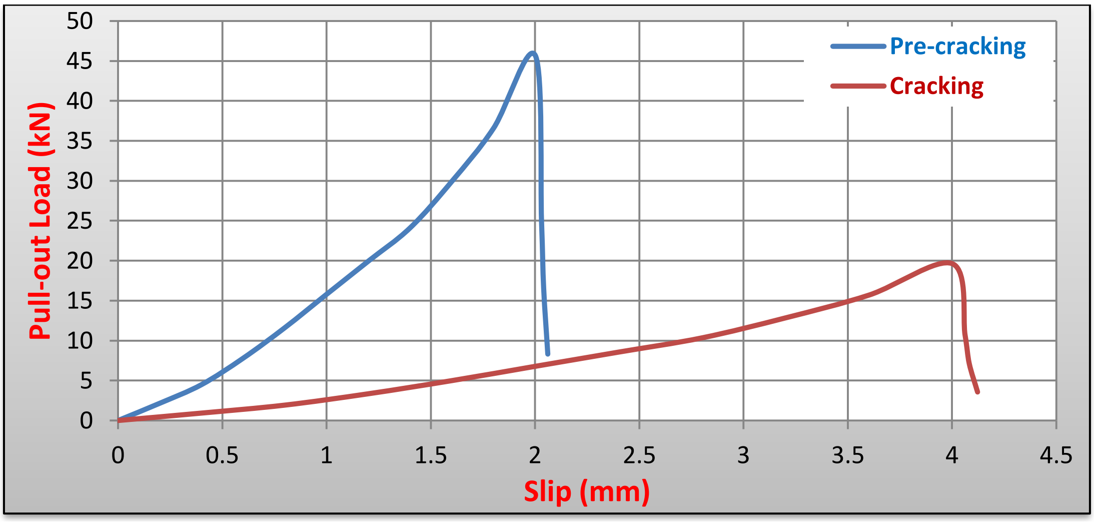

Fig. 7.33: Bond-slip relationship for Mix No. (2) Un-coated deformed bars

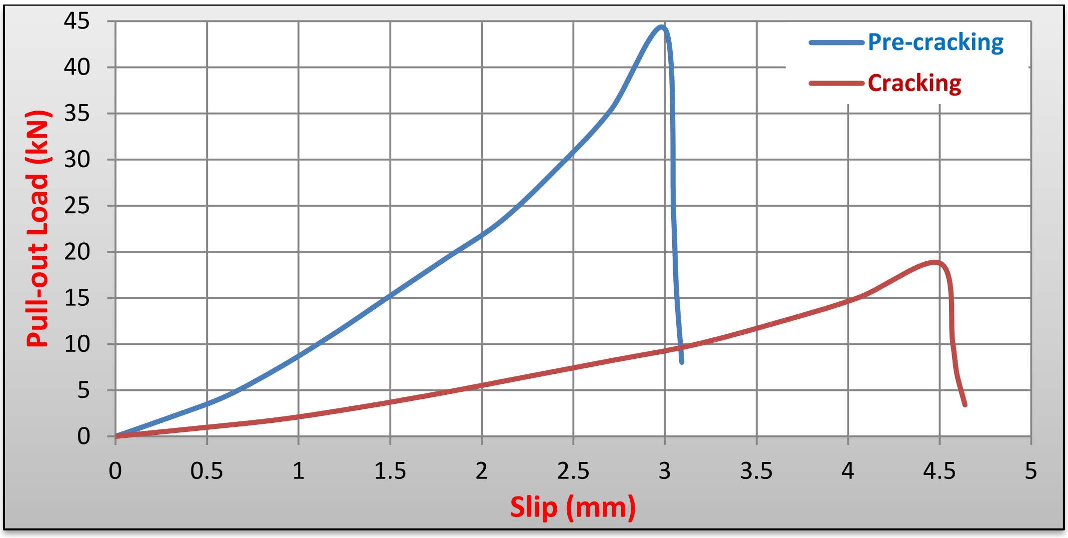

Fig. 7.34: Bond-slip relationship for Mix No. (2) Epoxy coated deformed bars

44MPa, w/c=0.32:

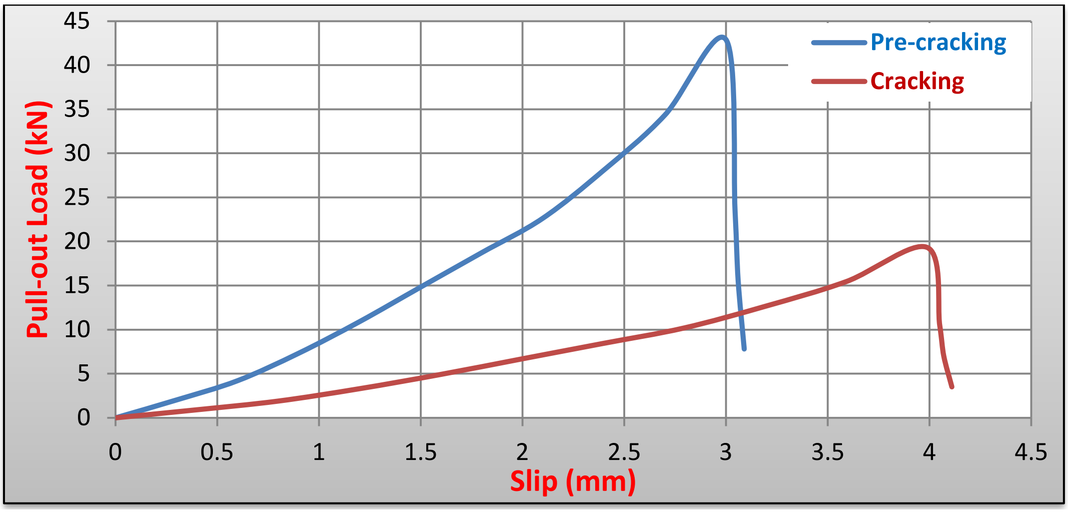

Fig. 7.35: Bond-slip relationship for Mix No. (3) Un-coated plain bars

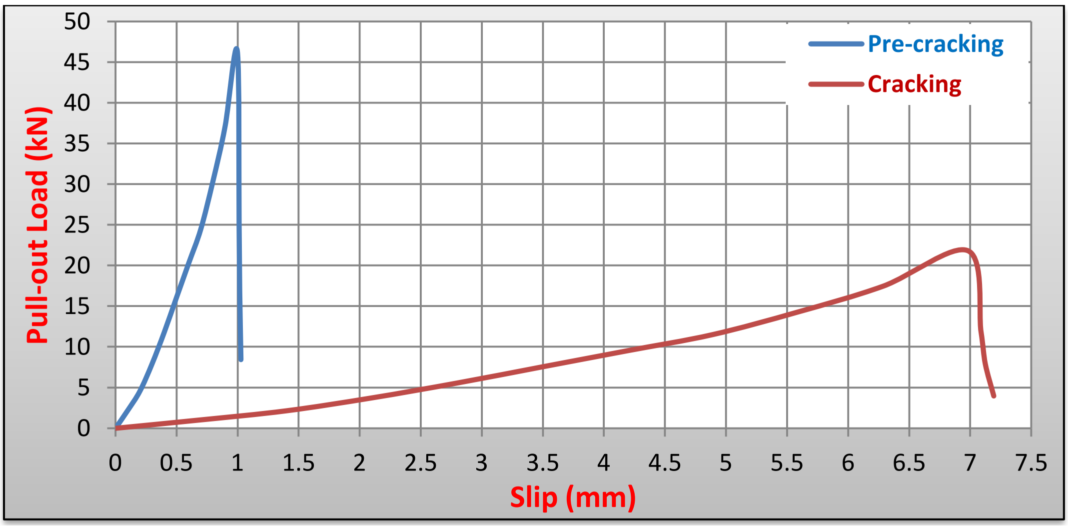

Fig. 7.36: Bond-slip relationship for Mix No. (3) Un-coated deformed bars

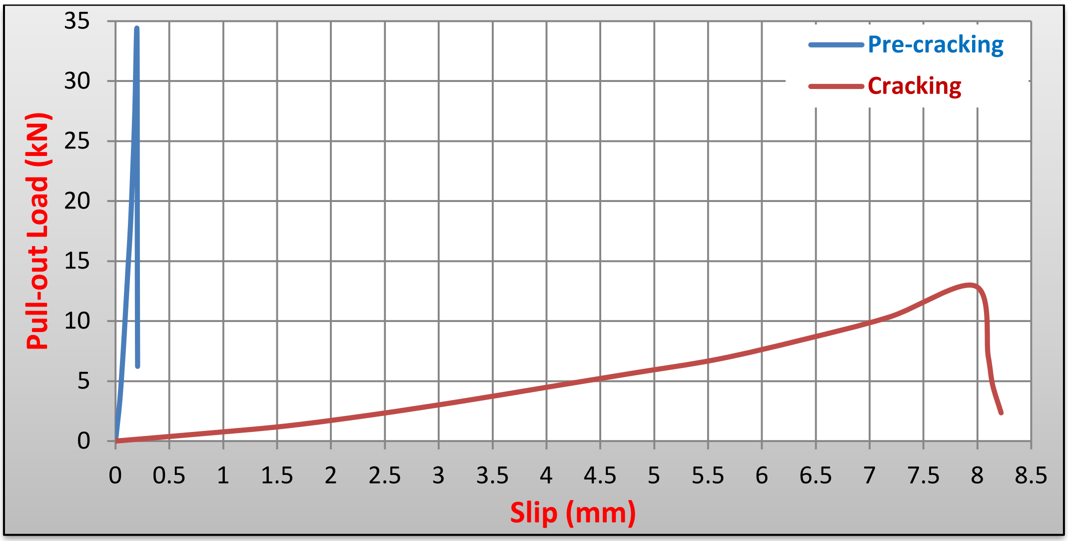

Fig. 7.37: Bond-slip relationship for Mix No. (3) Epoxy coated deformed bars

60MPa, w/c=0.32:

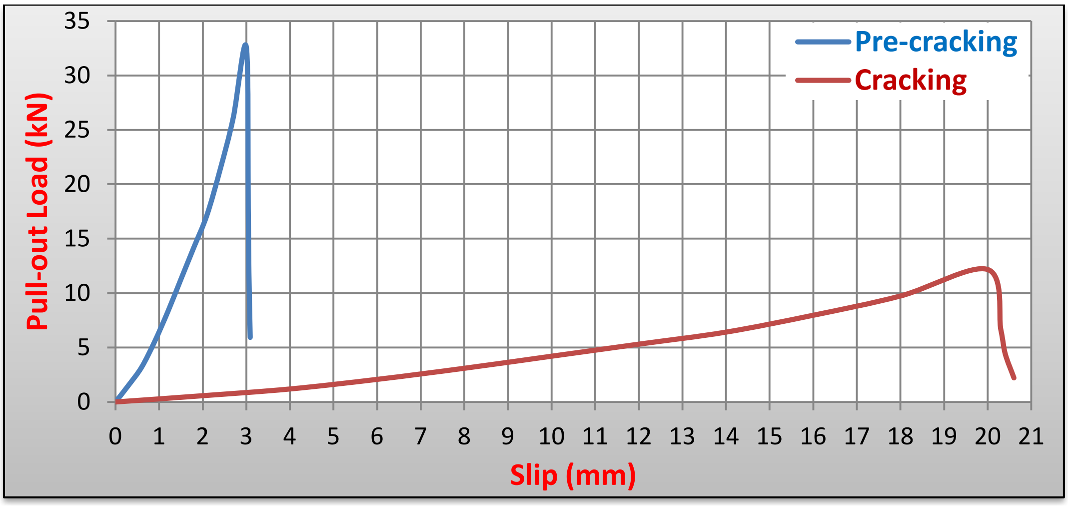

Fig. 7.38: Bond-slip relationship for Mix No. (4) Un-coated plain bars

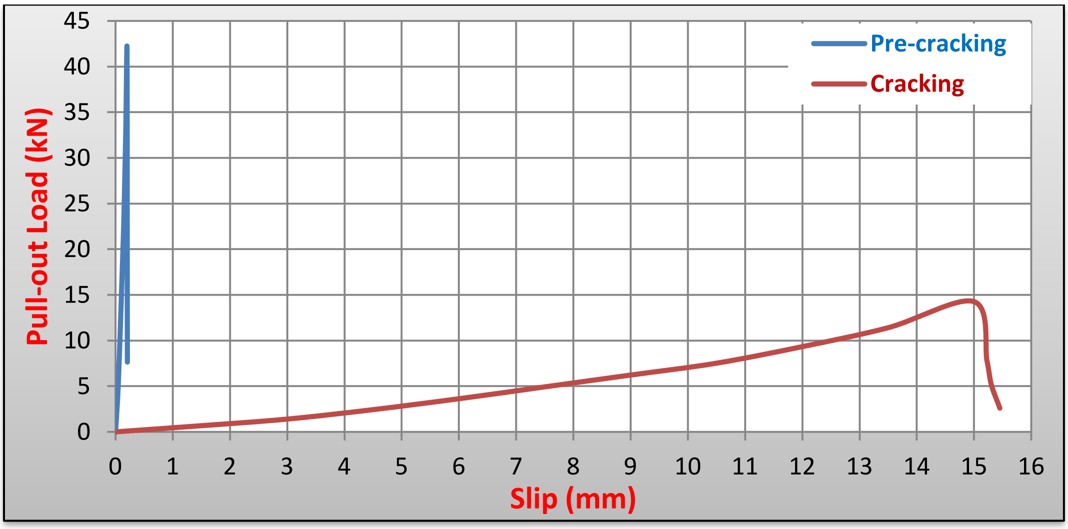

Fig. 7.39: Bond-slip relationship for Mix No. (4) Un-coated deformed bars

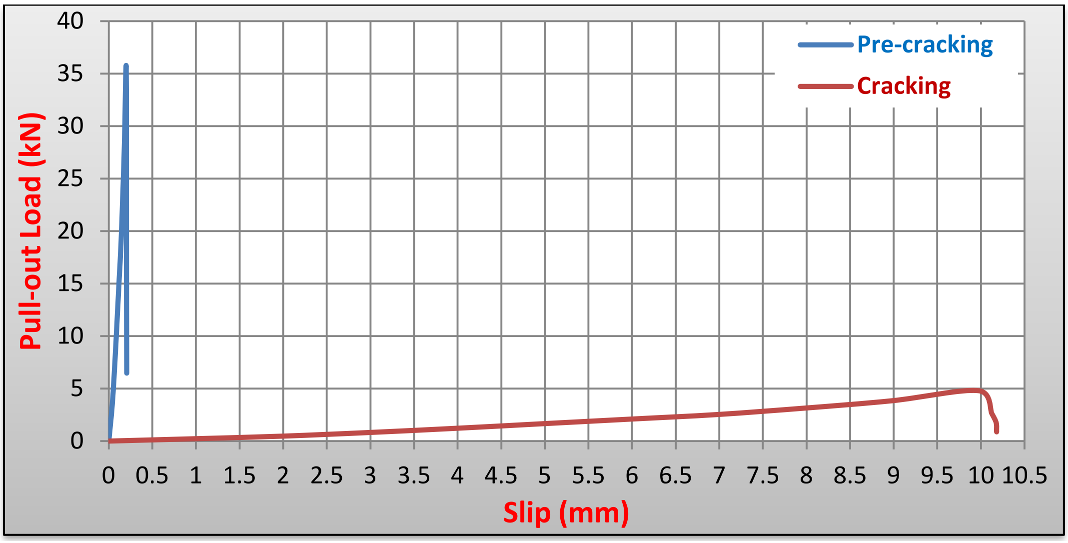

Fig. 7.40: Bond-slip relationship for Mix No. (4) Epoxy coated deformed bars

When studying corrosion effect on bond between concrete and steel bars, it is better to plot the relationships between pull-out load and slipping, than using the bond stress. The bond stress is the pull-out load divided by the area resisting the slipping. It is difficult to exactly determine this area at further degrees of corrosion. Even if the bond stress is calculated from the modified area, corroded area, an error will occur because there is no complete bonding between the bar and the surrounding concrete.

There are no results for severe corrosion stages for all concrete and steel types. All samples undergo total slipping at very low loading values when the crack width reached 4.0 mm or higher. However, the [60MPa] mix was the most durable one when reinforced with epoxy coated steel bars.

From the curves, it can be observed that the drop in bonding force between pre-cracking and cracking stages is higher in concrete mixes [44MPa, 0.32 w/c] and [60MPa]. This can be attributed to the sudden and wide cracks that formed on the surface of high strength concrete compared to the micro cracks for mixes [30 MPa] and [44MPa, 0.52 w/c]. These wide cracks decrease the friction and mechanical interlock at the concrete-rebar interface. Table 7.4 shows the bond strength for each type of concrete and steel at several degrees of corrosion; calculated using the initial area of the steel bars, and Table 7.5 shows the bond strength as a percentage of zero corrosion values at different degrees of corrosion.

Table 7.4: Bond strength at several degrees of corrosion

Concrete Type	Steel Type	Bond strength (MPa)	
		Pre-cracking	Cracking
30MPa, w/c=0.32	Plain	2.18	1.45
	Deformed Uncoated	5.31	1.55
	Deformed Coated	4.76	1.99
44MPa, w/c=0.52	Plain	4.3	1.95
	Deformed Uncoated	5.95	2.56
	Deformed Coated	5.77	2.42
44MPa, w/c=0.32	Plain	5.78	2.55
	Deformed Uncoated	6.02	2.91
	Deformed Coated	4.48	1.74
60MPa, w/c=0.32	Plain	4.37	1.61
	Deformed Uncoated	5.5	1.55
	Deformed Coated	4.63	0.64

Table 7.5: Bond strength as a percentage of zero corrosion values for different degrees of corrosion

Concrete Type	Steel Type	Bond strength as a percentage of zero corrosion bond strength (%)		
		Pre-cracking	Cracking	Severe Corrosion
30MPa, w/c=0.32	Plain	98.64	65.61	0
	Deformed Uncoated	109.5	31.96	0
	Deformed Coated	102.15	42.7	0
44MPa, w/c=0.52	Plain	96.37	43.72	0
	Deformed Uncoated	110.59	47.58	0
	Deformed Coated	119.21	50	0
44MPa, w/c=0.32	Plain	124.3	54.84	0
	Deformed Uncoated	98.21	47.47	0
	Deformed Coated	83.74	32.5	0
60MPa, w/c=0.32	Plain	81.53	30.04	0
	Deformed Uncoated	73.24	20.64	0
	Deformed Coated	66.52	9.2	0

From the results it can be concluded that higher strength concrete can withstand corrosion attacks for longer durations, but at cracking it will show faster deterioration than lower strength concrete.

7.4 Effect of Corrosion on Concrete Reinforcement Mechanical Properties

Figs. 7.41 to 7.47 show the different degrees of corrosion of steel bars after removing the bars from the concrete cylinders. Nearly 70% of all samples were attacked uniformly by corrosion. However, for epoxy coated samples, the corrosion attack was concentrated at the end of the bar, un-coated end, or at another part where holidays occurred.

Fig. 7.41: Un-coated bars, pre-cracking stage

Fig. 7.42: Uniformly corroded sample, plain bars, cracking stage

Fig. 7.43: Uniformly corroded sample, un-coated bars, cracking stage

Fig. 7.44: Concentrated corrosion, epoxy coated bars, cracking stage

Fig. 7.45: Un-coated bars, severe corrosion stage

Fig. 7.46: Un-coated plain bars, severe corrosion stage

Fig. 7.47: Total corrosion at bar end, epoxy coated bars, severe corrosion stage

The corroded bars were removed from the samples after performing the pull-out tests and then were tested in a tensile test to study the effect of corrosion on the tensile strength and steel ductility. The stress strain curves were plotted for each concrete and steel type at different corrosion degrees (Figs. 7.48 to 7.59).

The tensile stress was calculated by dividing the tensile load applied by the Universal testing machine by an average area for each bar (average between the area of the corroded embedded part and the un corroded area of the protruding part) and the strain was calculated by dividing the extension values taken from the machine LVDT by the bar initial length.

30MPa, w/c=0.32:

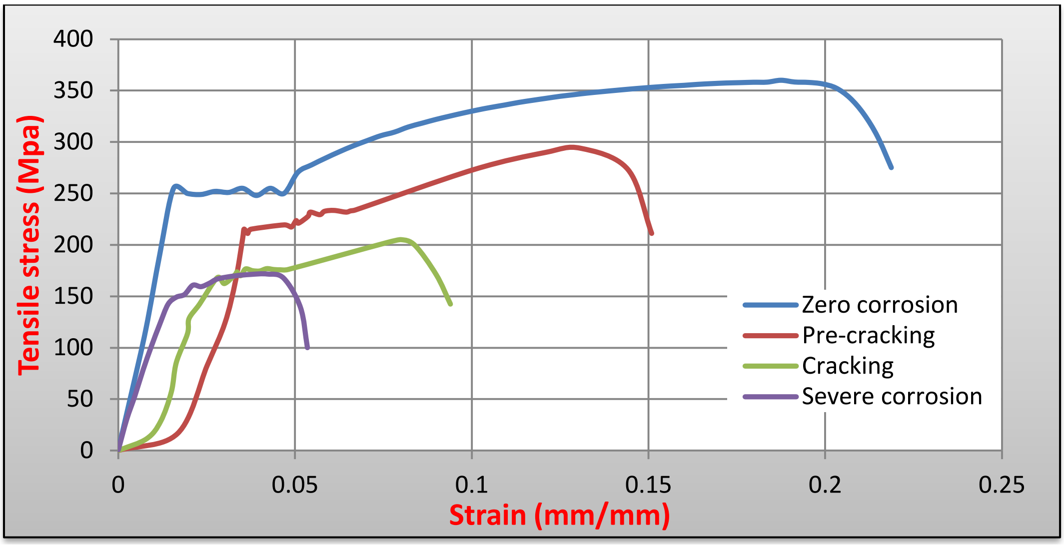

Fig. 7.48: Stress-strain curve for plain bars at each degree of corrosion, Mix No. (1)

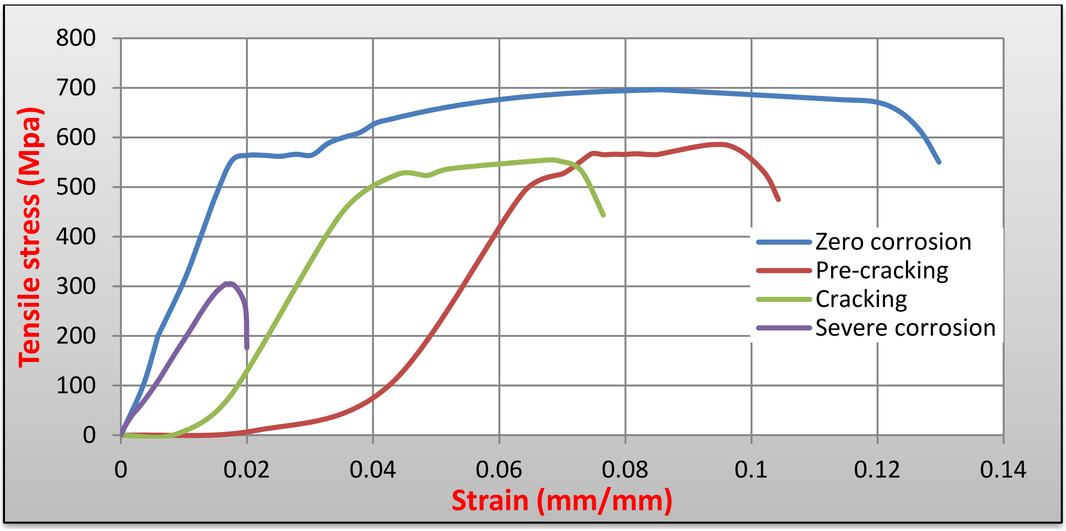

Fig. 7.49: Stress-strain curve for un-coated deformed bars at each degree of corrosion, Mix No. (1)

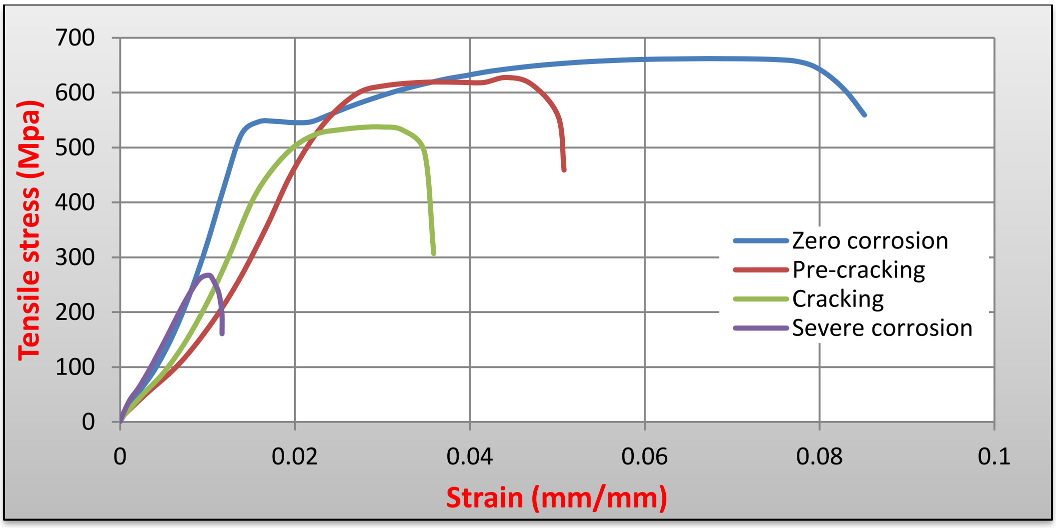

Fig. 7.50: Stress-strain curve for epoxy coated deformed bars at each degree of corrosion, Mix No. (1)

44MPa, w/c=0.52:

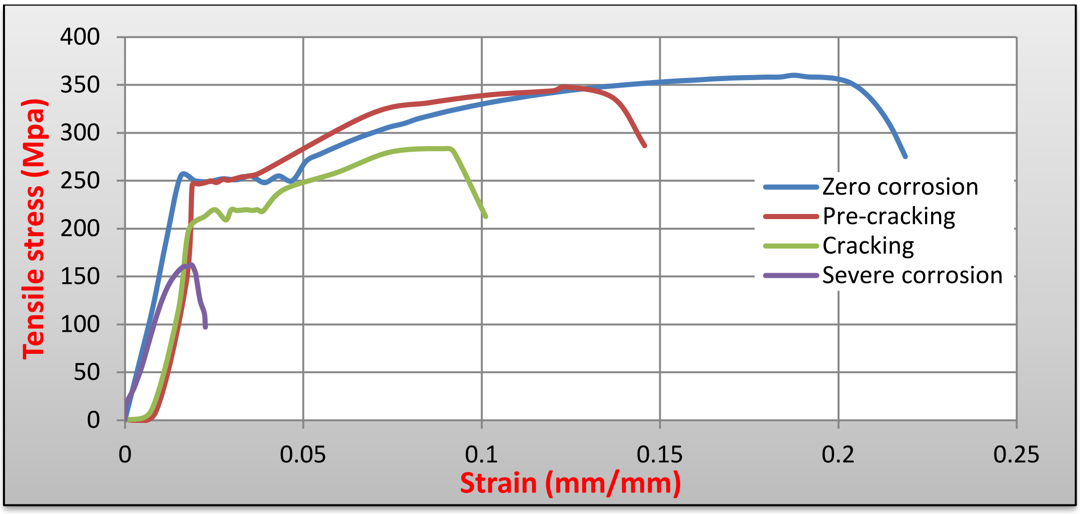

Fig. 7.51: Stress-strain curve for plain bars at each degree of corrosion, Mix No. (2)

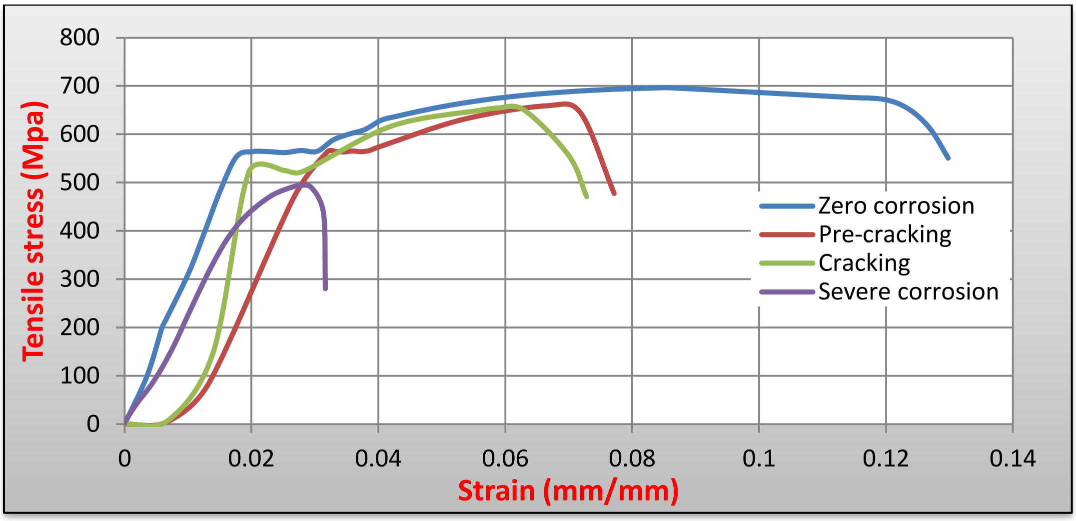

Fig. 7.52: Stress-strain curve for un-coated deformed bars at each degree of corrosion, Mix No. (2)

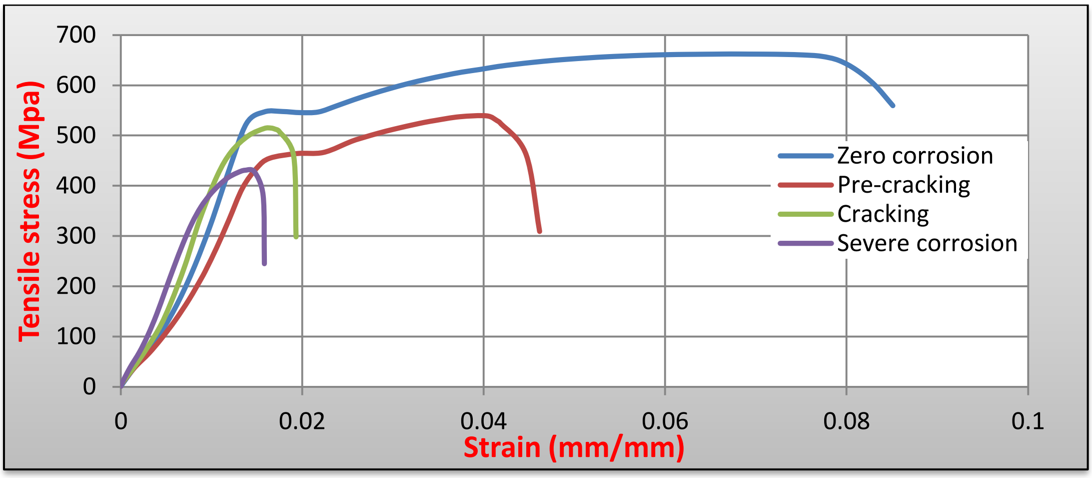

Fig. 7.53: Stress-strain curve for epoxy coated deformed bars at each degree of corrosion, Mix No. (2)

44MPa, w/c=0.32:

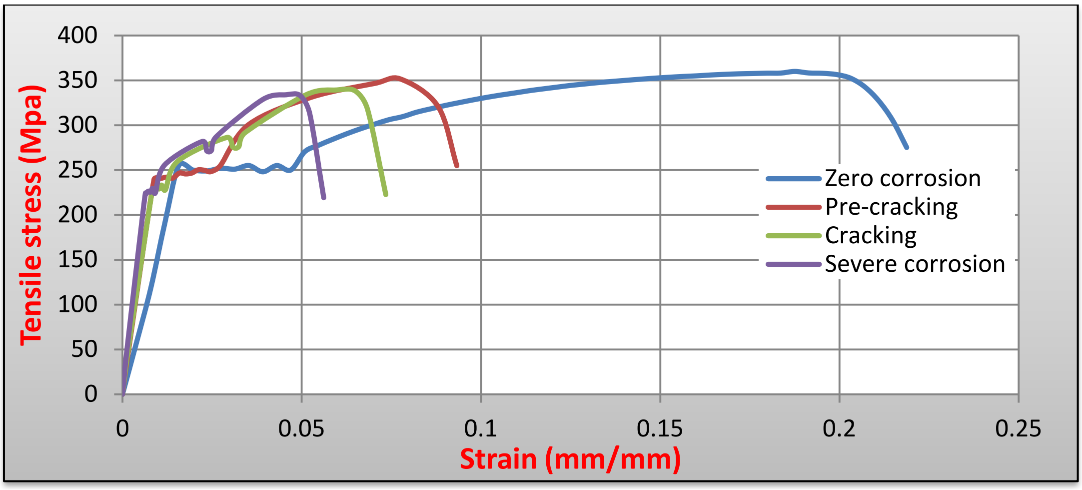

Fig. 7.54: Stress-strain curve for plain bars at each degree of corrosion, Mix No. (3)

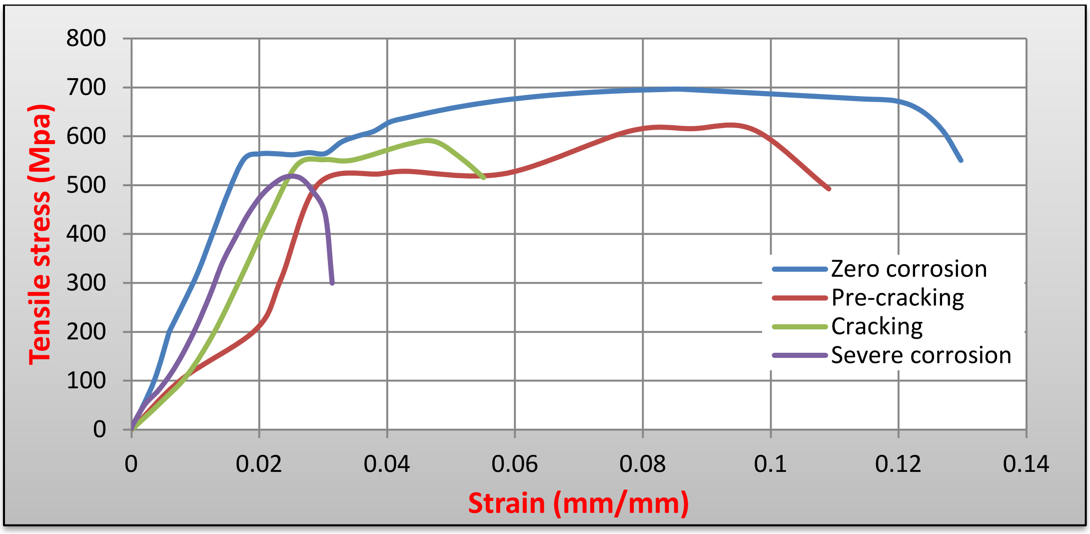

Fig. 7.55: Stress-strain curve for un-coated deformed bars at each degree of corrosion, Mix No. (3)

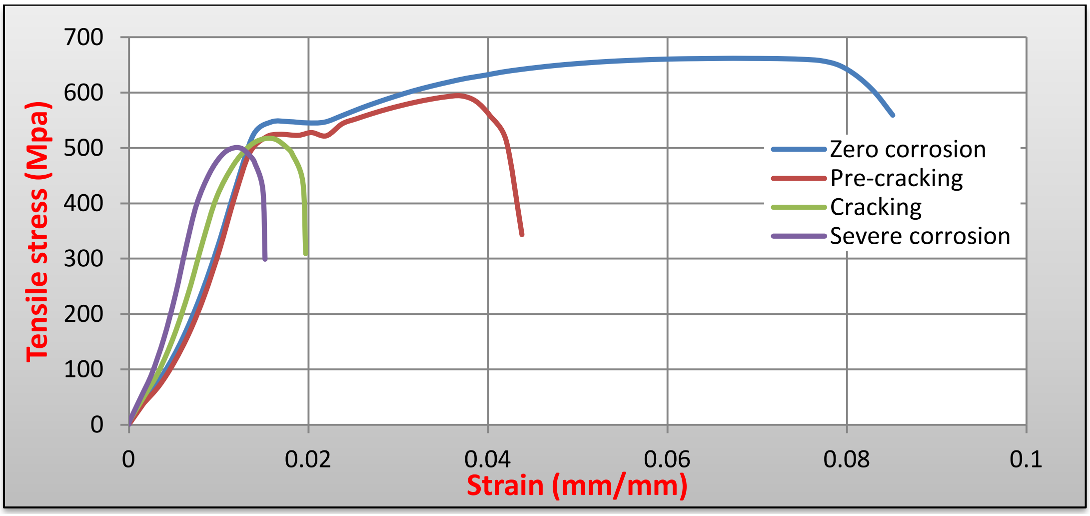

Fig. 7.56: Stress-strain curve for epoxy coated deformed bars at each degree of corrosion, Mix No. (3)

60MPa, w/c=0.32:

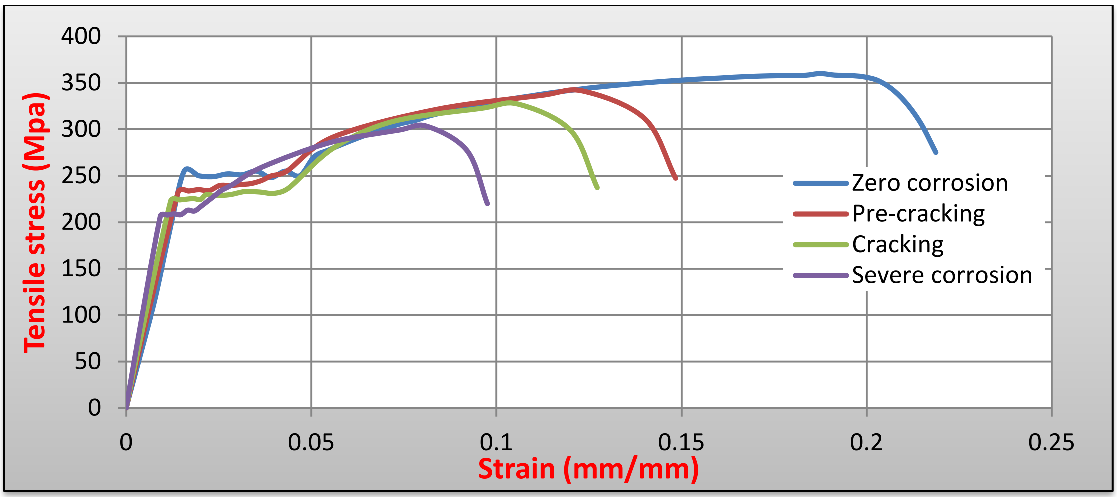

Fig. 7.57: Stress-strain curve for plain bars at each degree of corrosion, Mix No. (4)

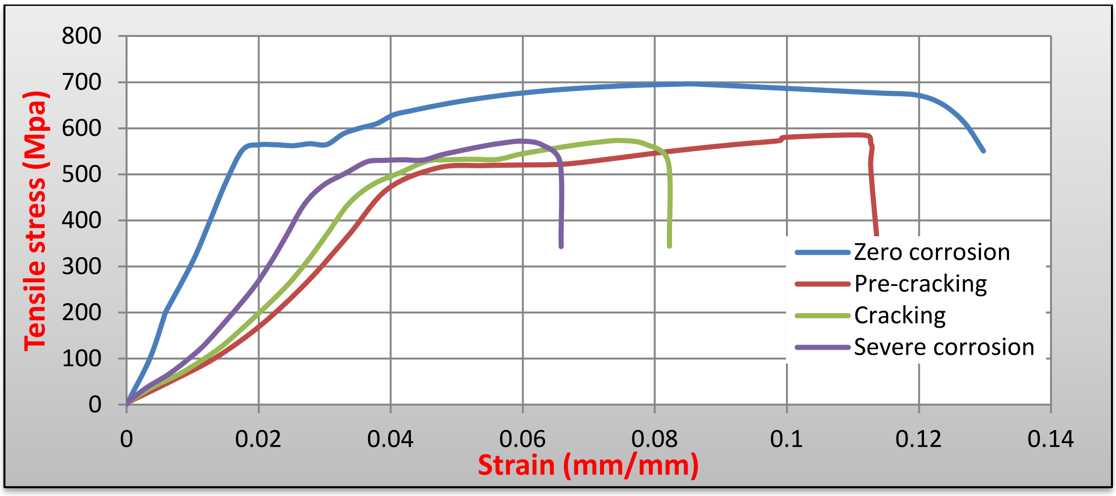

Fig. 7.58: Stress-strain curve for un-coated deformed bars at each degree of corrosion, Mix No. (4)

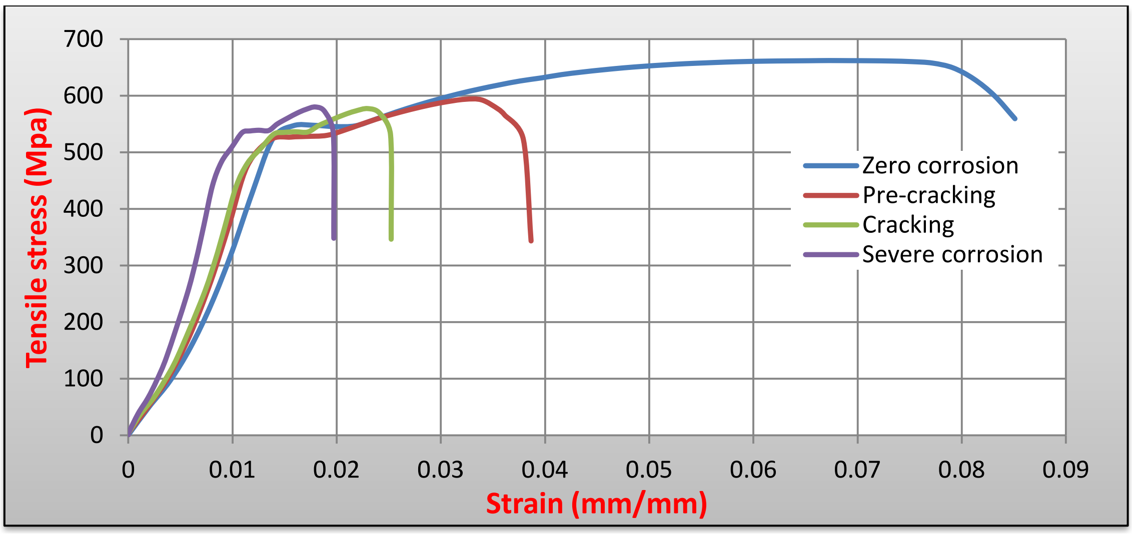

Fig. 7.59: Stress-strain curve for epoxy coated deformed bars at each degree of corrosion, Mix No. (4)

From the curves, it is observed that the reduction in steel tensile strength is inversely proportional to the increase in concrete strength. This is shown in the higher reduction values of tensile stresses for the 30 MPa concrete (mix No. 1) compared to the higher strength concrete. The minimum reduction in tensile stresses was observed in the 60 MPa concrete (mix No. 4).

On the other hand, the decrease in steel bars ductility is clearly obvious in all concrete mixes. As corrosion propagates, the steel bars failed at lower extensions compared to those before corrosion initiation. Nearly all steel types showed similarity in reduction of their ductility values.

When designing a reinforced concrete section, the designer is interested in the yielding values of steel, not the maximum values. All bars, plain and deformed, showed yielding regions in their stress-strain curves before corrosion. However, these regions started to disappear as the corrosion propagated from pre-cracking to severe corrosion stage.

From the previous results, it can be concluded that corrosion affects the steel mechanical properties negatively. This means that as corrosion propagates, the safety factor used in the designing process will be consumed. Corrosion looses the steel all its advantages. The high strength of steel is decreased and its ability to elongate upon loading is lost. Also the bond is lost between steel bars and the surrounding concrete which will force the structure to perform as plain concrete, leading to sudden failure at further degrees of corrosion.

7.5 Effect of Corrosion on Concrete Reinforcement Physical Properties

The effect of corrosion on steel bars physical properties was studied including the mass and rib loss for each type of steel at different degrees of corrosion. The mass loss was obtained as the difference between the mass of the corroded bar, after removal of the loose corrosion products, and its mass before corrosion. The ribs height were measured after the corrosion took place, and the rib profile loss was obtained as the difference between the rib height of the corroded bar and its height before corrosion. Tables 7.6 and 7.7 show the mass and rib profile loss of steel bars at different corrosion stages respectively.

From Table 7.6 it can be observed that the mass loss is greater in case of the [30MPa] and [44MPa, 0.52 w/c] mixes. The 60MPa mix showed the least mass loss percentage. This can be attributed to its high resistivity to corrosion, and when corrosion initiated it cracked suddenly at a low percentage of corrosion products.

By comparing these results with the bond-slip curves, it can be concluded that the bond increased with very small increase of the percentage of mass loss (pre-cracking stage), and then decreases with further increase of the mass loss (cracking and severe corrosion stages). The reason for the first increase of the bond was formation of a very thin rusty layer around the bar, which increases the concrete-steel friction. Furthermore, with the increase in the corrosion products, a friable layer formed around the bar leading to a significant decrease of the bond strength due to the loss of the surface friction and the degradation of the ribs height (Fig. 7.60).

Fig. 7.60: A friable layer formed around the bar at further degrees of corrosion

Table 7.6: Mass loss of steel bars at different degrees of corrosion

Concrete Type	Steel Type	Mass loss as a percentage of zero corrosion mass (%)		
		Pre-cracking	Cracking	Severe Corrosion
30MPa, w/c=0.32	Plain	0.8	2.6	3.5
	Deformed Uncoated	1.2	2.9	4.2
	Deformed Coated	1.6	2.4	3.6
44MPa, w/c=0.52	Plain	0.6	2.6	3.7
	Deformed Uncoated	0.4	1.6	4.2
	Deformed Coated	0.5	2.9	4.1
44MPa, w/c=0.32	Plain	0.4	0.6	2.9
	Deformed Uncoated	1	1.2	3.6
	Deformed Coated	1	1.1	3.3
60MPa, w/c=0.32	Plain	0.4	1.2	2.2
	Deformed Uncoated	0.5	1.7	2.9
	Deformed Coated	0.4	1.7	2.6

Table 7.7: Rib profile loss of steel bars at different degrees of corrosion

Concrete Type	Steel Type	Rib profile loss as a percentage of zero corrosion rib height (%)		
		Pre-cracking	Cracking	Severe Corrosion
30MPa, w/c=0.32	**Plain** (diameter loss)*	8.7	16.1	18.8
	Deformed Uncoated	69.2	98.56	(131.2)**
	Deformed Coated	81.2	92.1	(122.1)**
44MPa, w/c=0.52	**Plain** (diameter loss)*	7.6	16	19.1
	Deformed Uncoated	38.7	81.8	(132.1)**
	Deformed Coated	43.6	94.2	(130.9)**
44MPa, w/c=0.32	**Plain** (diameter loss)*	6.1	7.5	17.1
	Deformed Uncoated	63.9	69.6	(121.9)**
	Deformed Coated	63.1	66	(116.9)**
60MPa, w/c=0.32	**Plain** (diameter loss)*	6	11.1	14.7
	Deformed Uncoated	47.2	84.7	(108.4)**
	Deformed Coated	40.8	83.6	(103.9)**

*For plain bars with no ribs, the percentages were calculated from the total cross-sectional area of the bar.

**Results exceeding the 100% indicate that the corrosion causes total loss in the ribs and extends to the inner bar diameter.

A Numerical Model for Steel-Concrete Bond

8.1 Background

The bond between the concrete and reinforcing steel in RC structures allows longitudinal forces to be transferred from the reinforcement to the surrounding concrete. When studying cracked reinforced concrete, characterization of the bond behavior is one of the most important issues. Once a crack develops, the concrete stress near the crack is relieved, but the tension in steel can increase considerably. The high level of steel stress at the crack is transferred to the surrounding concrete through the interfacial bond *(Won 1991).*

This chapter describes an attempt to model the bond-slip relationship between concrete and rebar using the finite element software package ABAQUS.

ABAQUS, a suite of software application for finite element analysis and computer aided engineering, originally released in 1978. It is based on the finite element method that can solve problems ranging from relatively simple linear analysis to the most challenging nonlinear simulations *(ABAQUS 6.9-1).* Abaqus provides a variety of interactions methods for connecting two parts together.

8.2 Objective

The primary objectives of this chapter are to develop a finite element model which could correctly simulate the bond-slip relationship in a reinforced concrete member, to accurately predict the level of stress transferred by the bond, and to show how to introduce the effect of corrosion of steel reinforcement on the bond strength of RC members. This model will be based on the results obtained from the physical model of the pull-out samples. Other objectives are comparing previous RC models that included bond behavior, and to select the best modeling techniques available to accurately reflect the bond behavior.

8.3 Literature Review

The action of the steel/concrete bond is a complex force transfer phenomenon occurring between the reinforcing steel and the surrounding concrete in RC members. The existence of the bond is essential for these two materials to behave as a kind of composite material. Without bond, the rebar would not be able to resist external loads, and the RC member would behave exactly like a plain concrete member does.

The connection between the reinforcing bars and the concrete is also responsible for controlling of the crack opening behavior in an RC member *(Filho et al 2004).* Between significant cracks, the concrete still works and will absorb part of the tensile load from the rebar because the bond allows the load transfer between these two materials. Consequently, the strains resulting in the rebar are smaller than those that would be experienced under the same load in a single bar that is not embedded in concrete. This mechanism, attributed to the bond, reduces the width of the cracks that develop and increases the stiffness of the structure *(Xin Li 2007).*

Because of its importance, many researches have been conducted to characterize the constitutive bond-slip relationship. In the finite element analysis field, many different methods were also employed to represent the nature of the interaction between the concrete and reinforcement.

For better use of the bond mechanism in practical design and analysis, the bond slip relationship has been simplified to a linear or bilinear curve by many researchers. Several bilinear models were developed, such as the three segments model *(Nilson 1972),* the five segments model *(Guo & Shi 2003),* and the six segments model *(Tassios 1982);* Fig. 8.1 illustrates these three models. In Fig. 8.1, τ represents the bond stress, while S represents the magnitude of bond slip. The CEB-FIP MC90 suggested a four segments model, as shown in Fig. 8.2; Table 8.1 shows the characteristic values for the different parameters specified in this model. The CEB-

FIP model code for concrete structures was published in 1978 following approval by the Euro-International Committee for concrete (CEB). The publication was associated with the 8th Congress of the International Federation for Pre-stressing (FIP) in London in May 1978.

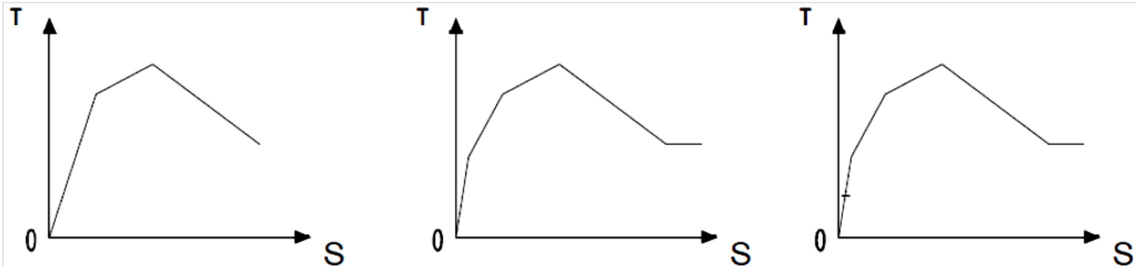

Fig. 8.1: Bilinear Bond Slip Relationships: a) Three Segments, b) Five Segments and c) Six segments

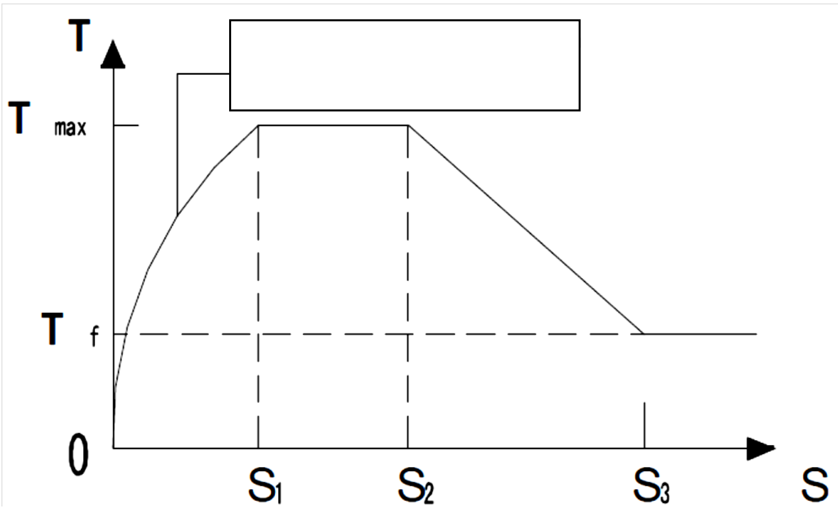

Fig. 8.2: CEB-FIP MC90 Model *(CEB-FIP, 1993)*

Engstrom found that the bond stress decreases more when the strain exceeds the yield strain than when the steel bar is still elastic. He modified the degrading part of the CEB model in order to consider the effect of yielding of the rebar (CEB-FIP 2000). Fig. 8.3 and Table 8.2 illustrate the different bond slip relationships under these two situations.

Table 8.1: Values of Parameters for CEB-FIP MC90 Model

	Unconfined concrete		Confined concrete	
	Good bond conditions	All other bond conditions	Good bond conditions	All other bond conditions
S_1	0.6mm	0.6mm	1.0mm	1.0mm
S_2	0.6mm	0.6mm	3.0mm	3.0mm
S_3	1.0mm	2.5mm	Clear rib spacing	Clear rib spacing
A	0.4	0.4	0.4	0.4
τ_{max} (MPa)	$2.0\sqrt{f_{ck}}$	$1.0\sqrt{f_{ck}}$	$2.5\sqrt{f_{ck}}$	$1.25\sqrt{f_{ck}}$
τ_f	0.15 τ_{max}	0.15 τ_{max}	0.40 τ_{max}	0.40 τ_{max}

* f_{ck} is the characteristic concrete compressive strength, MPa

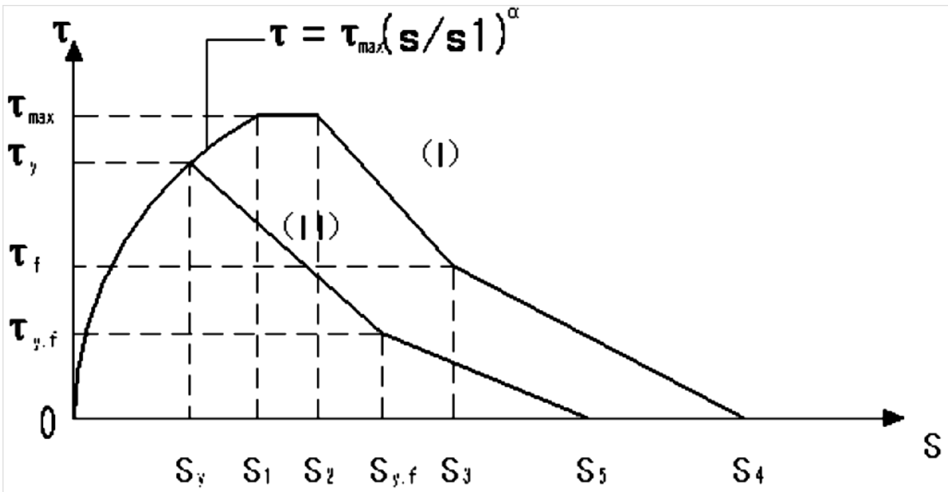

Fig. 8.3: Engstrom's Model (CEB-FIP 2000), (I) Steel Bar in Elastic Stage (II) Steel Bar in Plastic Stage

Table 8.2: Values of Parameters in Engstrom's Model (CEB-FIP 2000)

	S_1	S_2	S_3	S_4	τ_{max}	τ_f	α
Normal strength concrete	1.0mm	3.0mm	Clear rib spacing	$3S_3$	0.45 f_{cm}	0.4 τ_{max}	0.4
High strength concrete	0.5mm	1.5mm	Clear rib spacing	$3S_3$	0.45 f_{cm}	0.4 τ_{max}	0.3

* f_{cm} is the mean value of concrete compressive strength, MPa

Researchers also tried to establish equations to describe the bond-slip relationship mathematically. These equations can be used in simulating the bond behavior in finite element analysis. One equation was proposed by Nilson (1968):

$$u = 3.606x10^6 d - 5.356x10^9 d^2 + 1.986x10^{12} d^3 \qquad 8-1$$

Where

u: is the nominal bond stress, psi
d: is the local slip, in

Another equation was proposed by Mirza & Houde (1979):

$$u = 1.95x10^6 d - 2.35x10^9 d^2 + 1.39x10^{12} d^3 - 0.33x10^{15} d^4 \qquad 8-2$$

Where

u: is the nominal bond stress, psi
d: is the local slip, in

8.4 Existing FE Models for Reinforced Concrete

Unlike any other homogenous materials, which have uniform constitutive properties, reinforced concrete consists of two totally different materials working together to resist various types of loading. Therefore, modeling of bond-slip relationship and predicting the behavior of RC using finite element method is somewhat complex. Nowadays there exist three different FE models which are widely used to simulate reinforced concrete behavior. They are discrete, distributed and embedded models.

In the discrete model technique, concrete and steel are represented using two distinct elements. Usually a solid finite element is used to represent the concrete, while the reinforcing bar is simulated using a beam element. In this model, concrete and steel are totally independent parts. Therefore, special elements are placed at the interface between the concrete and steel to represent the bond mechanism between the two materials *(Xin Li 2007).*

When using the embedded modeling technique, the rebar is considered as an axial member that is built into the concrete element. Therefore, the rebar will have the same displacement as concrete. For this reason, it is said that this technique considered the bond between the concrete and the rebar to be perfect. In other words, the two materials are assumed to work together completely as one unit *(ASCE 1982).*

In the distributed modeling technique, the reinforcement is assumed to be smeared into every element of the concrete. The rebar is transferred to an equivalent amount of concrete and the reinforced concrete is considered as homogenous material in this model. Perfect bond is again assumed in this technique *(Xin Li 2007).*

Due to its simplicity of implementation, the distributed model is frequently used in practical structural design and analysis. However, the internal forces of the reinforcement bar can't be quantified in this model since the steel has been smeared. The discrete model is the only model of the three which can consider the bond slip mechanism directly because the concrete and steel are two separate entities, so it is very useful in more accurate RC simulations, despite the fact that the modeling process for this technique is the most complex. The embedded modeling technique falls between the distributed and discrete model in terms of complexity and ease of implementation.

Currently, most finite elements software packages such as ABAQUS, ADINA, ANSYS, and MSC/NASTRAN have their own concrete constitutive models and corresponding concrete and rebar elements. The issue is how to develop the three previous models using the combination of these elements and how to represent the bond, fracture and cracking behaviors..

8.5 Finite Element Modeling of Bond

In order to overcome the problem of considering the bond between concrete and steel rebar as if it is perfect, some dedicated elements have been developed to simulate the contact between concrete and rebar and presently they are widely used in the commercial finite element software.

In 1968, Bresler and Bertero developed a layered model to represent the bond. The concrete was divided into two regions: an inner “boundary layer” and an outer layer of undamaged concrete as shown in Fig. 8.4. This model was based on the idea that the bond only occurs in concrete closest to the steel bar. The thickness of the boundary layer was assumed to be 0.4 times the rebar diameter and consists of a special homogenized material. The boundary layer properties were based on the data included in the bond-slip relationship. This layer was able to transfer the stress and displacement from the reinforcement to the outer layer of concrete *(Bresler & Bertero 1968).*

In the same year (1968), *Nilson* was the first to use a connecting element. He introduced a double spring element to model the bond slip phenomena, as shown schematically in Fig. 8.5. This double spring element consisted of two springs, one acting parallel to the bar axis and one acting perpendicular to it. These two springs were used to transmit normal and shear forces between the nodes of concrete and reinforcement. The springs were not considered to have dimensions, and their stiffness was based on the characteristics of the bond-slip relationship. In 1991, the double spring element was modified into various possible unidirectional spring element configurations, as shown in Fig. 8.6.

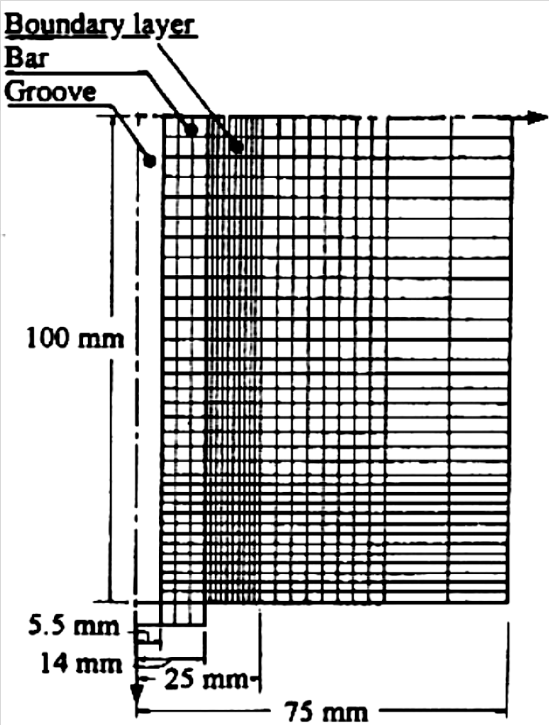

Fig. 8.4: FE Model according to Bresler & *Bertero (CEB-FIP 2000)*

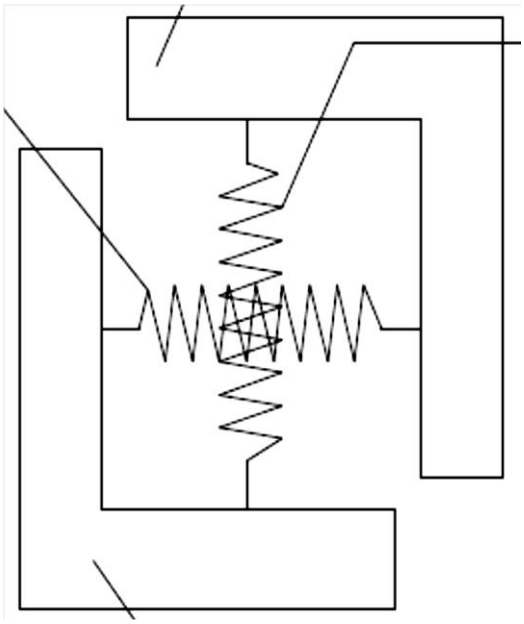

Fig. 8.5: FE Model according to *Nilson*

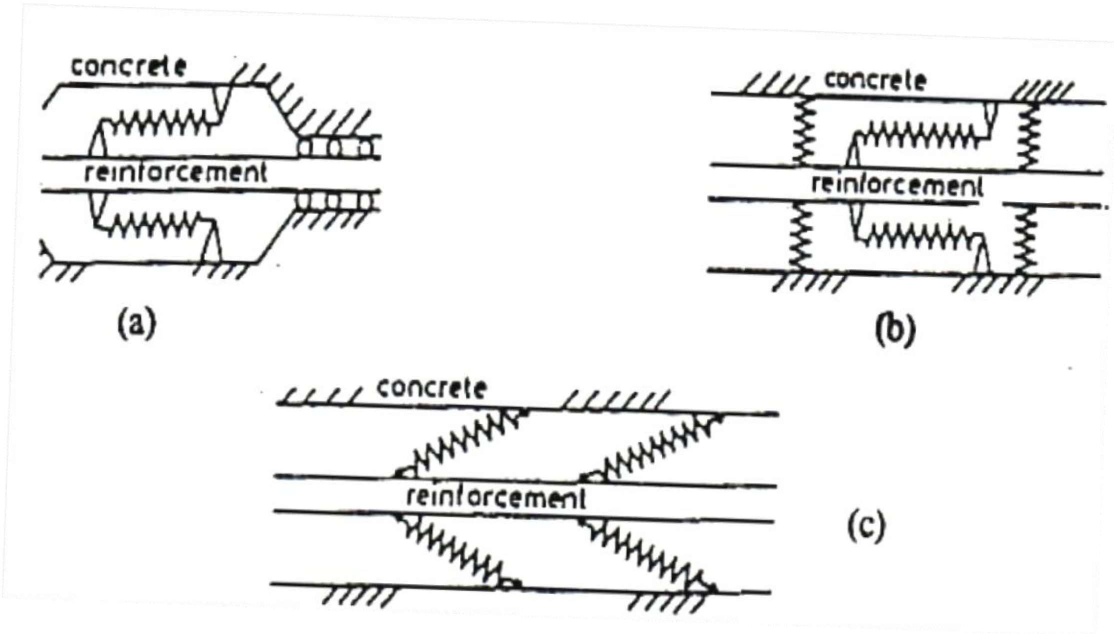

Fig. 8.6: The modified double spring element using various possible unidirectional spring element configurations *(Xin Li 2007)*

8.6 Proposed Model

Fracture and crack propagation in concrete depends to a large extent on the material properties in tension and the post-cracking behavior. Experimental studies *(Welch and Haisman 1969; Bedard and Kotsovos 1986)* indicate that the behavior of concrete after cracking is not completely brittle and that cracked region exhibits some ductility. As the applied loads are increased the tensile stress in the critical cross section of the member reaches the tensile strength (f_t).

The proposed FE model in this study consists of three contact parts: the steel bar, the concrete cylinder and an intermediate part that acts as the interface between the concrete and the reinforcement bar. The model shows the effect of reinforcement corrosion on the stresses in concrete. In this study, the bond between steel and concrete is simulated using intermediate elements and the corrosion effect is introduced as thermal expansion in the steel bar which causes internal stresses in the concrete leading to tensile cracks.

8.7 Corrosion Effect Model

This model is a 2D finite element model with the same dimensions of the experimental program samples as shown in Fig. 8.7. 2.0mm intermediate elements are used at the interaction between the steel bar and the concrete cylinder. Since the model is symmetry, therefore one quarter of the cylinder can be used in this model as shown in Figs. 8.8a and 8.8b using adequate boundary conditions.

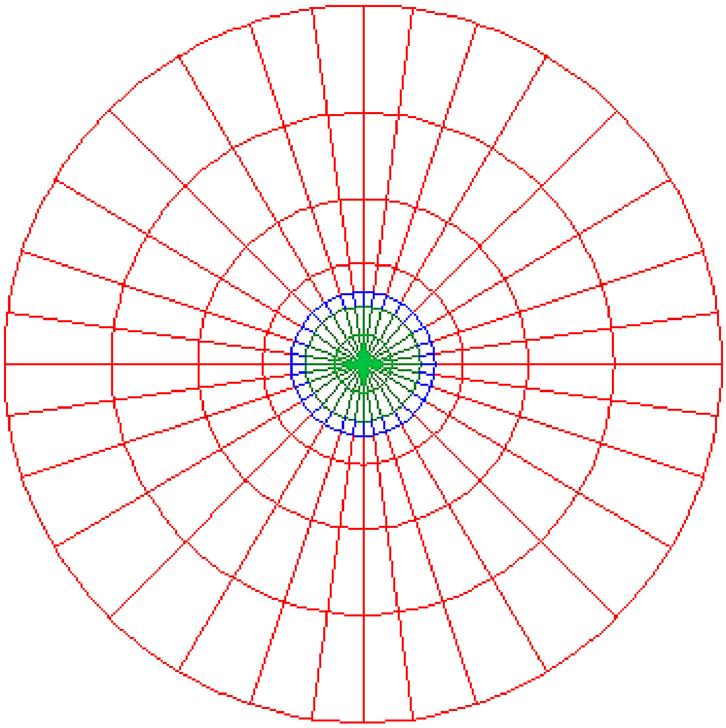

Fig. 8.7: 2D Plan of the concrete cylinder and the embedded bar

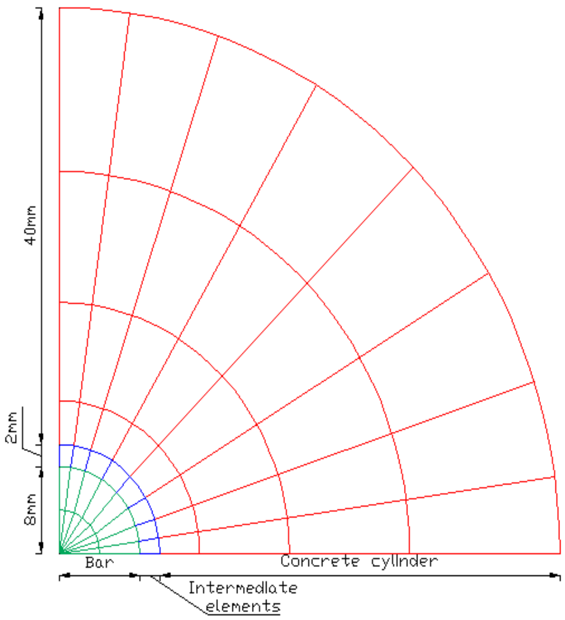

Fig. 8.8a: The 2D model Geometry

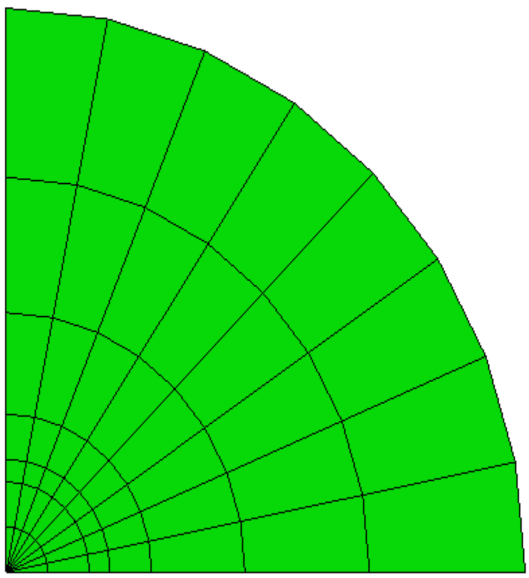

Fig. 8.8b: Abaqus mesh of the model

8.7.1 Model (1): Elastic Behavior for Steel and Concrete

8.7.1.1 Model Description

In this model both the concrete and steel are defined as linear elastic materials. This model uses the concrete properties for the 30 MPa concrete with the 240/350 steel bar embedded. The model parameters are shown in Table 8.3. Material properties are held constant for all concrete and steel elements. Properties of intermediate elements are exactly the same as concrete elements. Materials properties are defined using **Elastic* option in ABAQUS. All elements in the model were simulated using 3-node linear plane stress triangle (CPS3), and 4-node bilinear plane stress quadrilateral (CPS4) elements.

The **Elastic* option is used to define linear elastic model for a material. Its type is set to isotropic (*TYPE=ISOTROPIC*) to define isotropic behavior.

Table 8.3: Model No. (1) Parameters

Material	Density (kg/m^3)	Modulus of Elasticity (Pa)	Poisson's ratio	Expansion coefficient	Element thickness (mm)
Concrete (30MPa, w/c=0.32)	2222	$27.3x10^9$	0.2	$1.45\ x10^{-5}$	10
Steel (240/350)	7486	$200\ x10^9$	0.303	$1.23\ x10^{-5}$	10

8.7.1.2 Model Analysis

Figs. 8.9a to 8.9d show the Abaqus analysis for this model. From the figures it can be noticed that the maximum tension is at the interface between concrete and steel. Fig. 8.9b shows the stresses (S11), and it can be noticed that the maximum tensile stresses are 53 MPa and are located at the 2.0mm intermediate elements. From the experimental data, the maximum tensile stress for this type of concrete was 2.73 MPa; however, this model doesn't take into consideration the tensile behavior of concrete since concrete is defined using its modulus of elasticity only with no plastic behavior either for compression or tension.

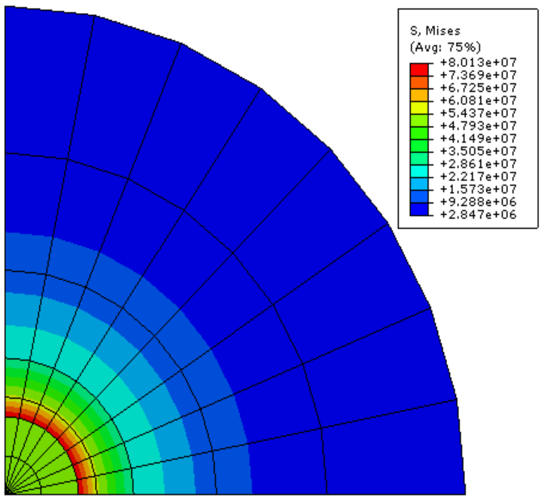

Fig. 8.9a: S,Misses (Model No. 1)

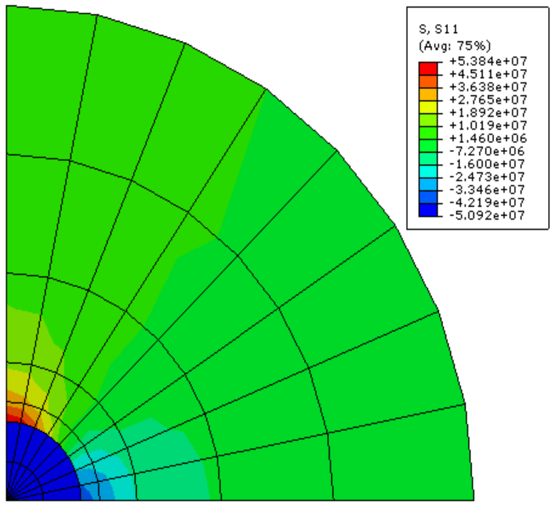

Fig. 8.9b: S,S11 (Model No. 1)

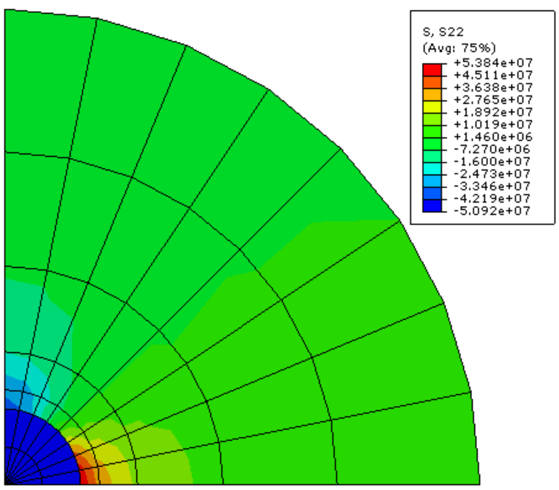

Fig. 8.9c: S,S22 (Model No. 1)

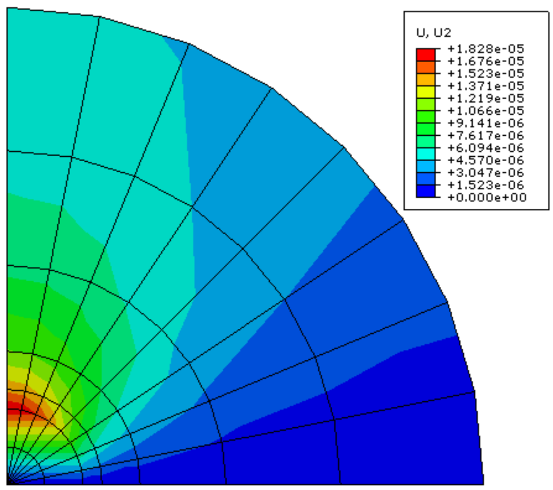

Fig. 8.9d: U,U2 (Model No. 1)

Therefore the concrete behaves the same in tension and compression and this can be shown in Figs. 8.10a to 8.10c, where the relations between different stresses and elongations with the corresponding temperature were plotted at node 803 located directly at the interface between steel and concrete.

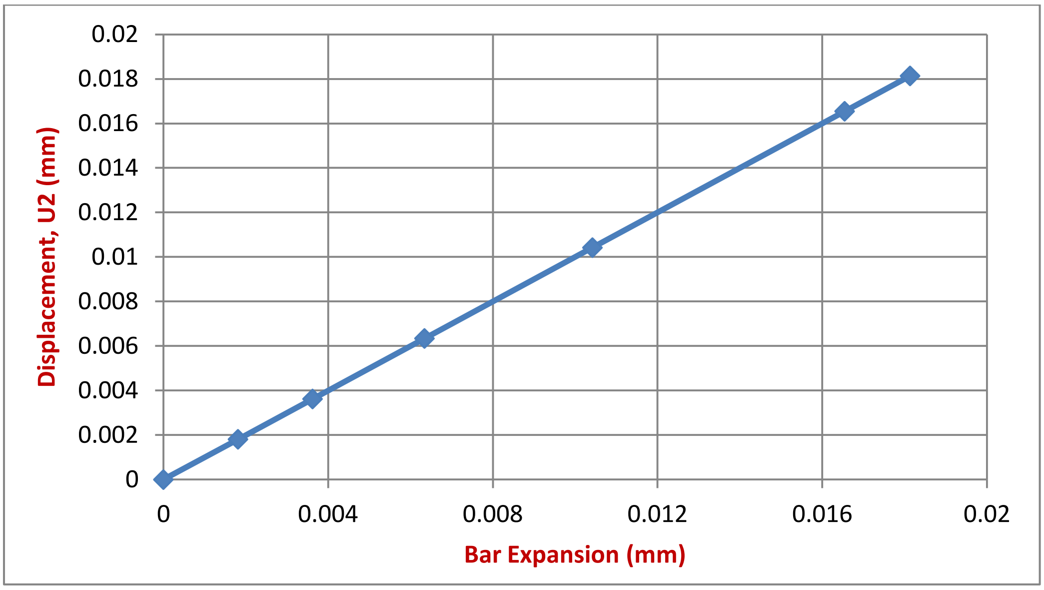

Fig. 8.10a: Displacement (U2) vs. Bar Expansion (Model No.1)

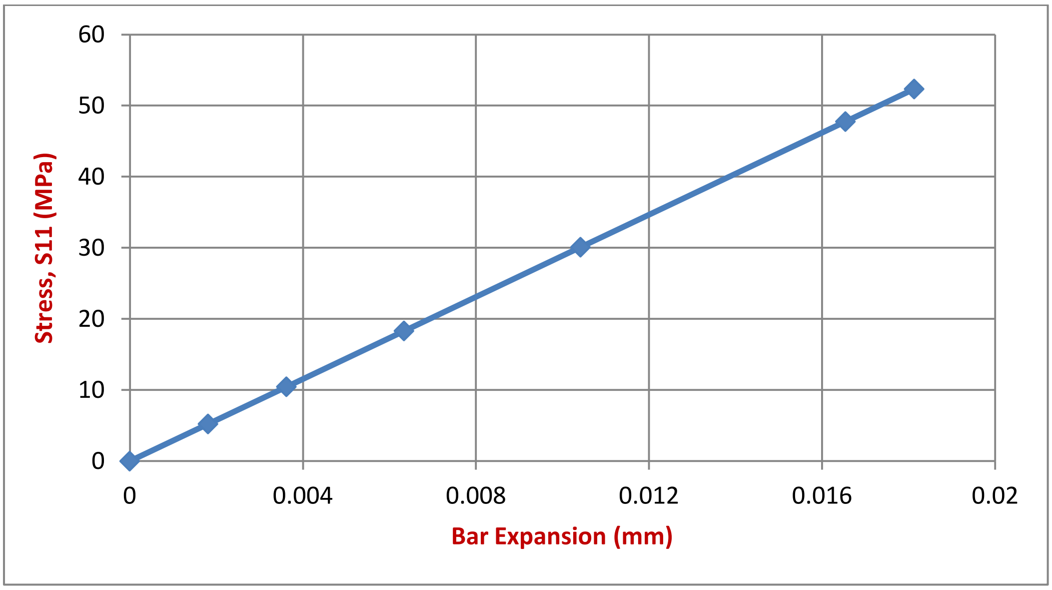

Fig. 8.10b: Stress (S11, tension) vs. Bar Expansion (Model No.1)

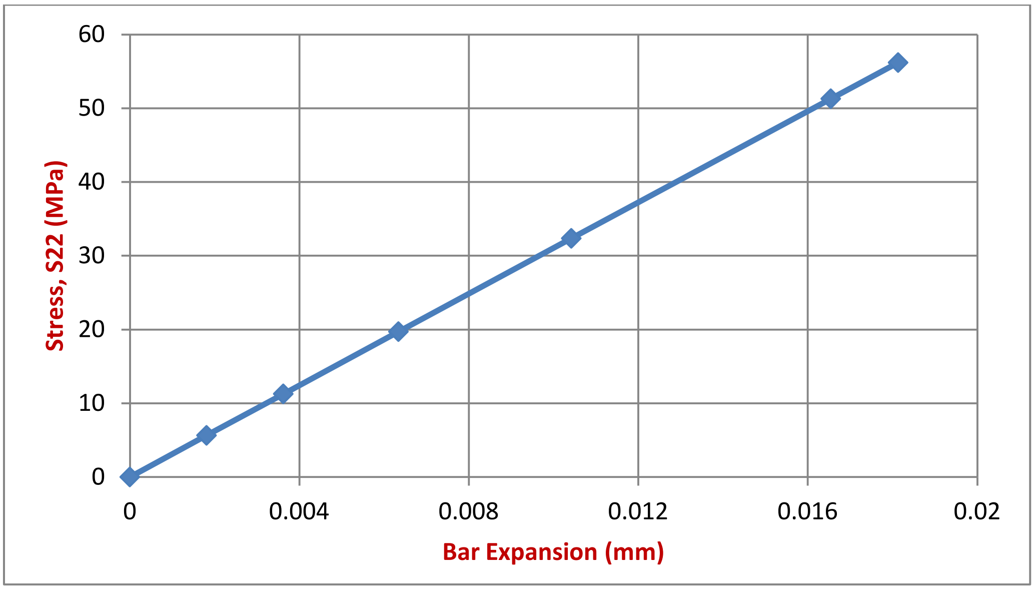

Fig. 8.10c: Stress (S22, compression) vs. Bar Expansion (Model No.1)

Node 803 is located directly at the interface; therefore it must experience the same elongation as the steel bar. By calculating the linear expansion of the steel bar where 8mm bar is subjected to a temperature difference of 200 °C, we can find that the maximum elongation will be equal to 0.01968 mm according to the following equation:

$$\Delta L = \alpha * L * \Delta T = 1.23 * 10^{-5} * 8 * 200 = 0.01968\, mm \qquad 8-3$$

This is typically the same elongation experienced by the numerical model at node 803 as shown in Fig. 8.10a.

From Figs. 8.10a and 8.1b, it is obvious that the behavior of concrete in both tension and compression is linearly elastic until failure and the modulus of elasticity is nearly the same for both cases. The maximum stresses at this node are approximately 55 MPa for both tension and compression.

8.7.2 Model (2): Steel (elasto-plastic) and Concrete (elastic)

8.7.2.1 Model Description

In this model steel is defined as elasto-plastic material and concrete is defined as linear elastic material. This model uses the concrete properties for the 30 MPa concrete with the 240/350 steel bar embedded. The model parameters are shown in Table 8.4. Material properties are held constant for all concrete and steel elements. Plasticity of steel is defined using the **PLASTICITY* option and the stress-strain curve shown in Fig. 8.11. Properties of intermediate elements are exactly the same as concrete elements. All elements in the model were simulated using 3-node linear plane stress triangle (CPS3), and 4-node bilinear plane stress quadrilateral (CPS4) elements.

Table 8.4: Model No. (2) Parameters

Material	Density (kg/m^3)	Modulus of Elasticity (Pa)	Poisson's ratio	Expansion coefficient	Element thickness (mm)
Concrete (30MPa, w/c=0.32)	2222	27.3x10^9	0.2	1.45 x10^{-5}	10
Steel (240/350)	7486	200 x10^9	0.303	1.23 x10^{-5}	10

8.7.2.2 Model Analysis

Figs. 8.12a to 8.12d show the Abaqus analysis for this model. From the figures it can be noticed that the maximum tension still occurs at the interface between concrete and steel. Fig. 8.12b shows the stresses (S11), and it can be noticed that the maximum tensile stresses remains 53 MPa and are located at the 2.0mm intermediate elements. This means that the plasticity of steel bar didn't affect the behavior of the model, and this can be considered correct since the stresses in the steel in the first model were approximately 50 MPa. This type of steel yields at 250 MPa, so the stresses are in the elastic zone and haven’t reached the plastic zone yet.

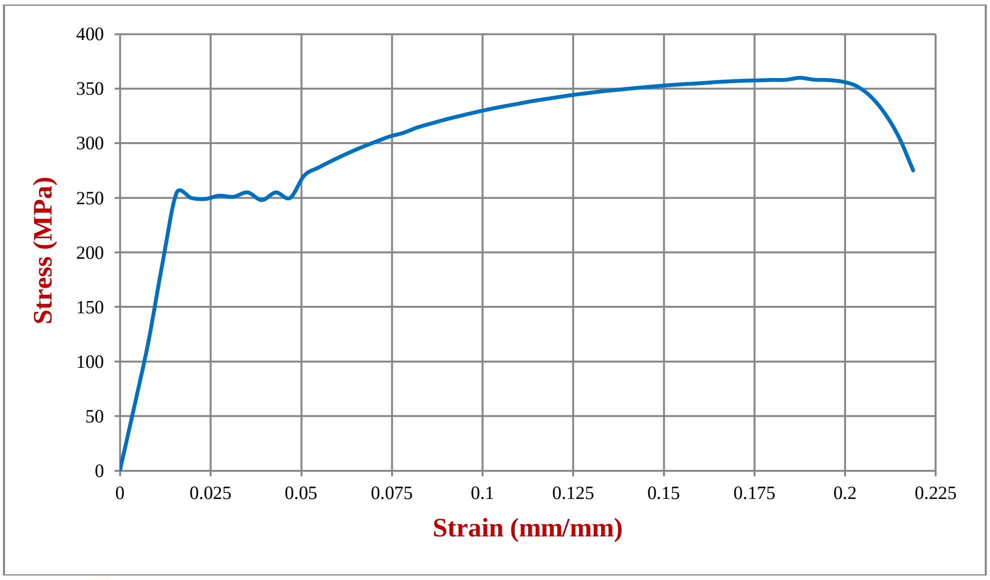

Fig. 8.11: Stress-strain relationship for 240/350 steel bar

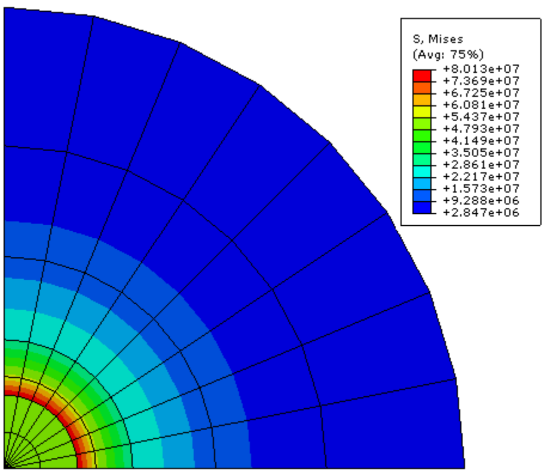

Fig. 8.12a: S,Misses (Model No. 2)

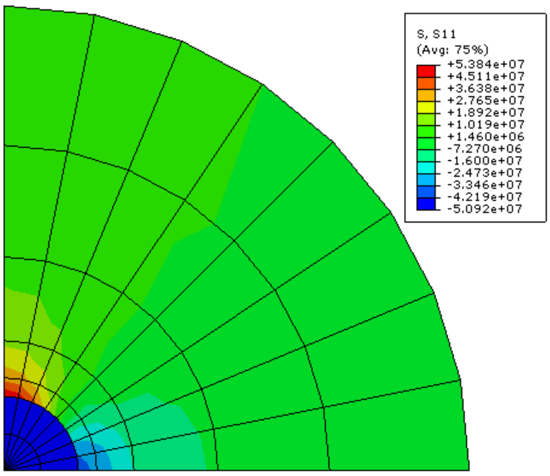

Fig. 8.12b: S,S11 (Model No. 2)

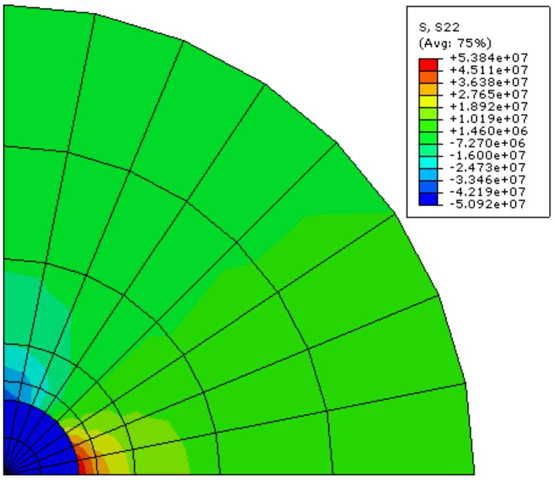

Fig. 8.12c: S,S22 (Model No. 2)

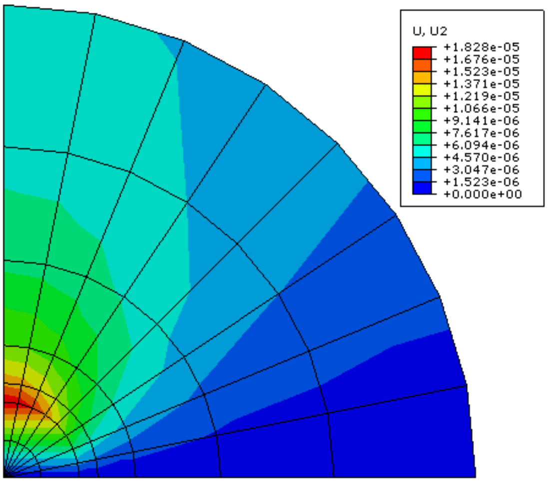

Fig. 8.12d: U,U2 (Model No. 2)

Therefore the concrete behaves the same in tension and compression as the first model and the plasticity property of steel has no effect on the concrete behavior. This can be shown in Figs. 8.13a to 8.13c, where the relations between different stresses and elongations with the corresponding temperature were plotted at node 803 located directly at the interface between steel and concrete.

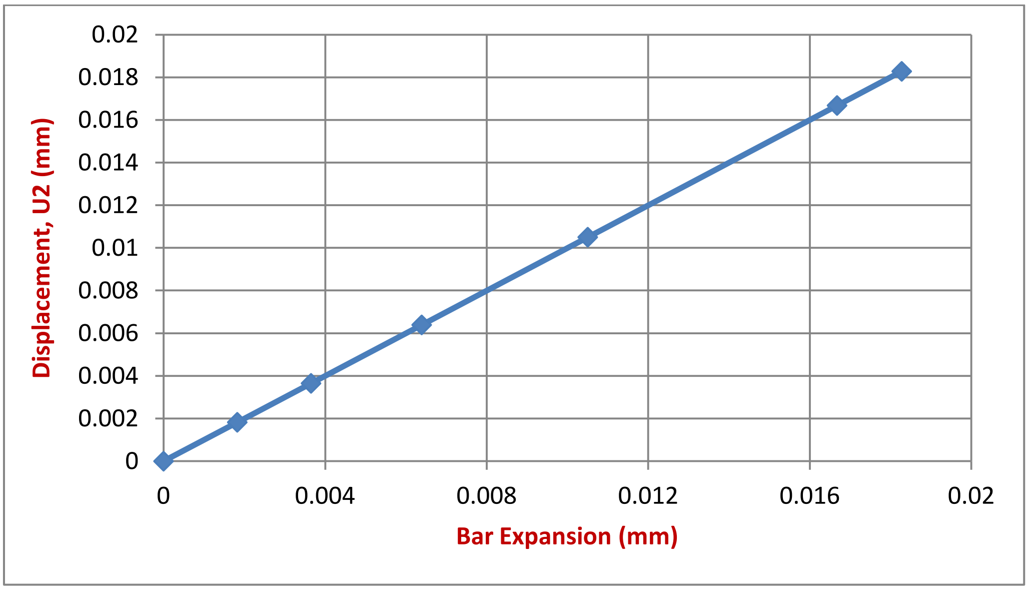

Fig. 8.13a: Displacement (U2) vs. Bar Expansion (Model No.2)

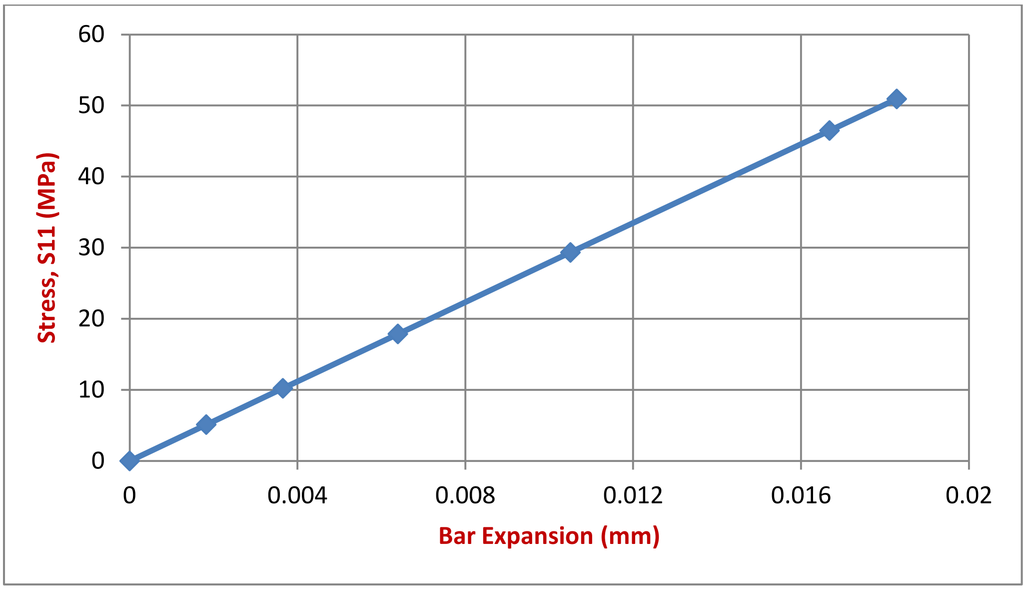

Fig. 8.13b: Stress (S11, tension) vs. Bar Expansion (Model No.2)

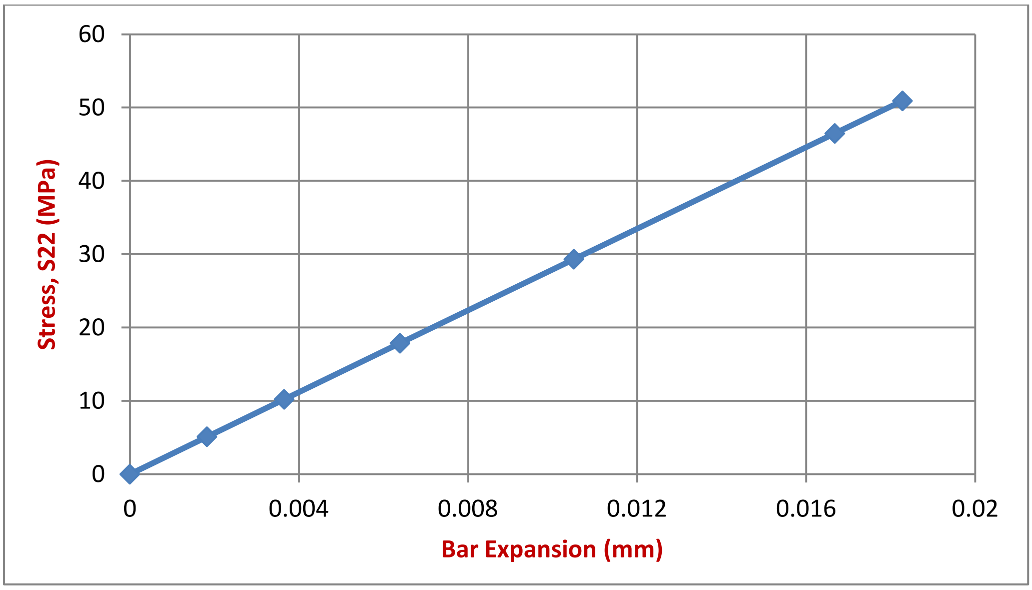

Fig. 8.13c: Stress (S22, compression) vs. Bar Expansion (Model No.2)

The figures show nearly the same behavior as model No.(1). The node still shows the same elongation and the stresses are nearly the same 52 MPa. This gives a conclusion that the steel plasticity has no effect if the stresses are below the steel yield strength. In the coming model, the concrete plasticity will be defined so as to investigate the plastic behavior of concrete when subjected to internal stresses resulting from the corrosion products.

8.7.3 Model (3): Steel (elastic) and Concrete (elasto-plastic)

8.7.3.1 Model Description

In this model concrete is defined as elasto-plastic material and steel is defined as linear elastic material. This model uses the concrete properties for the 30 MPa concrete with the 240/350 steel bar embedded. The model parameters are shown in Table 8.5. Material properties are held constant for all concrete and steel elements. Plasticity of concrete is assumed to be the same in both compressive and tensile behaviors and is defined using the **PLASTICITY* option and the stress-strain curve shown in Fig. 8.14. Properties of intermediate elements are exactly the same as concrete elements. All elements in the model were simulated using 3-node linear plane stress triangle (CPS3), and 4-node bilinear plane stress quadrilateral (CPS4) elements.

Table 8.5: Model No. (3) Parameters

Material	Density (kg/m^3)	Modulus of Elasticity (Pa)	Poisson's ratio	Expansion coefficient	Element thickness (mm)
Concrete (30MPa, w/c=0.32)	2222	27.3×10^9	0.2	1.45×10^{-5}	10
Steel (240/350)	7486	200×10^9	0.303	1.23×10^{-5}	10

8.7.3.2 Model Analysis

Figs. 8.15a to 8.15d show the Abaqus analysis for this model. From the figures it can be noticed that the maximum tension doesn't occur at the interface between concrete and steel, but it occurs somewhere after the interface. This can be confusing at the beginning, but this model works on six steps, so the behavior of the model along the six steps must be investigated. Fig. 8.15b shows the stresses (S11), and it can be noticed that the maximum tensile stresses are 13 MPa and located at a distance from the bar. Figure 8.15c shows the stresses (S22) which represent the compression stresses in the concrete cylinder. The maximum compressive stresses from the figures are approximately 28 MPa and located at the interface elements.

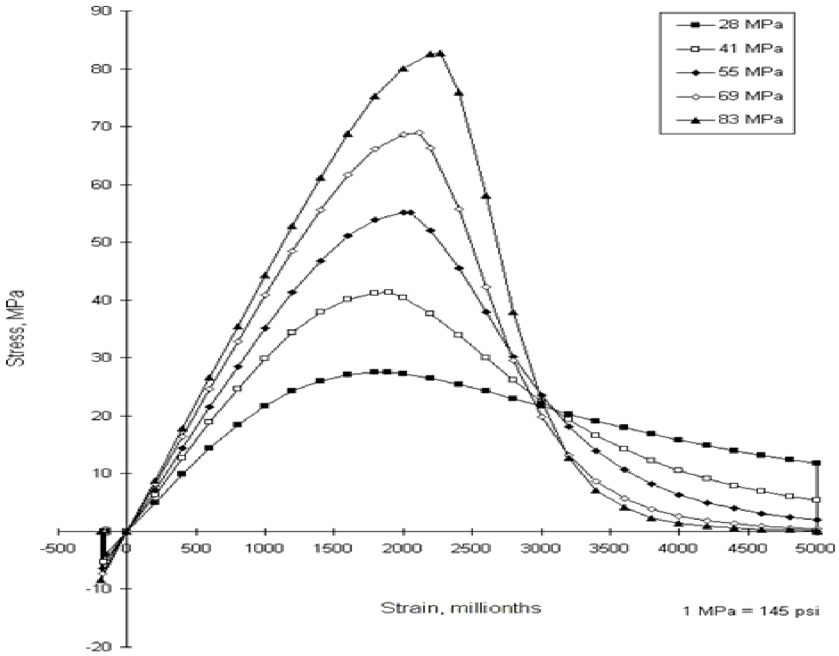

Fig. 8.14: Stress-strain relationship for concrete
[Optimized Sections for High-Strength Concrete Bridge Girders, FHWA]

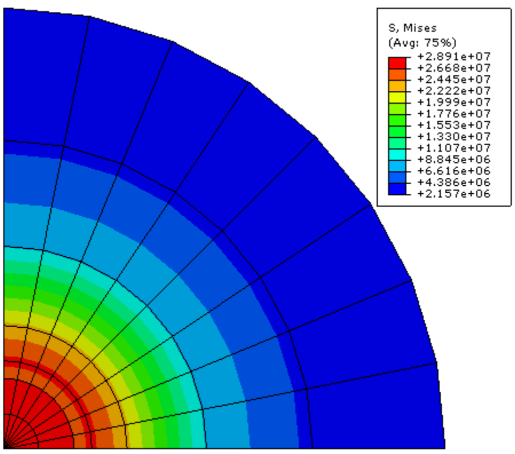

Fig. 8.15a: S,Misses (Model No. 3)

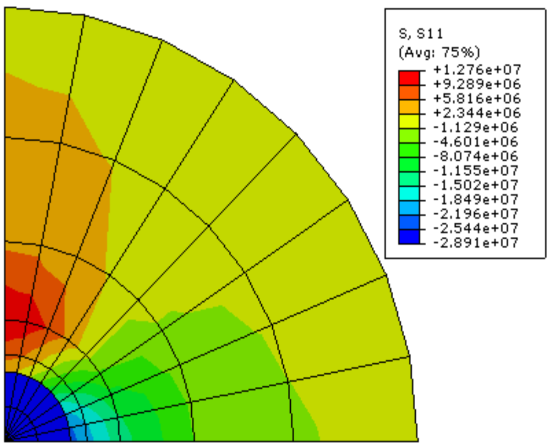

Fig. 8.15b: S,S11 (Model No. 3)

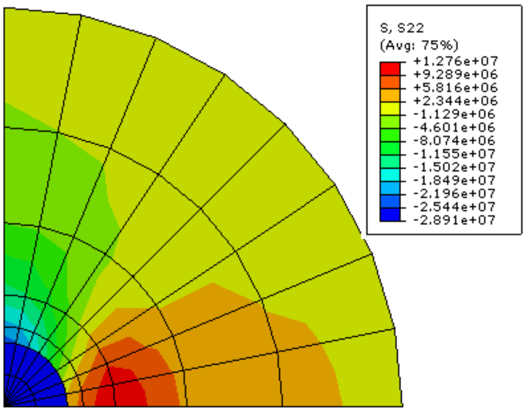

Fig. 8.15c: S,S22 (Model No. 3)

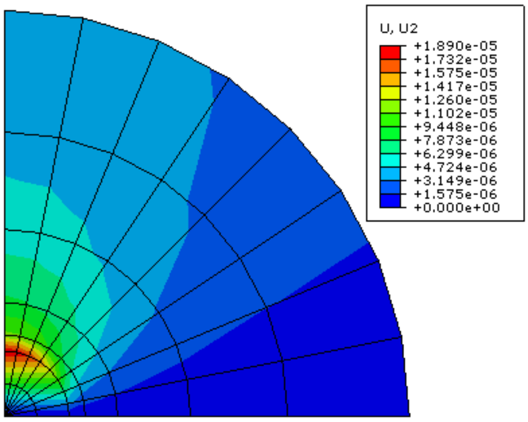

Fig. 8.15d: U,U2 (Model No. 3)

Figs. 8.16a to 8.16c show the behavior of the model along the six steps at the intermediate elements located at the interface between the steel bar and the concrete cylinder. In this model the behavior of concrete in tension (Fig. 8.16b) is different from its behavior in compression (Fig. 8.16c). In tension the concrete reached a maximum stress of 18.5 MPa. This exceeds the maximum tensile stress of this type of concrete which is equal to 2.73 MPa. However, the concrete behavior in compression showed that the maximum stresses were approximately 28 MPa, and this is below the compressive strength for this type of concrete 30 MPa.

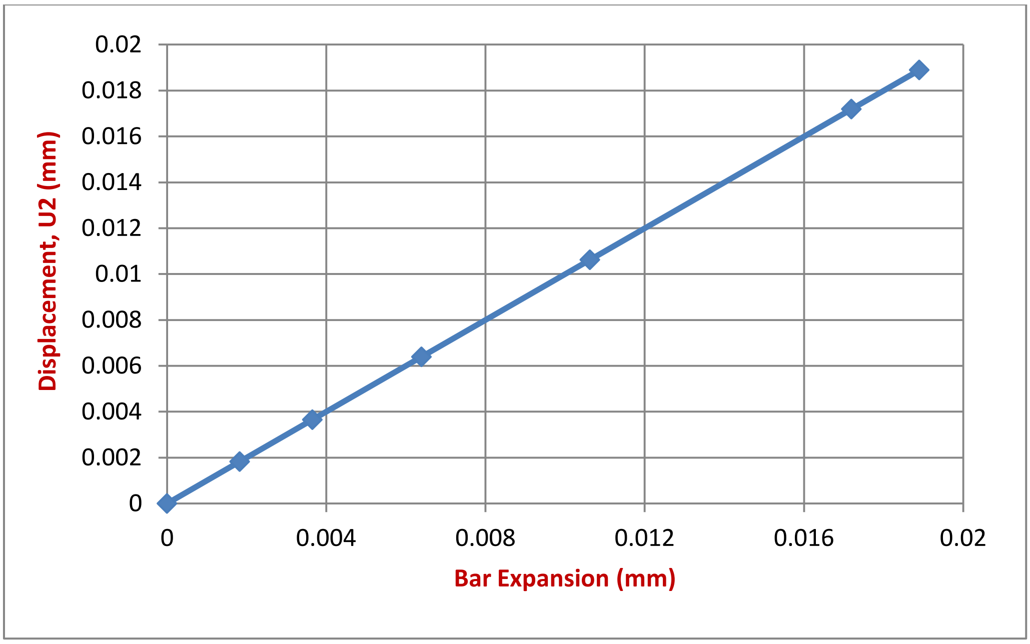

Fig. 8.16a: Displacement (U2) vs. Bar Expansion (Model No.3)

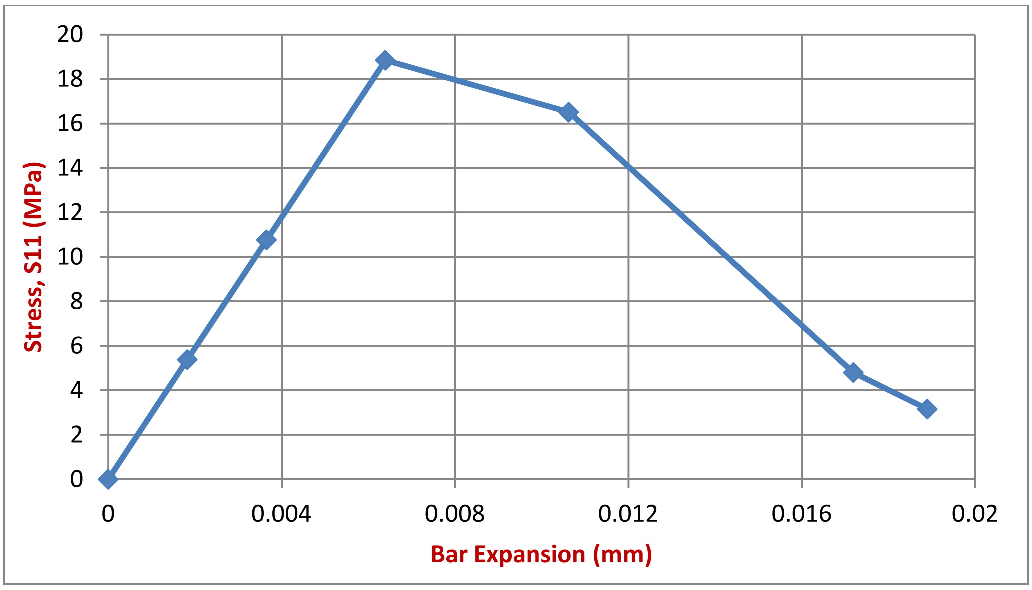

Fig. 8.16b: Stress (S11, tension) vs. Bar Expansion (Model No.3)

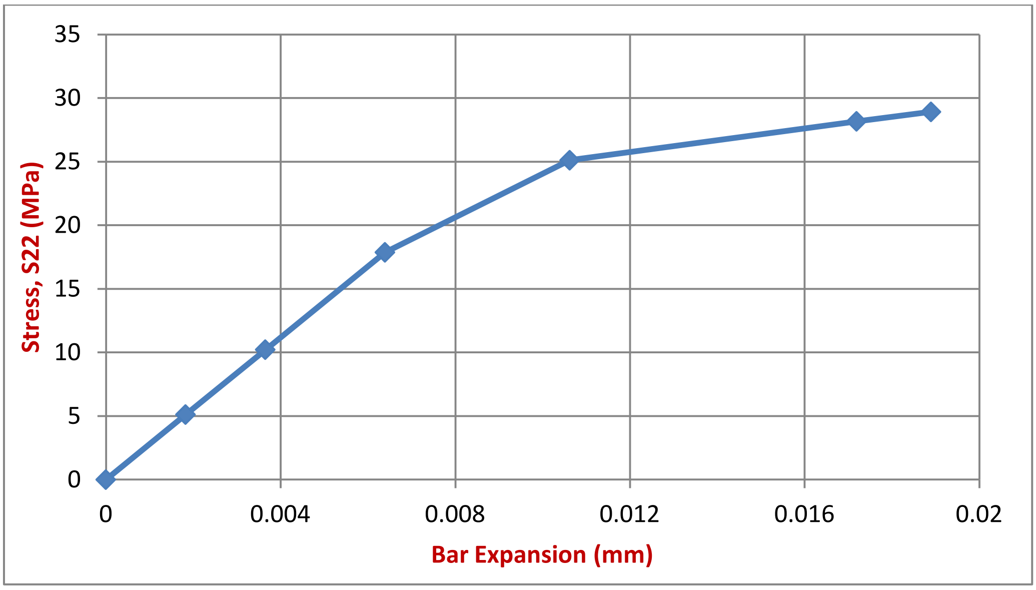

Fig. 8.16c: Stress (S22, compression) vs. Bar Expansion (Model No.3)

8.7.4 Model (4): Steel (elasto-plastic) and Concrete (elasto-plastic)

8.7.4.1 Model Description

In this model both steel and concrete are defined as elasto-plastic materials. This model uses the concrete properties for the 30 MPa concrete with the 240/350 steel bar embedded. The model parameters are shown in Table 8.6. Material properties are held constant for all concrete and steel elements. Plasticity of concrete in compressive behavior is defined using the stress-strain curve shown in Fig. 8.12 and the *CONCRETE* option in Abaqus, and its tensile behavior is defined using the *TENSION STIFFENING* and *FAILURE RATIOS* options. Properties of intermediate elements are exactly the same as concrete elements. Steel elements material properties are defined as those used in model No. (2). All elements in the model were simulated using 3-node linear plane stress triangle (CPS3), and 4-node bilinear plane stress quadrilateral (CPS4) elements.

Table 8.6: Model No. (4) Parameters

Material	Density (kg/m^3)	Modulus of Elasticity (Pa)	Poisson's ratio	Expansion coefficient	Element thickness (mm)
Concrete (30MPa, w/c=0.32)	2222	2.73×10^{10}	0.2	-----------	10
Steel (240/350)	7486	2×10^{11}	0.303	1.23×10^{-5}	10

The *CONCRETE* option is used to define the properties of plain concrete outside the elastic range in an Abaqus/Standard analysis. It must be used with in conjunction with the *TENSION STIFFENING* option. This option is used to define the retained tensile stress normal to a crack as a function of the deformation in the direction of the normal to the crack. The *FAILURE RATIOS* option is used to define the shape of the failure surface for a concrete model.

8.7.4.2 Model Analysis

Figs. 8.17a to 8.17d show the Abaqus analysis for this model. From the figures it can be noticed that the maximum tension doesn't occur at the interface between concrete and steel, but it occurs somewhere after the interface. However, this happens at the last step but at the beginning the maximum tensile stresses begin at the interface until reaching the maximum concrete tensile strength and then the stresses are transported to the un-cracked elements. Fig. 8.17b shows the stresses (S11), and it can be noticed that the maximum tensile stresses are 2.27 MPa and located at a distance from the bar. Fig. 8.15c shows the stresses (S22) which represent the compression stresses in the concrete cylinder. The maximum compressive stresses from the figures are approximately 23 MPa and located at the interface elements.

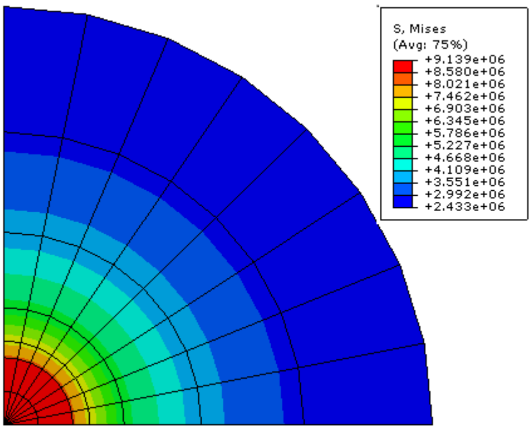

Fig. 8.17a: S,Misses (Model No. 4)

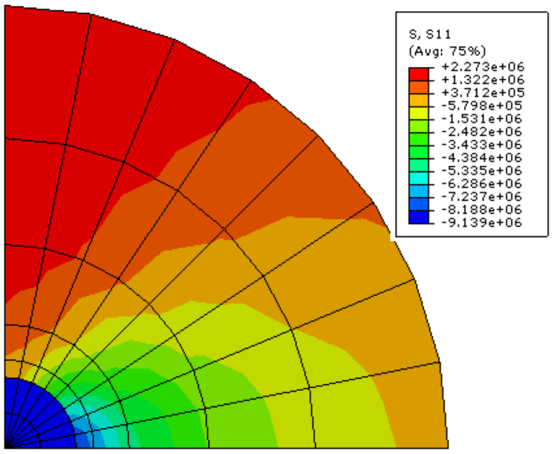

Fig. 8.17b: S,S11 (Model No. 4)

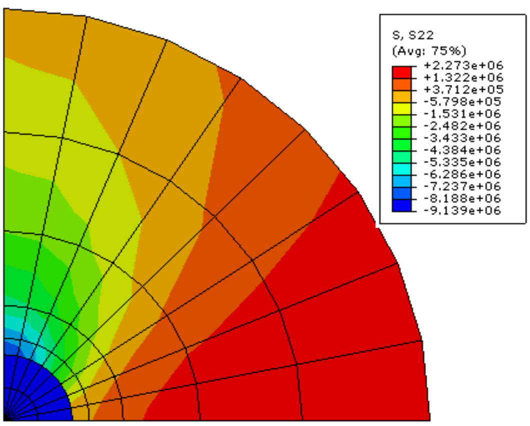

Fig. 8.17c: S,S22 (Model No. 4)

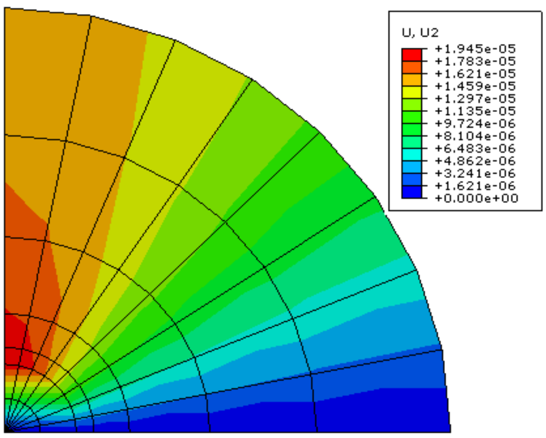

Fig. 8.17d: U,U2 (Model No. 4)

Figs. 8.18a to 8.18c show the behavior of the model along the six steps at the intermediate elements located at the interface between the steel bar and the concrete cylinder. In this model the behavior of concrete in tension (Fig. 8.18b) is different from its behavior in compression (Fig. 8.18c). In tension the concrete reached a maximum stress of 2.6 MPa. This is approximately the maximum tensile stress of this type of concrete which is equal to 2.73 MPa. However, the concrete behavior in compression showed that the maximum stresses were approximately 11 MPa, and this is below the compressive strength for this type of concrete 30 MPa.

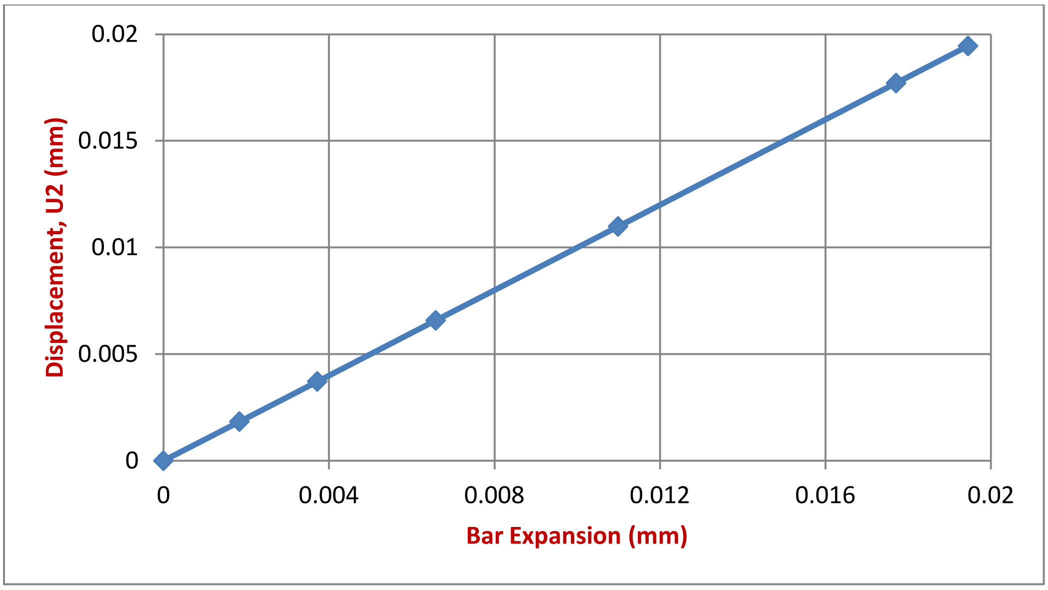

Fig. 8.18a: Displacement (U2) vs. Bar Expansion (Model No.4)

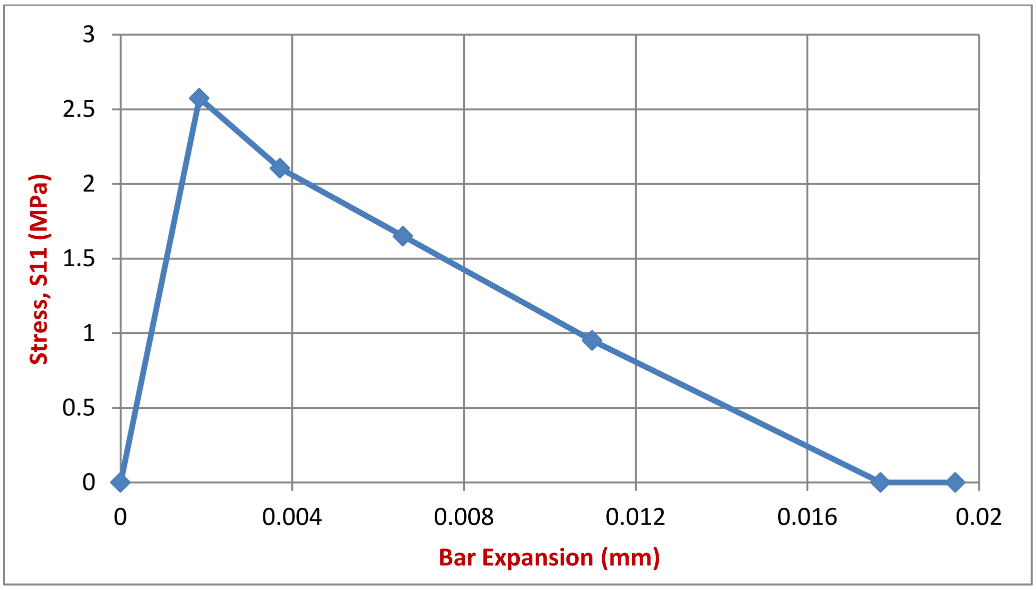

Fig. 8.18b: Stress (S11, tension) vs. Bar Expansion (Model No.4)

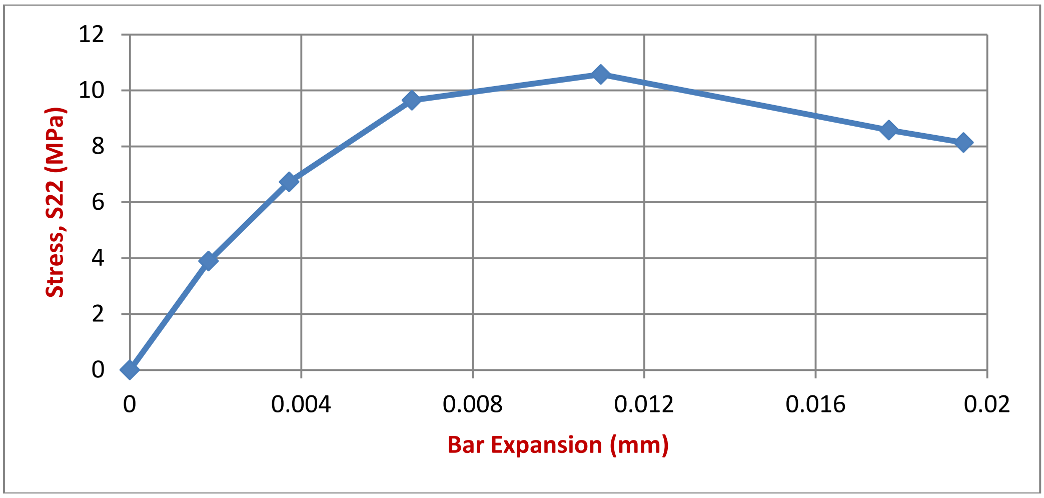

Fig. 8.18c: Stress (S22, compression) vs. Bar Expansion (Model No.4)

In order to ensure the type of boundary conditions used; a complete 2D circular model was developed as shown in Figs. 8.19a through 8.19d. The circular model showed nearly the same behavior as the 2D quarter circular model used in model No. [4].

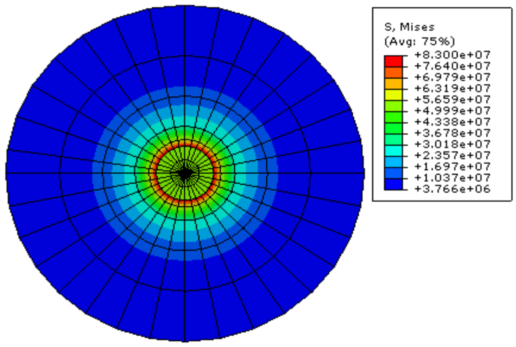

Fig. 8.19a: S,Misses (Model No. 5)

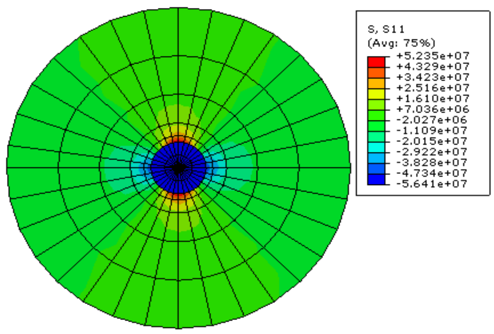

Fig. 8.19b: S,S11 (Model No. 5)

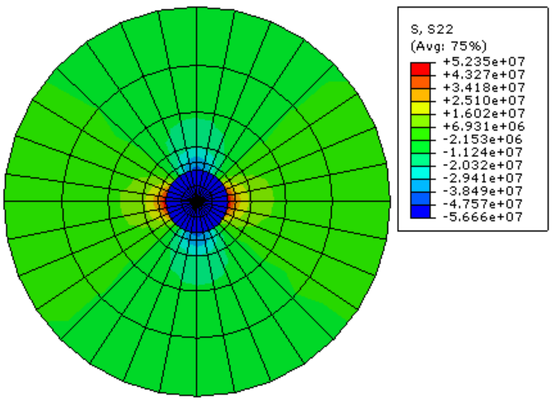

Fig. 8.19c: S,S22 (Model No. 5)

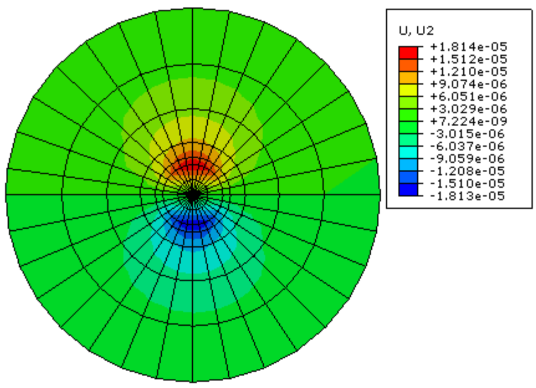

Fig. 8.19d: U,U2 (Model No. 5)

8.7.5 Model (5): Steel (elasto-plastic) and Concrete (elasto-plastic) 2D Circular

8.7.5.1 Model Description

This model is a complete circular 2D model (Fig. 8.20) which uses the same parameters as the previous model. The tensile behavior is defined using linear stress-strain before cracking and non-linear post-cracking behavior where tensile stresses decay to zero progressively to insure the numerical stability of the model. Since concrete is a composite material made primarily with aggregate, cement and water, its properties vary according to the mix proportion. Also, a variation in its mechanical and physical properties occurs within the same mix. This phenomenon had been considered when developing the numerical model, randomly some concrete elements were chosen and their materials properties had been changed to be stronger or weaker than the others.

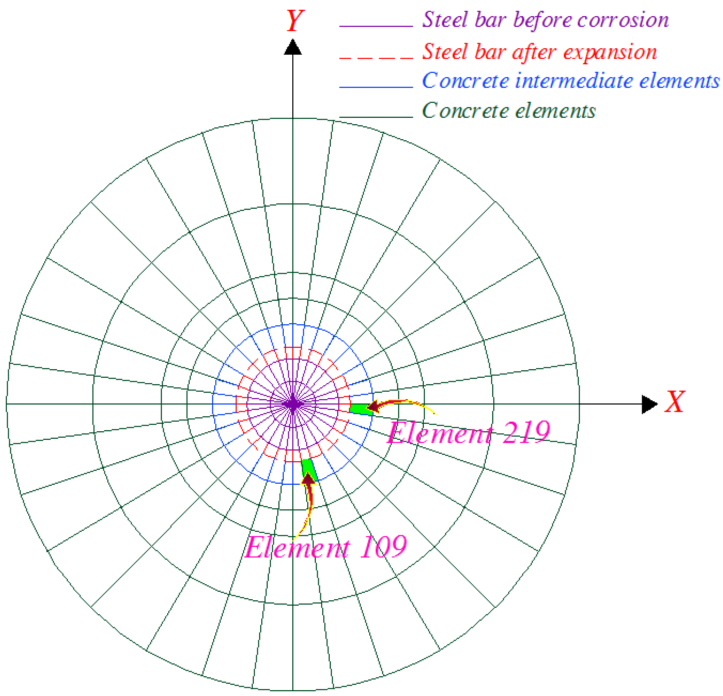

Fig. 8.20: The 2D model of cross-section [Model No. 5]

The cylinder cross-section is modeled using shell elements with three and four nodes. The material properties for the steel element representing the bar are; Yield strength F_s^y=240MPa, Elastic modulus E_s=200GPa and Poisson ratio μ =0.33. The material properties for concrete elements representing the cylinder are: Compressive strength F_c^u=30MPa, Elastic modulus E_c=27.3GPa and Poisson ratio μ=0.2. For the circular cross-section, the steel corrosion is simulated by radial expansion of steel bars ($\Delta\varphi$). The ratio of radial expansion to initial bar diameter (φ_0) gives the corrosion expansion strain:

$$\varepsilon_{corr} = \frac{\Delta\varphi}{\varphi_0} \qquad 8-4$$

The applied corrosion expansion strain varied from zero to $3x10^{-3}$ and the axial logarithmic strain in the x-direction (ε_x) is used to detect the development of cracks over the cross section. The cracking of concrete is simulated using the smeared method where the effect of discrete fracture created in localized zone is simulated by an equivalent reduction in tensile stress over wider zone, The tensile strength for concrete is fixed to F_c^t = 3MPa with corresponding tensile strain of ε_c^t=10^{-4}. Beyond the fracture limit a smooth decaying of tensile stress is assumed to insure a numerical stability in the calculations. To represent the localized variation in concrete properties at element size, 10% of concrete elements were assigned 10% reduction in their material properties while another 10% of elements were assigned 10% increase in their properties. Both types of elements were selected randomly.

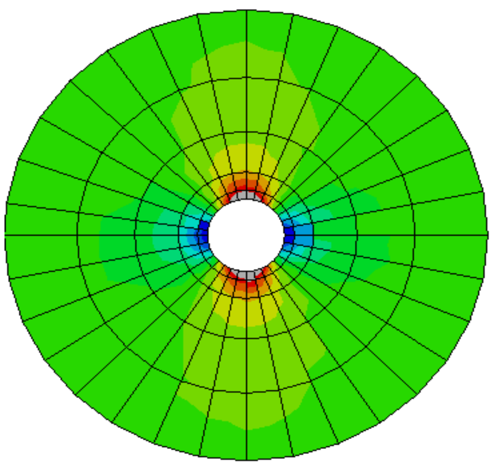

Fig. 8.21a: ε_{corr} = 0.9‰

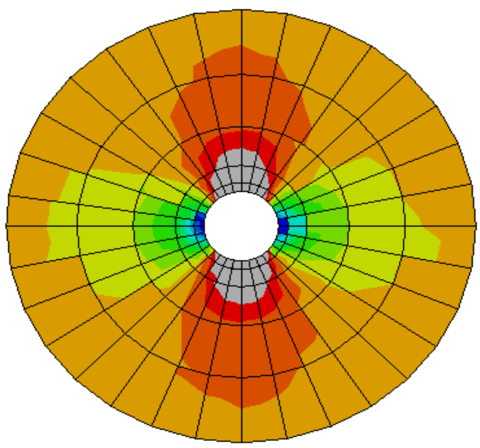

Fig. 8.21b: ε_{corr} = 1.0‰